Ebbs and Glows: Quantifying Small RNA Concentrations in *C. elegans*

Richard Boeri Decal

A thesis submitted in partial fulfillment of the honors requirements for the degree of Bachelor of Arts

April 2011

Division of Natural Sciences

New College of Florida

Ebbs and Glows:

Quantifying Small RNA Concentrations in *C. elegans*

Richard Boeri Decal

New College of Florida, 2011

Abstract

The recent discovery of RNA interference (RNAi) has revolutionized our understanding of RNA biology and genetic regulation. Researchers have mounted an international effort to elucidate RNAi pathways in order to harness them for their therapeutic potential. *Caenorhabditis elegans*, a model organism widely used to study RNAi, has distinct silencing pathways for interfering RNAs derived from endogenous and exogenous sources. Although the exogenous RNAi pathway has been largely mapped, endogenous RNAi pathways remain largely uncharacterized. In particular, RNA Helicase A (RHA-1) is an actor in endogenous RNAi whose function remains unknown. *C. elegans* deficient in RHA-1 exhibit a phenotype similar to animals deficient in ERI-1, a component of the endogenous 26G RNAi pathway. To test whether RHA-1 works in the 26G pathway, we measured changes in 26G interfering RNAs in worms deficient in RHA-1, ERI-1, and both RHA-1 and ERI-1. The preliminary data indicates that RHA-1 is not involved in 26G RNA biogenesis, but may be working further downstream in the pathway.

Katherine Walstrom

Division of Natural Sciences

To Madhuri Shukla, with love.

If you wouldn't have let me borrow your printer that late afternoon,

I wouldn't have been able to graduate.

This thesis is dedicated to you as per our agreement.

Ack

Thank you to Dr. Gregory Dubois-Felsmann, a New College alum slash science superstar who generously funded my project.

nowledge

To Dr. Walstrom for sponsoring my project and letting me bumble around the lab, and for your aiding me throughout my undergraduate career. You helped me achieve many of my academic conquests, so I thank you for your support. A special thanks to Dr. Thomas for lending me your lab expertise. Thank you to my committee, Dr. Shipman and Dr. Hart for being a solid source of career and life advice.

ments

I would not have gotten by without a little help from my friends: Lucy, Simon, Erin and my family. I especially thank Sara and the members of Zee dorm for putting up with my temporary lapses in sanity. I am indebted to TM for sharing the location of his secret thesising hole. Last but not least, thank you to the series of space-time events affectionately named New College.

Stay hungry. Stay foolish.

Contents

List of Figures

List of Tables

Chapter 1

Introduction

"A four-year-old child could understand this report. Run out and find me a four-year-old child, I can't make head or tail of it."

-Groucho Marx in *Duck Soup*

"Sometimes a scream is better than a thesis."

-Ralph Waldo Emerson

1.1 Background

1.1.1 A Brief Overview of Gene Expression

DNA is a molecule used as a blueprint to synthesize biological products in all cells. These instructions are encoded using sequences of the nucleotides adenine, thymine, guanine, and cytosine (A, T, G, and C, respectively) within regions of DNA termed "genes". The instructions are decoded by cells to synthesize proteins, the basic mechanistic unit of life.

Gene expression is highly controlled (Figure 1.1) because it would be counter-productive to express the entire gene arsenal constantly. For example, it would be harmful for a cell to synthesize proteins used in division during its growth phase. Gene expression can occur at various points in the protein synthesis pathway using different strategies. The control point that has recieved the most attention for much of the past century is the transcriptional level, where DNA sequences (promoters, enhancers,

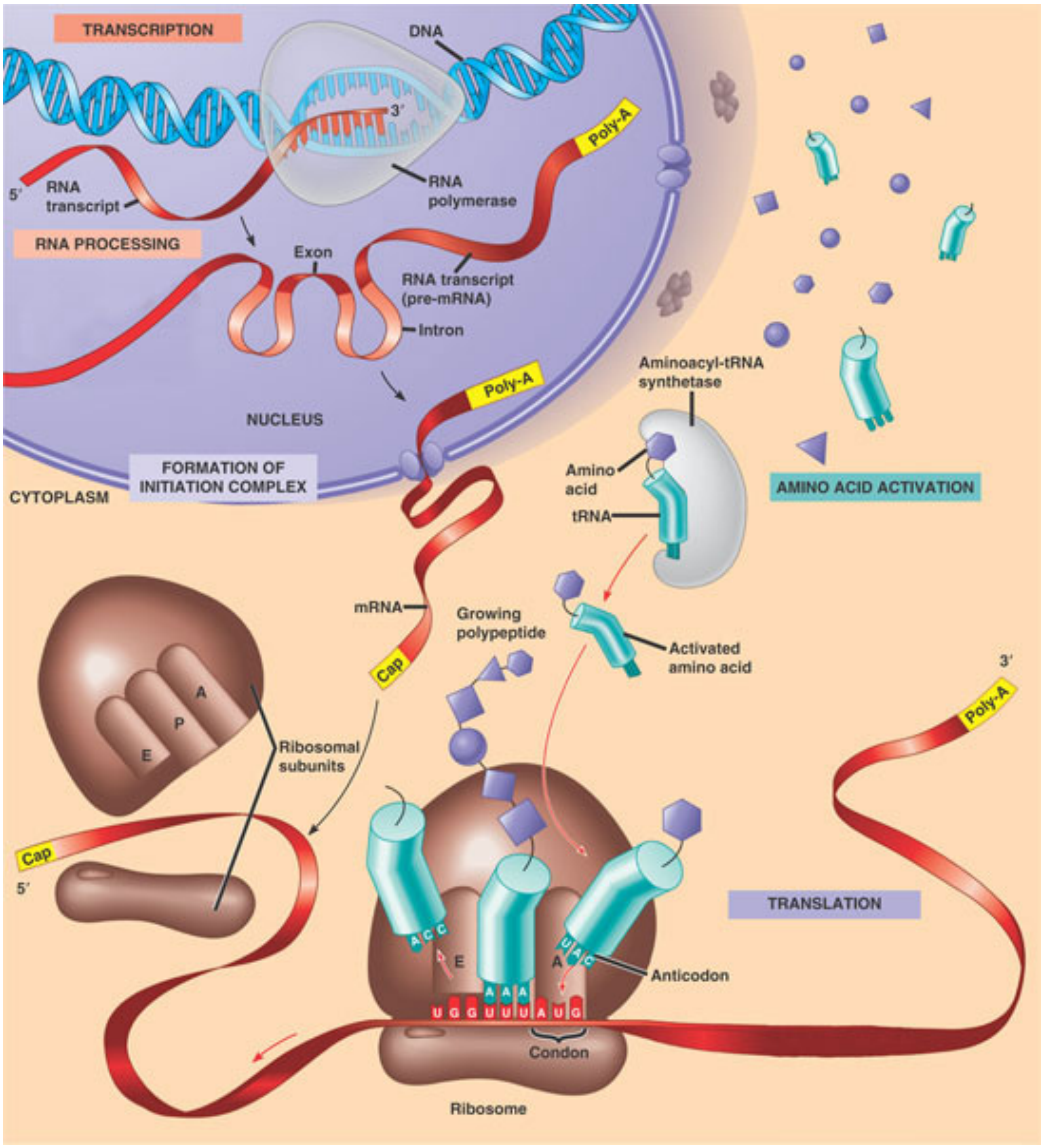

Figure 1.1: Gene Expression Overview - In a process called transcription, RNA polymerase II is recruited to genes. It slides down the DNA helix, unwinding the two strands to access the DNA bases. The polymerase uses nucleotides complimentary to the DNA sequence to synthesize an RNA copy of the gene. This intermediate "**m**essenger" **RNA** (**mRNA**) is processed before being exported from the nucleus to the cytoplasm. There, large ancient cellular machines called ribosomes "translate" the nucleic acid code into the protein code. Nascent proteins are folded into their proper shape, processed, and transported to its final destination. mRNAs can be recycled by other ribosomes to produce several protein copies. Picture courtesy of PBWorks.

and insulators) and transcription factors (activators and repressors) orchestrate the transcription machinery.

However, the majority of the human genome is not transcribed into protein transcripts[1]. Some genes encode RNAs responsible for regulating most cellular processes, including differentiation, gene expression, protecting the genome from instability, and metabolism[2,3]. Among these RNAs are small (<25 nucleotide) RNAs responsible for silencing genes[4], termed **s**mall **i**nterfering **RNA** (**siRNA**). siRNAs achieve gene silencing through a mechanism called **RNA i**nterference* (**RNAi**), a fundamental cellular process[5–8].

1.1.2 An Overview of Canonical RNA Interference Pathways

RNAi is an ancient biological mechanism which traces its origin to the common ancestor of humans, fish, flowers, worms, and yeast[9] (see Figure 1.2). The RNAi effect and its components are implicated in many fundamental cellular roles. RNAi is an epigenetic mechanism, meaning it modifies gene expression heritably without editing the DNA sequence of those genes. Epigenetic mechanisms are the basis for differentiation of cells that contain identical copies of DNA (reviewed by Gibney *et al*[10]). One particular RNAi pathway involving miRNAs is capable of regulating upwards of 60% of mammalian mRNAs[11]. RNAi is essential for proper development, and mutations to RNAi components are often developmentally lethal. RNAi prevents foreign genetic matter originating from transposons[12] or viruses[13] from damaging the host genome and is believed to be a primordial immune system.

RNAi negatively regulates genes in a potent, sequence-specific, and sometimes reversible manner[4]. This reversibility gives RNAi some advantages over other transcriptional silencing strategies. For example, methylation of residue Lysine 9 on Histone 3 is a repressive epigenetic modification that triggers events that pack DNA,

*The discovery of siRNAs' role in genetic silencing garnered the 2006 Nobel Prize in Physiology or Medicine.

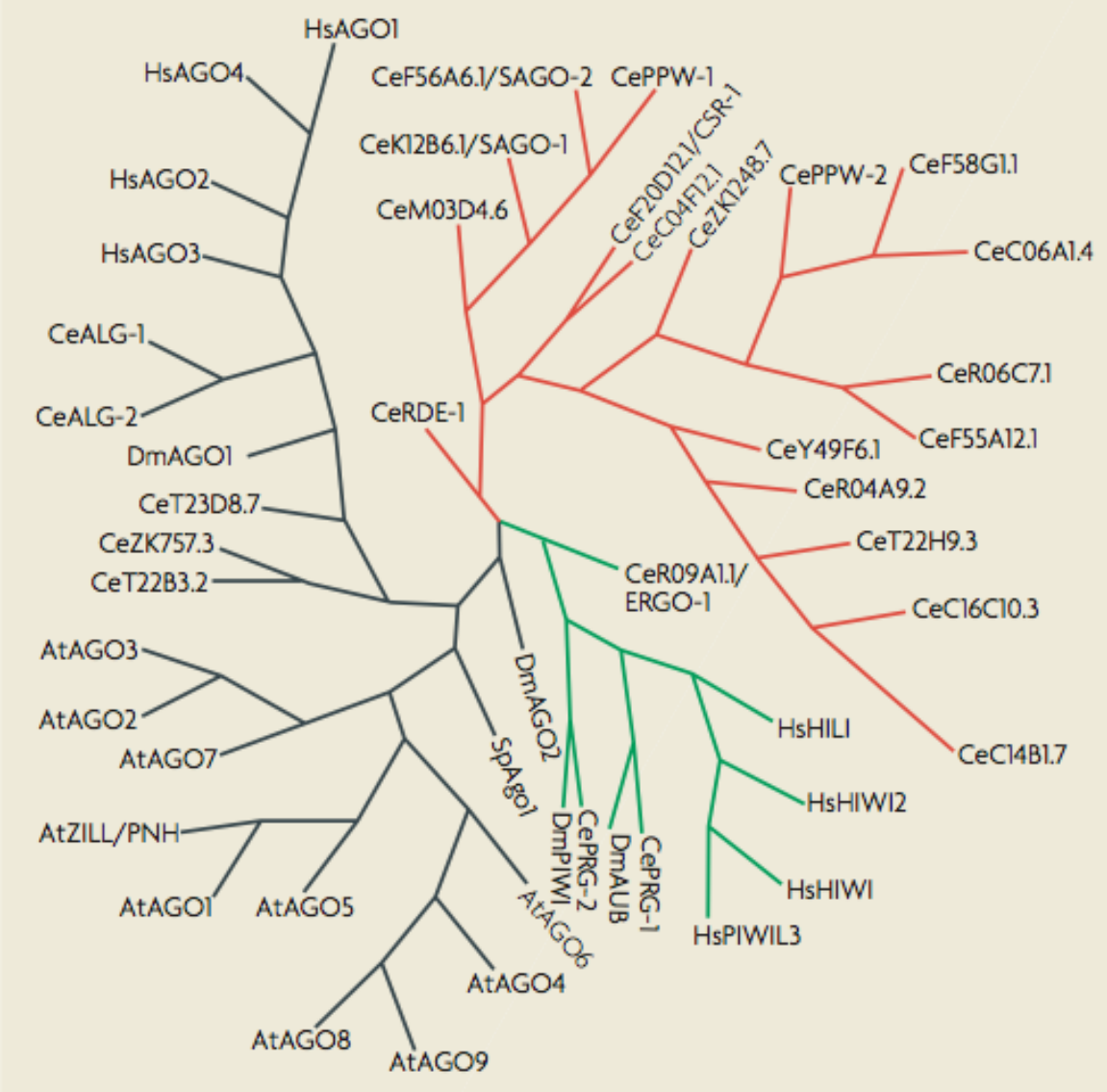

Figure 1.2: Evolutionary Lineage of Argonautes - Argonautes are a central RNAi component. Pictured is a phylogenetic map of *C. elegans*, *D. melanogaster*, *A. thalia*, *S. pombe*, and *H. sapiens* argonautes. The common ancestor of all these distantly related species had RNAi pathways nearly a trillion years ago, and they modern argonautes still have high sequence conservation. Interestingly, *C. elegans* has an expanded collection of argonaute proteins. Picture taken from Yigit *et al.*[14].

which sterically exclude the transcriptional machinery from those genetic regions. Additionally, siRNAs degrade mRNAs regardless of their genomic origin, making it an effective way to silence high copy-number genes which are distributed across the genome.

siRNAs silence genes by degrading mRNAs before they can be used as translational transcripts (see Figure 1.3). The workhorse of the interference pathway is the **R**NA-**i**nduced **S**ilencing **C**omplex (**RISC**), a large multi-protein machine that uses siRNA to identify and degrade mRNAs homologous to the siRNA. Briefly, siRNA are synthesized, processed, and loaded into the RISC complex. This siRNA-RISC complex hybridizes exclusively with mRNA that perfectly compliment the siRNA strand. Successful base-pairing of siRNA with its target mRNA triggers cleavages by Argonaute, the RISC endonuclease component.

Besides being a powerful biological tool, RNAi has many applications in biotechnology. It has revolutionized our scientific ability with its rapid, inexpensive, and effective nature. No longer hampered by the laborious process of generating mutants, scientists can rapidly knock down genes of interest using high throughput techniques. As a therapeutic, RNAi has promise for treating many diseases including AIDS[16,17] and cancer[18] (reviewed by Castanotto[19] and Barik[20]).

1.1.2.1 siRNA Biogenesis and Regulation

In general, siRNAs originate from long double-stranded RNA. Pre-siRNA are recognized by the endoribonuclease "Dicer" (DCR-1 in *C. elegans*) and "diced" into mature siRNAs[22] (mechanism detailed in Section 1.1.2.2). Mature siRNAs are double stranded, approximately 21 nucleotides long, and have a characteristic symmetric 2-nucleotide 3' overhang[21,23]. This length is sufficiently long to recognize any

Note to the reader: Due to many aliases assigned to the main RNAi components, I will adhere to the *C. elegans* naming conventions in order to simplify the my overview and because my experiments were conducted *C. elegans*.

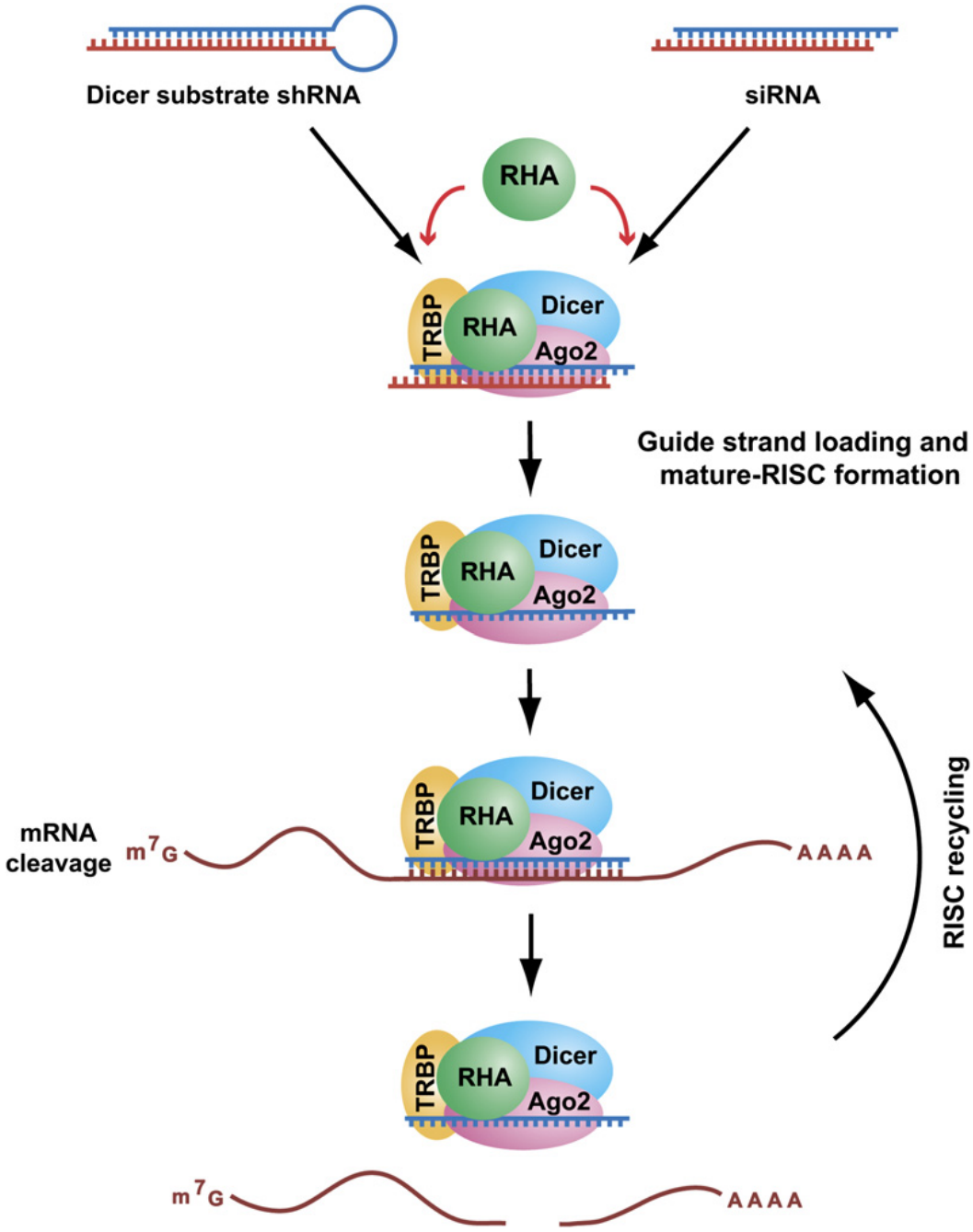

Figure 1.3: Schematic of a Canonical RNAi Mechanism - In humans, **R**NA **h**elicase **A** (**RHA**) promotes the association of siRNA with argonaute of RISC. Once the siRNA guide strand is loaded into RISC, it acts as an argonaute cofactor for potent and sequence-specific degradation of mRNA. The RISC can reuse the siRNA guide strand, so catalytic amounts of siRNA are sufficient to destroy many mRNAs. Picture modified from Robb *et al* [15].

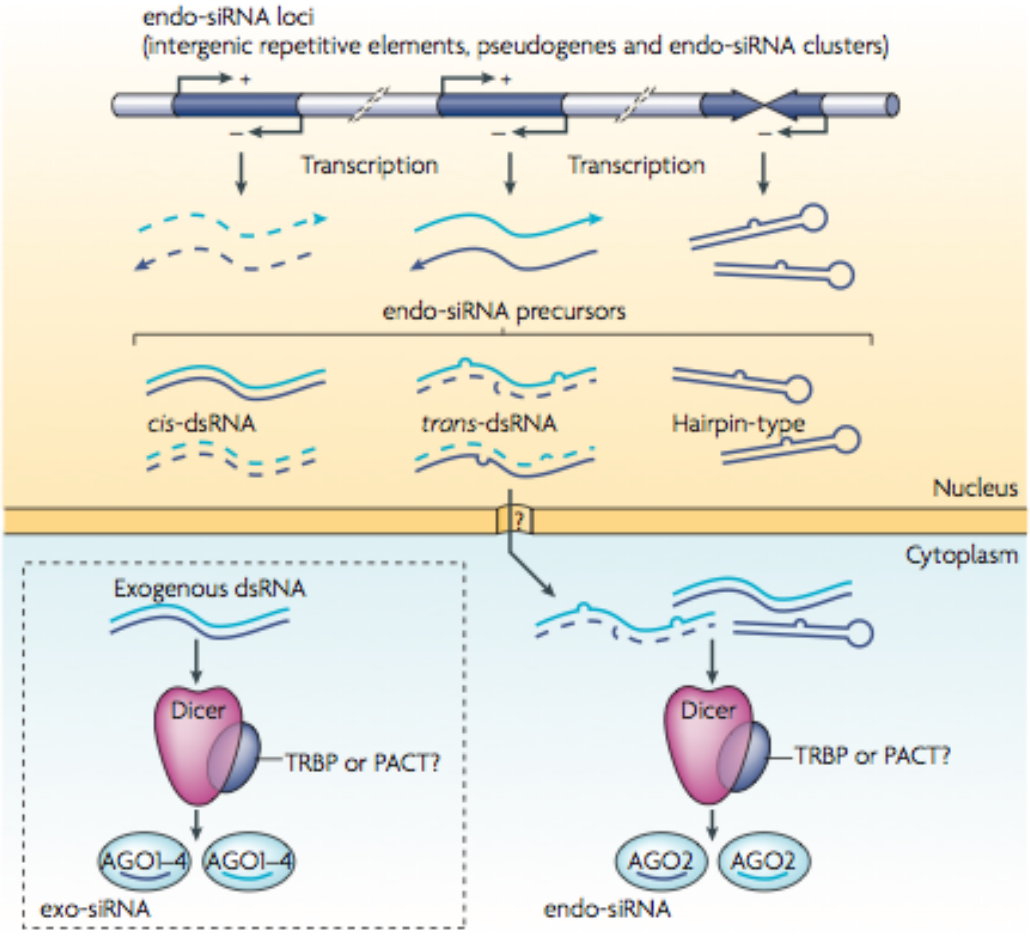

Figure 1.4: siRNA Biogenesis Pathways - Endogenous siRNA precursors are **d**ouble-**s**tranded **RNAs** (**dsRNAs**). These pre-siRNA are processed by Dicer into mature siRNA which then associate with endogenous argonautes. Inset: exogenous pre-siRNA are also processed by Dicer and used to program the exogenous RISC complex. Note: in *C. elegans*, the exo-RISC argonaute component is called RDE-1, TRBP is called RDE-4, and the endo-RISC argonaute component is called ERGO-1. Picture taken from Kim *et al*[21].

mRNA target, and statistically has the best ratio of sequence specificity to off-target effects[24].

Organisms can quickly and impermanently silence genes by altering siRNA concentration. siRNA concentration is controlled by a variety of mechanisms, including regulating initial transcription, siRNA amplification by **R**NA-**D**ependent **R**NA **P**olymerases (**RdRPs**), degeneration by ERI-1, and janitorial depletion by cytoplasmic nucleases[23]. Changing the activity of these mechanisms can dramatically change siRNA levels.

1.1.2.2 Overview of Dicer Proteins

The structure of siRNAs is a clue that they are processed using an RNAse III-like mechanism[5]. To identify the siRNA processing component, a combination of epitope tags, coimmunoprecipitation, and radio-labeled dsRNA were used to screen candidate proteins[5]. These studies identified Dicer as the enzyme responsible for processing dsRNAs into siRNAs *in vivo*[22,25]. Dicer then relinquishes the siRNA to the Argonaute, the "slicer" of the RNAi pathway. Dicer has substrate promiscuity, and is largely responsible for the short half life of long dsRNA in most eukaryotic cells[22].

Eukaryotic Dicer is comprised of a helicase domain, a PAZ (**P**IWI/**A**rgonaute/**Z**wille) domain, two RNAse III domains, and a **ds**RNA-**b**inding **d**omain (**dsRBD**) (see Figure 1.5)[22,27]. The enzyme has an axe-like shape, with the helicase and PAZ domains forming the "handle" and the two RNAseIII domains forming a monodimer "blade". The end of dsRNAs are recognized and anchored at one end of Dicer by the PAZ domain. At the other end of Dicer, the monodimer harbors two Mg^{2+} catalytic centres responsible for "dicing" activity. The centres are separated by the width of dsRNA and slightly offset, which is the structural basis for the siRNA overhangs[25,28]. Between the PAZ and RNAseIII domains is a flat, positively charged surface which

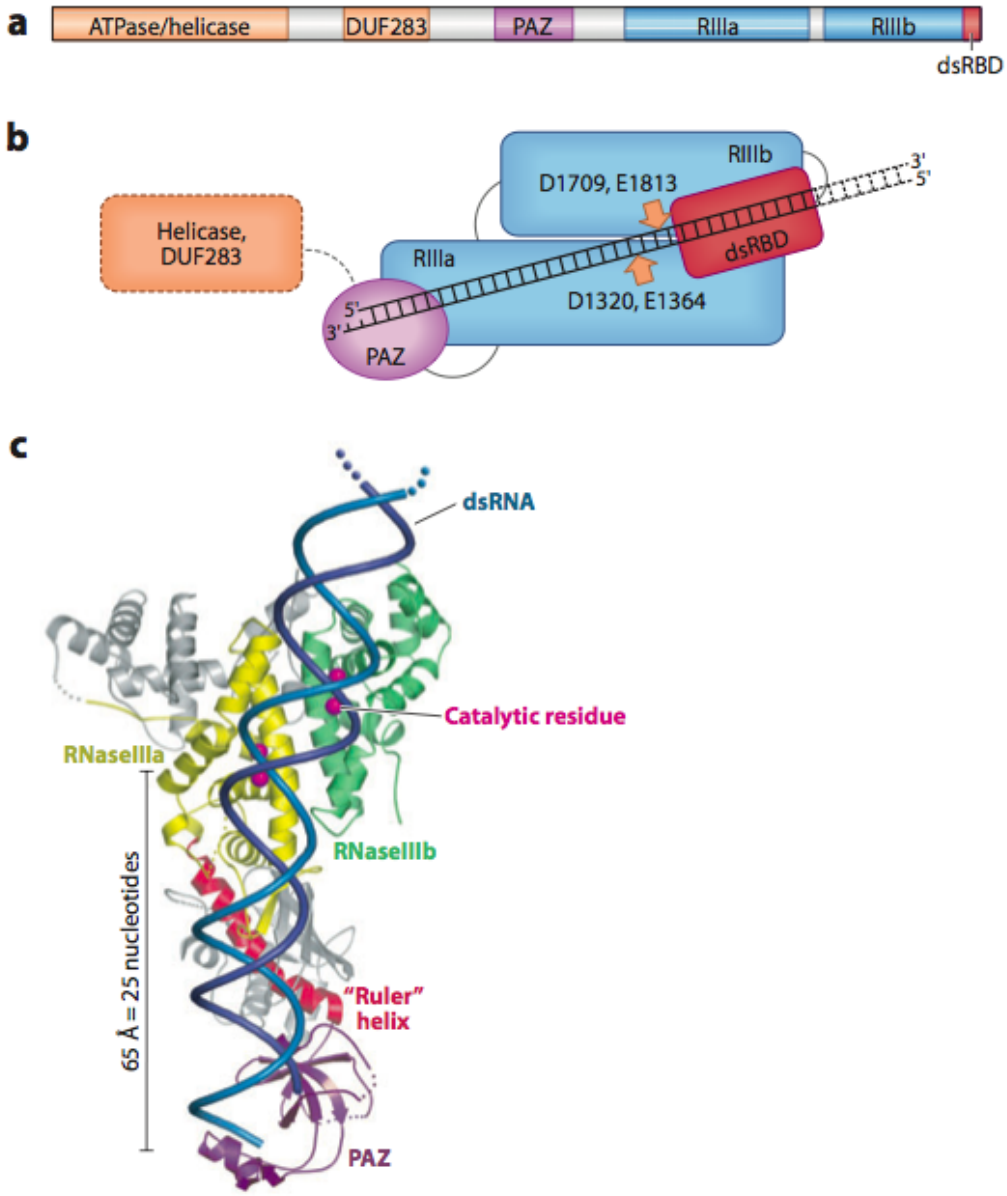

Figure 1.5: The Structure of Dicer Enzymes - Dicer is comprised of a helicase, PAZ, RNAse III, and dsRNA-binding domains (**A**). (**B**) shows a schematic of the Dicer tertiary structure with a siRNA bound. The arrows indicate the location of cleavage sites. The X-ray co-crystal structure (**C**) of Dicer-dsRNA shows the siRNA anchored in the PAZ domain and adjacent to the catalytic residues. The distance between the PAZ and catalytic domains is indicated. Picture taken from Liu *et al* [26].

interacts with the dsRNA phosphates[25].

Dicer is sometimes called a molecular ruler because it produces dsRNAs of precise lengths. The structural basis for this precision is a "ruler helix" which separates the PAZ "anchor" and RNAseIII "dicing" center. The length of this helix determines the length of the siRNA[25].

1.1.2.3 Overview of Argonaute Proteins

After siRNA are created, they associate with primary **Argo**nautes (**AGO**s) to activate the RISC complex. Small RNA-AGO complexes are broadly responsible for genomic surveillance and gene regulation[29,30]. In particular, siRNA-AGO is the core functional unit of the RISC[31,32]. siRNAs are used as a guide by AGO to cleave the correct mRNA target[33].

First, the guide strand of the siRNA needs to be loaded into the AGO. There are two prevailing models for how AGO selects the correct strand[34]. In both models, strand selection is achieved by sensing the inherent asymmetric thermodynamic profile in siRNAs. In the first model, a Dicer-2-R2D2 (homologous to DCR-1 and RDE-4 in *C. elegans*) separate the duplex RNA and load the correct one into AGO[26,35]. Dicer binds the stable end of the duplex while R2D2 selects the less stable end. In the other model, AGO loads both siRNA strands and uses their thermodynamic instability to differentiate the strands[35]. Once it has determined which is the guide strand, AGO cleaves and discards the passenger strand[36,37].

AGOs have a N-terminal, PAZ, middle (Mid), and PIWI domain[26] (see Figure 1.6). The PIWI domain has an RNase H-like fold containing a conserved "DDH" motif (two aspartate and one histidine residue) which correspond to the catalytic center of AGO (see Figure 1.7). The PAZ, N-terminal, PIWI, and Mid domains form a positively charged crescent-shaped channel which stabilizes the siRNA and mRNA. Additionally, the PAZ domain has a fold which interacts with the 3' over-

hang of siRNA, and the Mid domain has a pocket which binds the 5' end. This is consistent with biochemical studies[38] that demonstrated the precise complimentary base-pairing of the 5' end was more important than the 3' end in successful cleavage.

One notable class of AGO proteins, called the PIWI proteins, direct a distinct RNAi pathway. They use a distinct class of small **P**IWI-**i**nteracting **RNA** (**piRNA**) to cause genetic silencing. Interestingly, these piRNAs are formed independant of Dicer and Drosha[21]. In general, PIWIs are required for worm fertility[14].

1.1.3 An Overview of *C. elegans*-specific RNAi Mechanisms

At this point, I will overview some nuances of *C. elegans* RNAi biology, since we will use it as a model organism to test our hypothesis.

C. elegans has many specialized RNAi mechanisms driven by its expansive repertoire of no less than 27 unique argonautes (shown in Figures 1.2 and 1.7). The functions of all these argonautes are not known, but some are redundant and others are unique in function.

Unlike mammals, *C. elegans* can use foreign RNA for RNAi. In mammals, exogenous dsRNAs are quickly destroyed by interferon[7]. *C. elegans*, on the other hand, processes ingested* or injected[32] siRNA mimics for use in an exogenous RNAi pathway[40,41].

The exogenous RNAi pathway is very similar to the canonical RNAi model reviewed above. DCR-1 and RDE-4[42] (homologous to Dicer and TRBP, respectively) process exogenous dsRNA into primary exo-siRNA[32]. This exo-siRNA binds the primary argonaute RDE-1 (**R**NA interference-**de**ficient phenotype; homologous to Ago2) to activate exo-RISC.

Endogenous siRNA precursors are also processed by DCR-1[43] before associating with the primary argonaute of the endo-RISC pathway, ERGO-1[32]. *ergo-1*

*The animals can be fed dsRNAs using liquid containing dsRNAs or bacteria over-expressing siRNAs[39]

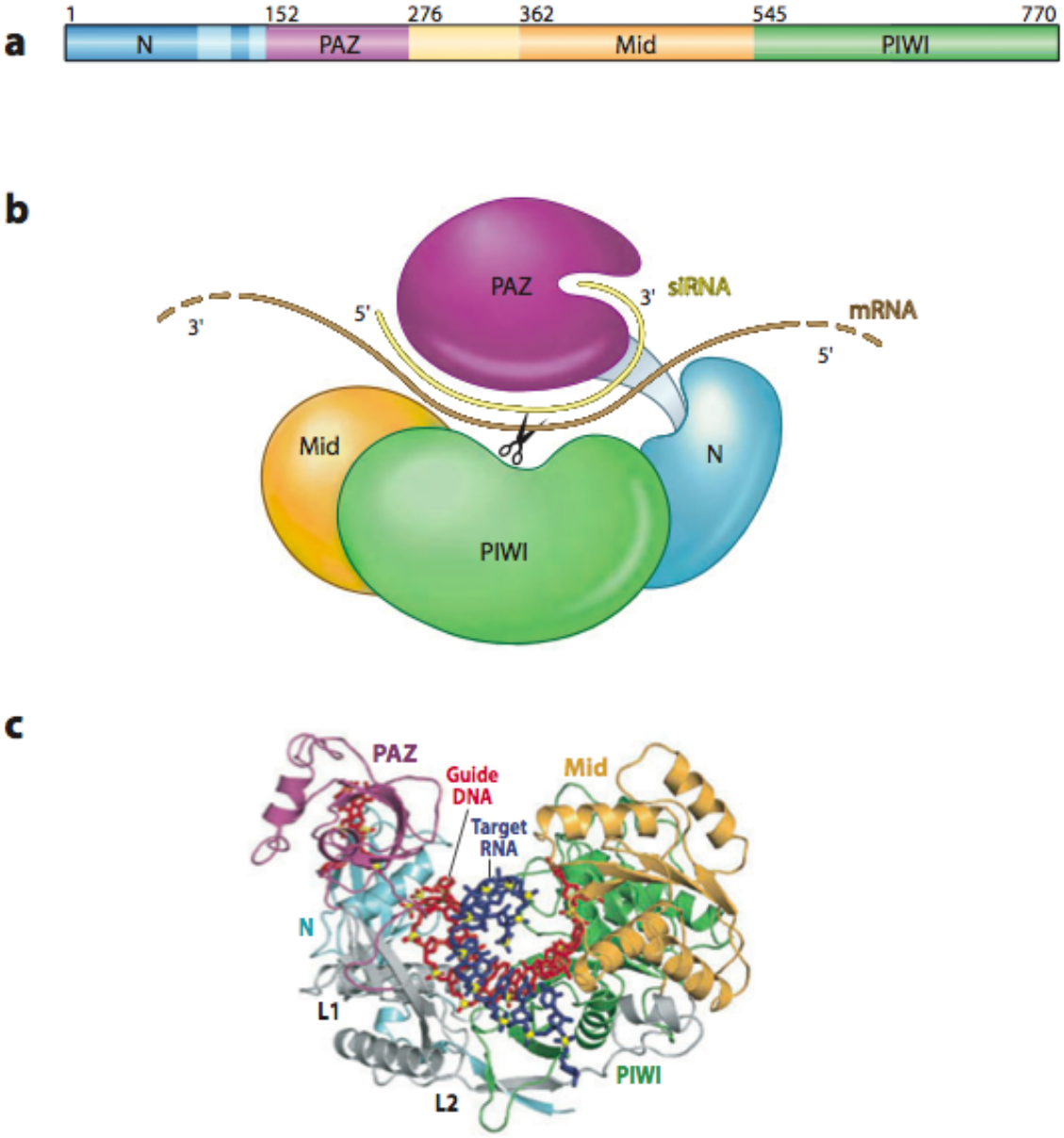

Figure 1.6: The Structure of Argonaute Proteins - The primary structure (**A**) and schematic (**B**) of arganaute shows the relationship between its N-terminal, PAZ, middle (Mid), and PIWI domains. As in Dicer, the PAZ domain recognizes and anchors the end of siRNA. Successful base-pairing with target transcripts positions the mRNA backbone in the "slicing" catalytic center (represented as a pair of scissors). The X-ray cocrystallization (**C**) of siRNA-mRNA-Ago demonstrates the base-pairing, and curvature of the siRNA. Picture taken from Liu *et al*[26].

Figure 1.7: Sequence Alignments of *C. elegans* Argonaute Proteins - *C. elegans* has many unique AGOs. The conserved "DDH" motif is necessary for slicer activity[26]. The secondary AGOs (highlighted) are missing this motif and do not have slicer activity. Picture taken from Yigit *et al.*[14].

(**e**ndogenous **R**NAi-deficient Ar**go**naute) deficient animals are sensitive to exogenous RNAi and have increased endo-siRNA concentrations. The molecular basis for the interaction between endogenous and exogenous RNAi is discussed later.

Additionally, both the endo- and exogenous RNAi have sequential "primary" and "secondary" pathways[7,44–46]. Following mRNA cleavage by primary RNAi, the degradation products are used as a template for unprimed synthesis of an anti-sense strand by RdRPs[45,47,48]. The resulting dsRNA is processed by Dicer into secondary siRNAs[32] (see Figure 1.8). Each of these secondary siRNA are distinct RdRP products[47]. These secondary siRNAs are used exclusively by **s**econdary **AGO**s (**SAGOs**) in what is called secondary RNAi which silences genes. The secondary RNAi pathway amplifies the original primary siRNA signal[7]. Secondary siRNAs are vastly more abundant than primary siRNAs, and are essential for proper interference in *C. elegans*[45].

1.1.3.1 Specific Classes of Small RNA

In *C. elegans*, a subset of 26 nt-long endogenous primary siRNA which invariably start with a guanine nucleotide are named the "26G RNAs"[50]. They are found in high concentrations in sperm, and are important for spermatogenesis and oogenesis (see Figure 1.9). Worms deficient in the 26G RNAi pathway have a temperature sensitive sterile phenotype[50]. The target mRNA cleavage products are used as a template to synthesize secondary siRNAs of 22 nt length that invariably start with a guanine nucleotide, called the 22G RNAs. Some 26Gs originate from a specific region of the X chromosome and are called "the X cluster" called the X-cluster RNAs[32].

Another class of small RNAs, called the 21U RNAs, are believed to be the piRNAs of *C. elegans*[29,52,53]. These RNAs have a Dicer-independent biogenesis, are invariably 21 nt in length, and have a 5' monophosphate and uracil. They are expressed in the germline. Ruby *et al* identified over 15,000 unique 21U RNAs in *C. elegans* in

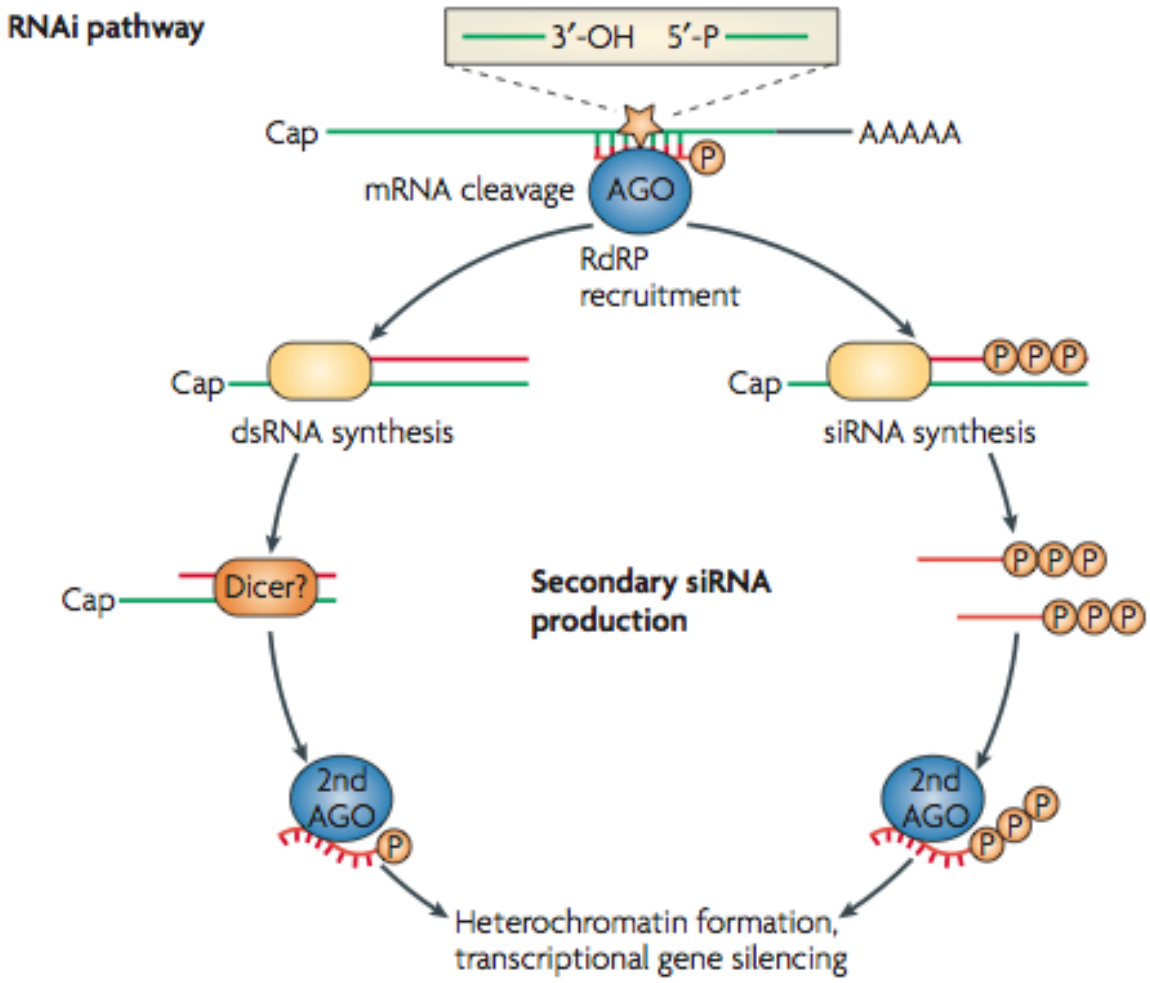

Figure 1.8: Model for Secondary siRNA Synthesis - RNAi has sequential and distinct rounds of silencing. The first, or primary, round of RNAi cleaves mRNA targets which are used as substrates for RdRPs to make secondary siRNA. These secondary siRNA are used by secondary RISC proteins in genetic silencing. Picture taken from Hutvagner *et al* [49].

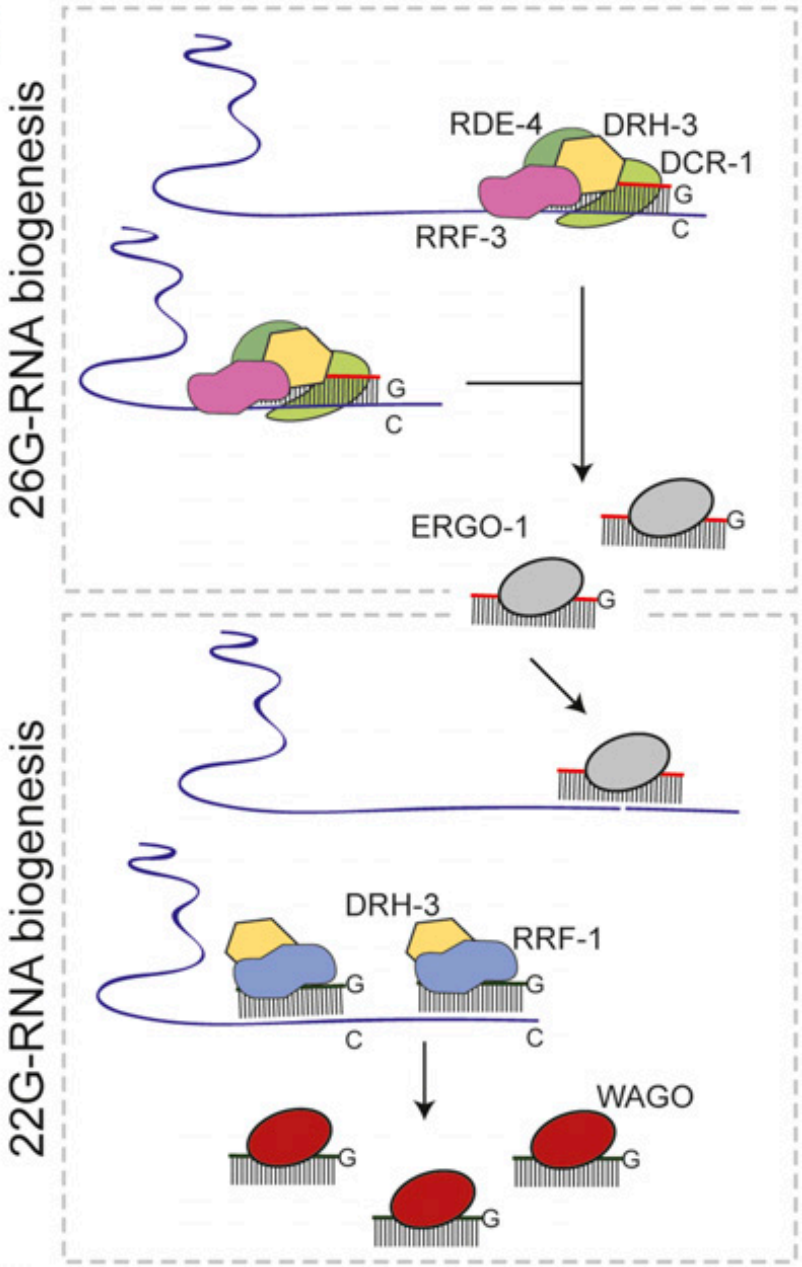

Figure 1.9: Model for 26G and 22G RNA Biogenesis - 26G and 22G RNAs are primary and secondary siRNAs which are synthesized in sequential rounds. First, distinct RdRPs synthesize 26G RNAs by using primary argonaute targets as a template. These 26G RNAs are used with ERGO-1 to degrade targets. These 26G targets are, in turn, used by distinct RdRPs to form 22G RNAs. These 22G RNAs are used by worm-specific **AGO**s (**WAGO**s) for RNAi silencing. Picture taken from Vasale *et al*[51].

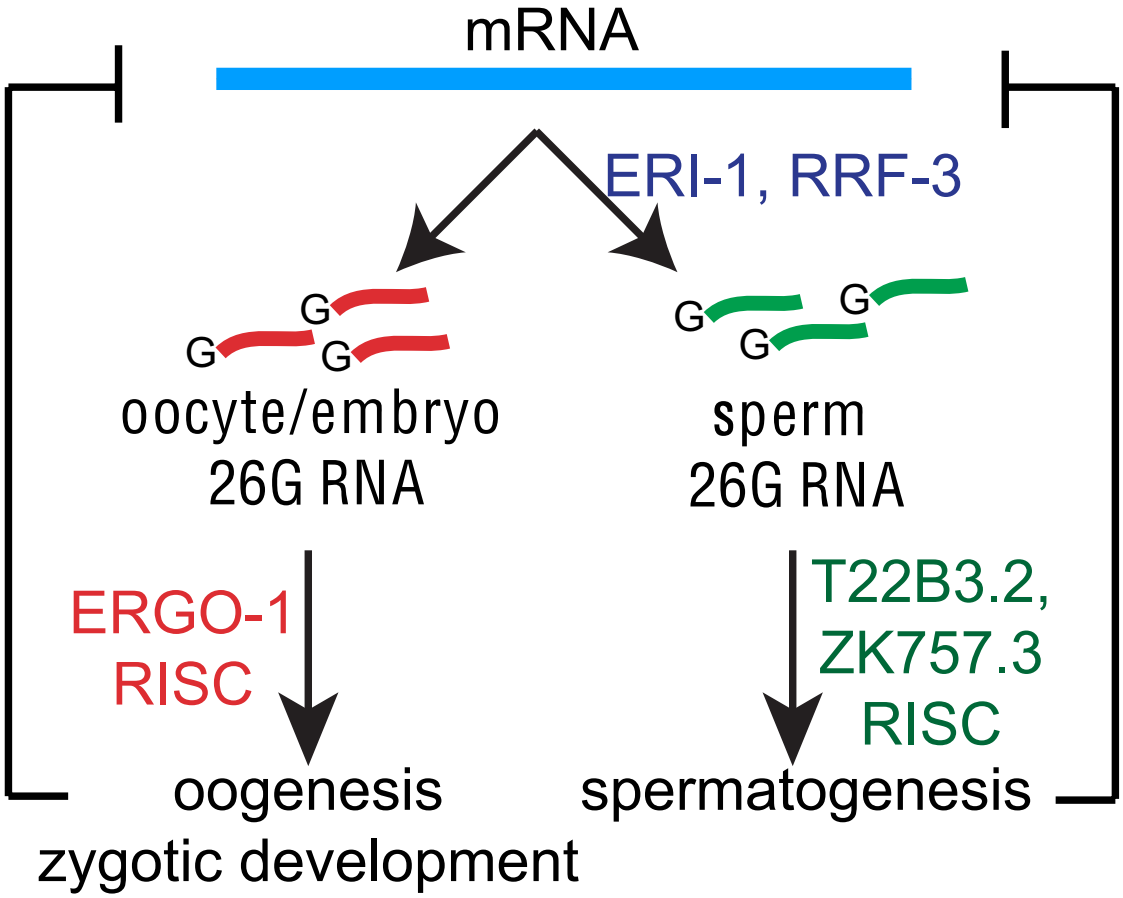

Figure 1.10: Proposed Model for 26G RNA Biogenesis and Function - Oocytes and sperm have different requirements for proper 26G RNA function. The 26G RNAs have distinct roles in these cell types. ERGO-1, T22B3.2, and ZK757.3 are all argonaute proteins. Picture taken from Han *et al*[50].

2006[53]. These 21U RNAs depend on PRG-1, a germline protein, to accumulate[52]. The developmental profile of PRG-1 and the 21U RNAs overlap perfectly[29]. Worms deficient in germline cells did not express PRG-1 or 21U RNAs[29]. *prg-1* mutants had a temperature-sensitive sterility phenotype.

Finally, *mi*cro*RNA*s (*miRNA*s) are a class of small RNA conserved across eukaryotes and play a fundamental role in genetic regulation[54–56]. They use a unique mechanism of RNAi that does not involve perfect base-pairing or mRNA cleavage[57–59]. The exact mechanism by which miRNAs repress expression is not clear, but they seems to preventing translation or by stimulating RNA degradation.

1.1.3.2 The ERI-1 Pathway

Wildtype *C. elegans* lacks the RNAi effect in neuronal tissue[39,60]. The discovery of viruses using proteins to disable RNAi[61] led to a hypothesis that an endogenous inhibitor of RNAi was causing the intrinsic RNAi resistance in neurons. One study[41] screened 50,000 *C. elegans* strains, each with a single gene knockout, in a neuron-localized GFP background. These strains were fed GFP-silencing siRNAs and monitored for changes in GFP fluorescence. Most strains did not properly silence the GFP gene since their neurons lacked RNAi. However, one mutant strain potently decreased fluorescence. This **e**nhanced **R**NA**i** phenotype worm was named the *eri-1* mutant.

The *eri-1(mg366)* mutation consists of a 23 base-pair insertion encoding a premature stop codon in the open reading frame T07A9.5 in *eri-1*, upstream of the evolutionarily conserved domains of *eri-1*[41]. This mutation causes an *eri-1* null phenotype.

eri-1 encodes ERI-1, a cytoplasmic inhibitor of endo-RNAi[62]. Specifically, it seems to modify the duration and cell-type specificity of RNAi[23,41]. ERI-1 is an evolutionarily conserved protein with a DEDDh-like 3'-5' exonuclease domain and

SAP/SAF-box DNA-binding domain. Both *eri-1* splice variants encode these conserved nuclease domains. The SAP domain is speculated to stabilize interactions between its DEDDh domain and dsRNA[41].

eri-1 animals accumulate endogenous and exogenous siRNA in all tissues relative to wild-type[23,41]. Biochemical studies showed human and worm ERI-1 produced similar protein products[41]. One model proposes that ERI-1 functions as an endoribonuclease to degrade the 3' overhangs of double stranded siRNA, a structural prerequisite for RISC loading[23,41]. In this model, *eri-1* mutants have enhanced RNAi because there are more siRNAs available for use in RNAi.

The *eri-1* mutant has a higher proportion of males due to chromosomal nondisjunction (Him phenotype)[41]. Additionally, mutants have a temperature-dependent sterility due to defects in spermatogenesis[41,63]. ERI-1 and Dicer act in a common pathway necessary for sperm development[50,63]. These mutants also lack 26G RNAs, evidence that *eri-1* is involved in 26G-siRNA biogenesis.

Curiously, *eri-1* mutants are very sensitive to exogenous RNAi even though ERI-1 only inhibits endogenous RNAi. One model proposes there is a limited reagent shared between endo- and exo-RNAi pathways[64] (see Figure 1.11). ERI-1 presumably associates with this limited reagent, and deletion of ERI-1 releases the reagent for use in exo-RNAi. In general, secondary AGOs cause competition between the endo- and exogenous RNAi pathways. Deficiencies in endo-RISC components results in enriched activity of exo-RISC[32].

1.1.3.3 RNA Helicase A

Helicases are an important class of enzyme which mechanically wind and unwind nucleic acids. RNA helicases unwind dsRNA fueled by ATP-hydrolysis[65]. RNA helicases are involved in nearly every aspect of RNA metabolism, and they are necessary for RNAi[66]. Understanding the role of helicases in RNAi is paramount for

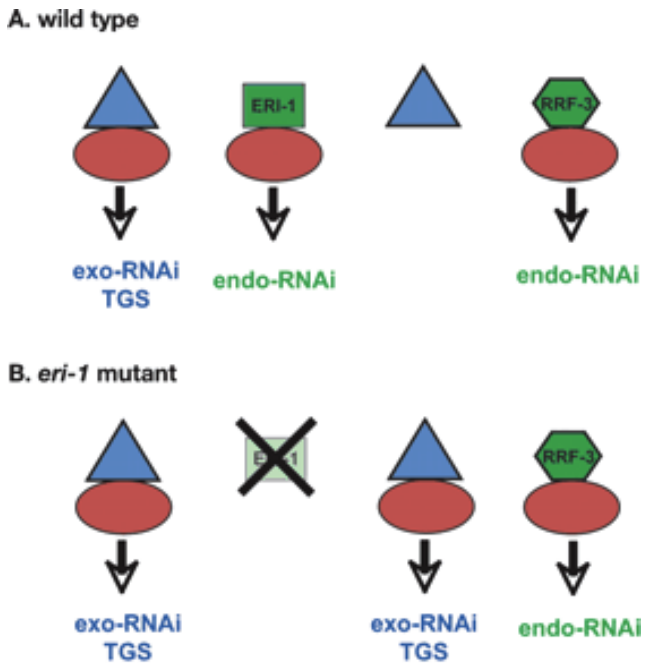

Figure 1.11: ERI-1 Limited Reagent Theory - One model to explain how loss of endogenous components improves exogenous components posits a limited reagent used in both pathways. ERI-1 presumably sequesters this reagent during endo-RNAi, and loss of ERI-1 makes these limited reagents available to exogenous RNAi, making exogenous RNAi more active. Picture modified from Lee *et al*[64].

therapy because they are frequently involved in viral biology[26]. *C. elegans* encodes 134 helicases[67], some of which fulfill roles not based on their helicase abilities[66].

RNA Helicase A (also known as RHA-1[68], DDX9[66], dhx9, LKP, NDHII, and Maleless[69]) has received much attention because of its many functions. It is highly conserved and involved in transcription, splicing, nuclear export, translation, and RNAi[66,70–72]. RHA is often conscripted by viruses including the human T-cell leukemia virus[73], foot-and-mouth disease virus[74], respiratory syncytial virus[75], Hepatitis C[76], and HIV[77,78].

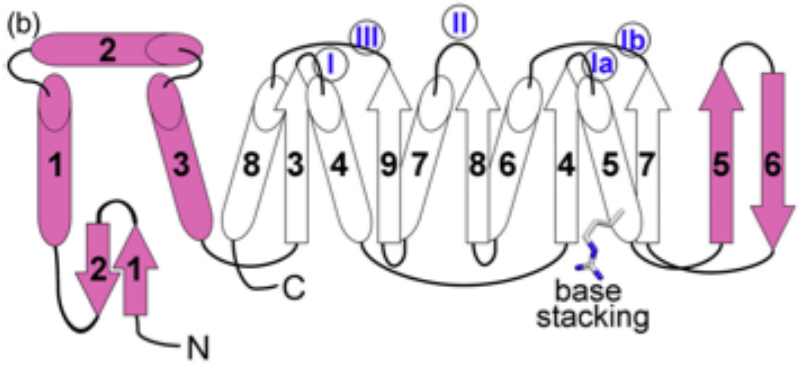

Figure 1.12: Schematic of Human RNA Helicase A Structure - The red parts of the schematic represent the DEIH domains, and the blue ones represent the helicase domains. Picture taken from Schutz *et al*[79].

RHA is also a part of the RNAi machinery[15,71] (see Figure 1.3). Animals deficient in RHA have lower gene silencing due to reduced recruitment of siRNA to Argonaute[15,66] (Ago2 is the human homologue of the *C. elegans* RDE-1). This, along with other data, suggest a model where RHA loads siRNA into argonaute along with the rest of the RISC[15,66] (see Figure 1.3).

RHA is a DEIH-box protein containing all the signature helicase motifs[66,79]. DEAD-box proteins have a conserved helicase core with two linked RecA-like domains[80]. The regions up and downstream of these RecA-like domains are highly variable and modulate the activity and substrate specificity of the helicase. The RecA-like domains form a continuous RNA binding site as well as the catalytic cen-

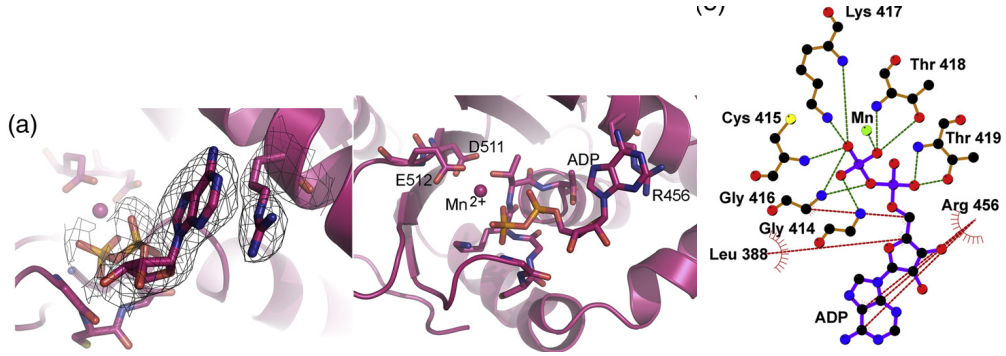

(a) Election density map of ADP in the catalytic cener, showing the base-pair stacking interaction.

(b) Structure of RHA catalytic center with important residues indicated.

(c) Molecular Interctions of ADP in the RHA active site.

Figure 1.13: Human RNA Helicase A Core Structure - Pictures taken from Schutz *et al* [79].

ter for nucleotide triphosphate hydrolysis.

When bound to ATP and dsRNA, the helicase forms a compact structure (step 1, Figure 1.14). This conformation surrounds and stabilizes the dsRNA. The enzyme then changes conformation to kink the RNA backbone, introducing local thermodynamic instability in the duplex (step 2, Figure 1.14). This instability is sufficient to separate short RNA duplexes, and one strand diffuses out of the enzyme (step 3, Figure 1.14). The helicase hydrolyses ATP and adopts a conformation with low affinity for RNA (step 4, Figure 1.14). After the second RNA strand and ADP leaves the helicase cleft (step 5, Figure 1.14) the cycle repeats [81].

1.1.4 *C. elegans* as a Model Organism

C. elegans (Figure 1.15) is an established eukaryotic model organism popularized in the 1970s by Sydney Brenner [82]. It has biological features which make it convenient for study, including its short development cycle (see Figure 1.16), transparent body, and simple body plan for a eukaryote. They are also resilient and inexpensive to maintain. *C. elegans* have 5 autosomal chromosomes and a pair of sex chromosomes;

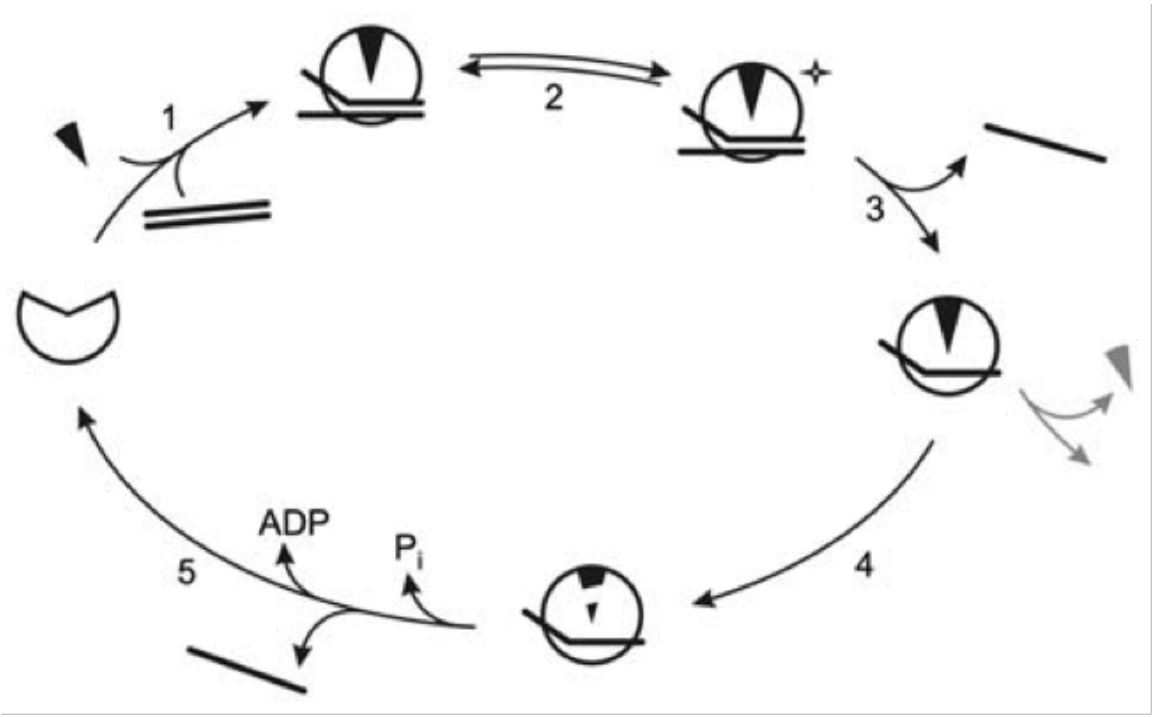

Figure 1.14: Model for DEAD Helicase Activity - This is a possible catalytic mechanism for DEAD-box helicase-mediated RNA duplex unwinding. The steps are described in the text. Picture modified from Hilbert *et al*[81].

hermaphrodite worms have XX sex chromosomes and the rarer males have XO sex chromosomes. Geneticists have developed an arsenal of genetic tools to manipulate *C. elegans* genes, and practically any mutant is available via worm stock centers*. Sequence analysis shows conservation of *C. elegans* small RNAs with distantly related organisms[59], making it a good model for use in this study.

C. elegans with null *rha-1* have a temperature-sensitive defect in germline transcriptional silencing[68], consistent with previous experiments showing RHA an is important transcriptional regulator. At the restrictive temperature, the animals become sterile due to defects in gametogenesis.

*The Caenorhabditis Genetics Center - http://www.cbs.umn.edu/CGC/

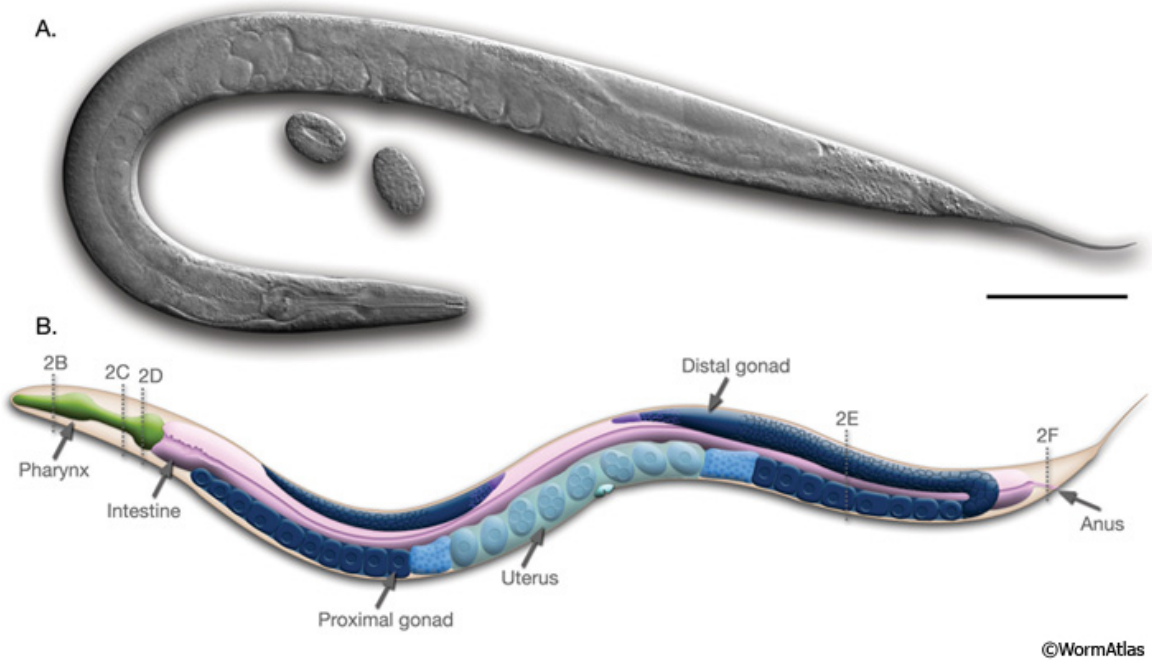

Figure 1.15: Anatomy of *C. elegans* - *C. elegans* is a clear nematode about 1 mm in length. The body plan is often described as a "tube inside of a tube". **(A)** is a differential contrast image (DIC) image of an adult *C. elegans* hermaphrodite (scale bar = 0.1 mm). **(B)** is a schematic of the nematode anatomy. Picture courtesy of Worm Atlas: wormatlas.org.

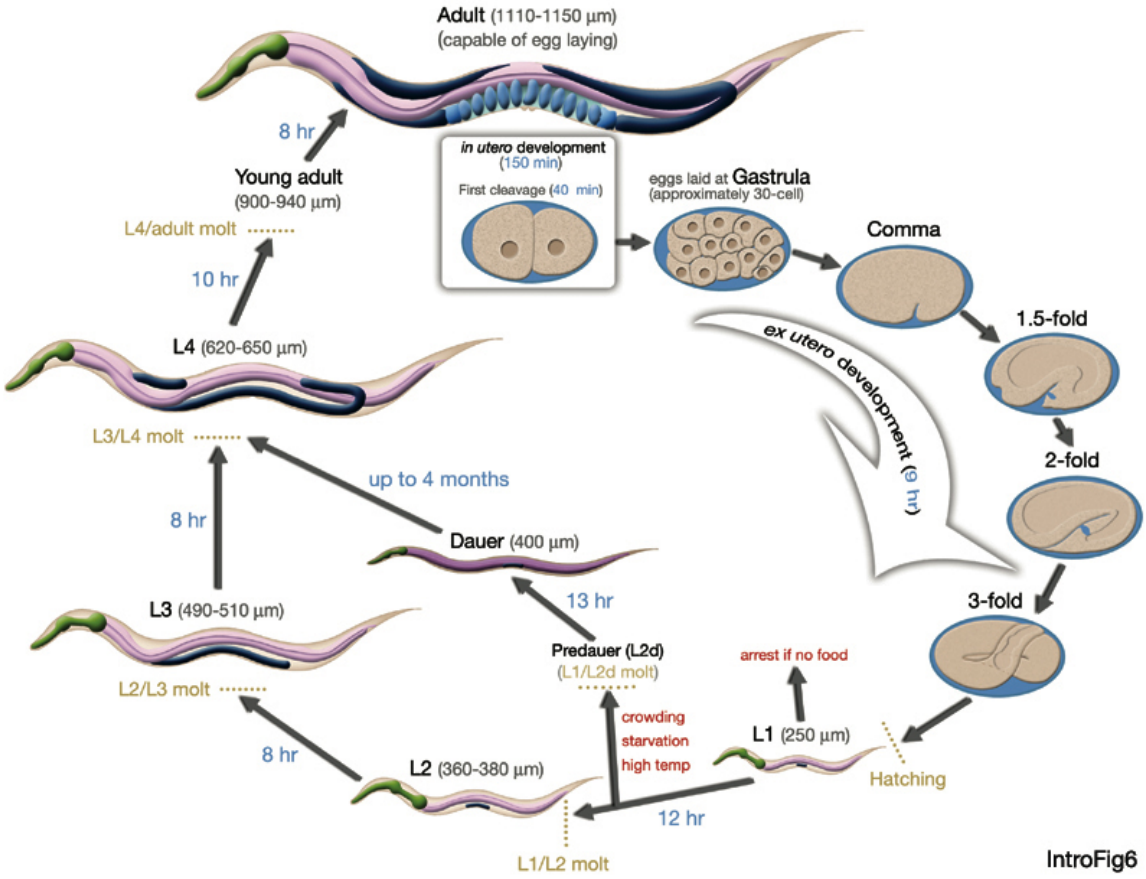

Figure 1.16: Developmental Cycle of *C. elegans* - *C. elegans* development occurs in stages named L1, L2, L3, L4, and finally adult. These stages take a specific amount of time at different temperatures. Picture courtesy of Worm Atlas: wormatlas.org.

1.2 Current State of the Field

The discovery of RNAi mechanisms in *C. elegans* has spurred a tremendous international effort to work out the biochemistry of the pathway. However, most studies in *C. elegans* have been focused on components of the exogenous pathway, and many endo-RNAi pathways remain to be understood. In particular, RHA is known to be involved in endogenous RNAi but its role is yet to be understood.

1.3 Current Research

rha-1 and *eri-1* are individually important for sperm development, and loss of function mutants exhibit similar phenotypes. This led us to hypothesize that RHA-1 acted with ERI-1 in a common RNAi pathway. To test this hypothesis, we measured the cellular concentration of small RNAs from various RNAi pathways in *eri-1* and *rha-1* mutants as well as *rha-1;eri-1* double mutants. We then calculated the RNA expression relative to wild-type animals. Changes in relative expression would be evidence that RHA-1 regulates the gene being measured.

We tested representative small RNAs including the 26G siRNAs, 21U piRNAs, and X-cluster RNAs. We also tested miRNAs and a snRNA as candidates for an internal reference gene. In this study we show that *rha-1* is not involved in the 21U RNA pathway. We also have preliminary evidence that *rha-1* does not alter the concentration of X-cluster RNAs of the 26G RNAi pathway. This suggests that *rha-1* is not involved in 26G siRNA biogenesis, although it is possible it acts downstream of biogenesis.

Chapter 2

Materials & Methods

"If at first you dont succeed, try try again.

Then quit. No sense being a damn fool about it."

-W.C. Fields

"We are scientists dammit, go measure something!"

-Dr. Benjamin Newberry, waving a ruler

All PCR reactions were conducted on a PTC-100 Thermal Controller made by M. J. Research. See Appendix A for buffer preparations.

2.1 Worm Strains

All worms strains (listed in Table 2.1) were obtained from the *C. elegans* Stock Center. For details on worm stock maintenance, see Appendix B.2.

Strain name	Description
N2	A wild-type strain originally described by Brenner[82].
rha-1(tm329)	A deletion mutation of *rha-1* (encoding RHA-1).
eri-1(mg366)	An insertion mutation of *eri-1* (encoding ERI-1).
rha-1(tm329);eri-1(mg366)	A double mutant.

Table 2.1: List of Worm Strains Used - All worm strain stocks were verified using single worm PCR before use.

2.2 Worm Genotype Verification

We verified the genotype of our worm stocks using agarose gel electrophoresis. Gel electrophoresis is a technique used to resolve mixtures of DNA based on length, which can be compared to known DNA size standards to calculate the size of the DNA. In this way, we can verify each allele in each strain by detecting bands of the correct size. The method involves loading DNA in one end of an agarose gel, immersing it in buffer, and creating an electric field along the gel using electrodes. The negatively charged DNA molecules are attracted to the positive terminal, and thus are slowly pushed through the gel in its direction. Longer DNA molecules can not fit through the smaller crevices in the gel matrix and thus are forced to take a torturous route. On the other hand, shorter DNA molecules travel faster and farther in the same amount of time. A loading dye such as Orange G makes the DNA mixture colored to make loading wells easier and to monitor the progress of the electrophoresis. The DNA bands can be visualized using commercially available dyes such as GelRed, which fluoresce exclusively when bound to DNA.

However, gel electrophoresis cannot detect single genes from a single worm, so the sequences of interest must be amplified. To do this, we used the **P**olymerase **C**hain **R**eaction (**PCR**). PCR is a cyclic reaction made possible by Taq, a thermostable DNA polymerase isolated from extremophile bacteria. The reaction employs a pair of olignucleotides called "primers" that anneal to a desired sequence on both strands of the DNA (in our case, flanking the sequences we wished to genotype). Primers are a requirement for Taq to polymerize nucleotides into a stand complimentary to the template DNA strand (Figure 2.1). As the PCR progresses, more DNA is available for primers to bind to, and amplification proceeds exponentially (Figure 2.2).

To isolate DNA from nematodes, we thoroughly digested all their proteins using a serine protease. First, a lysis mixture was prepared by mixing 1 μL of 10 mg/mL Proteinase K into 50 μL of lysis buffer. This lysis mixture was dispensed into PCR

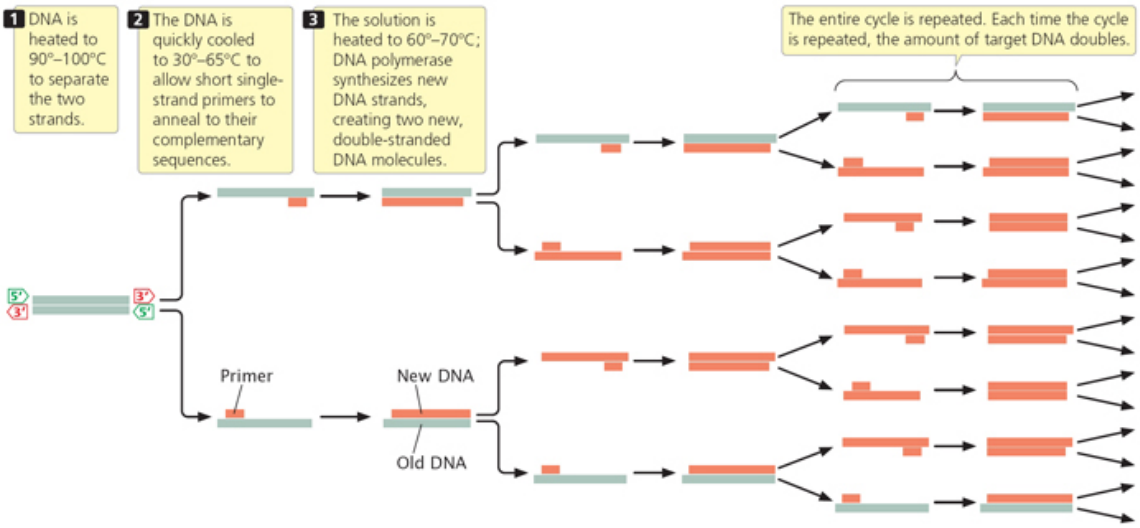

Figure 2.1: Steps of PCR - PCR is a cyclic reaction that amplifies DNA sequences using primers. First, the strands are separated so that the DNA bases can be bound by PCR components. The DNA is then permitted to form complimentary base pairs again. Quickly cooling the reaction with excess primer gives primers a thermodynamic advantage for binding. Finally, the reaction is increased to a temperature where Taq is physiologically active, and it elongates the primer to make a copy of the template strand. Picture courtesy of Nature Education: nature.com.

Number of PCR cycles (*n*)	Number of double-stranded copies of original DNA (2^n)
0	1
1	2
2	4
3	8
4	16
5	32
6	64
7	128
8	256
9	512
10	1,024
20	1,048,576
30	1,073,741,824

Figure 2.2: PCR Amplifies DNA Exponentially - Each PCR cycle doubles the copies of the template sequence. The rate of amplification increases exponentially as the reaction proceeds. The amplification continues until all dNTPs in the reaction mixture are depleted. Picture courtesy of Nature Education: nature.com.

Stock Reagent	Amount Used per Reaction
Nanopure water	13 μL
10X PCR Buffer (Qiagen)	2.5 μL
Forward Primer (10 μM)	1 μL
Reverse Primer (10 μM)	1 μL
1 mM dNTPs	2.5 μL
S. Taq (5 U/μL)	0.07 μL

Table 2.2: Single Worm PCR Reaction Mix - The PCR mixture used for to PCR a single worm. The forward and reverse primers used are listed in Table D.1. S. Taq is a mixture of Taq (Qiagen) and Tgo (Roche) in a 25:1 unit ratio in Taq buffer (Qiagen).

Stage 1 (1 repeat)	**Stage 2** (40 repeats)	**Stage 3** (5 repeats)
94°C for 30 sec,	92°C for 30 sec, 58°C for 30 sec 72°C for 30 sec	72°C for 5 min

Table 2.3: Parameters for Single Worm PCR - The 92°C stage melts double stranded nucleotides. This is followed by a 58°C stage to annealing primers with their complimentary sequence. The primer remains annealed through the 72°C stage, where S. Taq DNA polymerase elongates the primer. This reaction is cycled 40 times to amplify the template DNA.

tubes in 5 μL aliquots. One adult nematode of the appropriate strain was placed in lysis mixture before it was covered with mineral oil. The worms were then digested at 60°C for one hour, followed by a 15 minute 95°C incubation to denature the Proteinase K, which would otherwise digest the PCR enzymes in the next step.

We prepared a PCR mixture (Table 2.2) and mixed 20 μL of it with the digested worm under the mineral oil. PCR was performed on this genomic DNA using the parameters shown in Table 2.3, yielding a high concentration of our target DNA. Finally, 10 μL of the PCR reaction was mixed with Orange G loading dye and analysed using a 1.2% agarose gel run in 1X SB buffer alongside protein size standards.

2.3 Worm Collection

Worms were grown on seeded **r**ich **NGM** (rNGM) plates until most were adults and then washed into a 15 mL centrifuge tube using M9 buffer. To clean the bacteria off the worms, they were pelleted in a clinical centrifuge at 2250 rpm and transferred to a 1.5 mL Eppendorf tube. We continued washing the worms with M9 and pelleted them at 2250 rpm for 1 minute until the supernatant was clear of bacteria. This step also helped wash bacteria out of the guts of the worms. At this point, if the worms were to be harvested for eggs, we proceeded with an egg preparation protocol (see next section). Otherwise, the volume of worms was measured after chilling the tube on ice to pack their bodies. All supernatant was removed from the tube before it was flash frozen with liquid nitrogen and stored at -80°C.

2.3.1 Synchronizing Worms

Using worms that are the same age is convenient for quantitative studies because it reduces variability in small RNA concentrations. This can be simulated by synchronizing young worms to the same stage of development by hatching them in the absence of food. *C. elegans* has a developmental feature which halts larval development at the L1 stage until they are fed.

To collect eggs, cleaned mixed-stage worms in 0.5 mL of M9 were mixed with 0.5 mL of 2 N NaOH/bleach. The latter reacts with worm bodies, dissolving everything except the worm eggs. The tube was vortexed until the hermaphrodite bodies began to break open. Promptly, the reaction was terminated by diluting into 12 mL of M9 in a 15 mL tube. The eggs were pelleted and transferred to a fresh 1.5 mL Eppendorf tube. The bleach was removed by repeatedly pelleting the worms at 12,000 rpm for 1 minute and washing with M9 until the smell of bleach was gone. The eggs were transferred to a 6 cm Petri dish containing 6 mL of M9 and shaken at 60 rpm until

the larvae were hatched. The larvae were pelleted in 15 mL centrifuge tubes at 4000 rpm for 1 minute and grown on rNGM plates. The moment the young adults began to lay eggs, the worms were stored as described in the previous section.

We used synchronized worms to determine the mirVana RNA purification kit was unnecessary to extract RNAs (results in Section 3.2). Due to difficulties with egg preparations, we decided to abandon the synchronization step and instead use mixed stage worms for the relative quantitation experiments.

2.4 Quantifying Small RNA Concentrations in *C. elegans*

2.4.1 Isolation of Small RNA from *C. elegans*

To isolate RNAs from worms, we used the TRIzol reagent (Invitrogen) as per the manufacturer's directions (see Appendix C.1). This is a technique that homogenizes tissues and cells and yields RNA, DNA, and protein fractions from the tissues. At this point, the RNAs were purified using either a mirVana Isolation Kit (Ambion) or a standard ethanol precipitation, detailed below.

The RNA fraction was concentrated using a series of ethanol precipitations as described previously[83] (see Appendix C.2 for procedure). In an aqueous environment, the negatively charged RNA phosphate backbone is stably solvated. Adding a high concentration of ethanol disrupts these intermolecular forces, permitting the phosphates to form ionic bonds with positive ions in solution. This disruption of this solvent shell causes RNA to precipitate.

Finally, the RNA was quantified and tested for purity using **u**ltra**v**iolet/**vis**ible (**UV/Vis**) light spectroscopy (see Appendix C.3 for procedure and example calculation). The UV/Vis spectrometer shines a beam of light of a specific wavelength at

the solution, and a detector measures the amount of light absorbed by the sample due to electronic transitions. A plot of absorbance versus wavelength is produced. RNA, DNA, and proteins have characteristic absorbance signatures, and the amplitude of the absorption peaks can be used to measure their concentration in solution.

2.4.2 Relative Quantitation Using RT-qPCR

Gel staining of PCR products is not quantitative because the amount of PCR product produced at the end of a reaction depends on the concentration of dNTPs in the solution and not on the concentration of the template. To accurately quantify concentration of small RNAs in *C. elegans*, we used **R**eal **T**ime **Q**uantitative **PCR** (**RT-qPCR**), a highly sensitive PCR technique[84] that can be scaled up efficiently[85,86]. The RT-qPCR instrument monitors the production of PCR product by measuring DNA dye fluorescence at every cycle of the reaction, so measurements can be taken during a phase where PCR kinetics are reproducible[87,88].

However, RT-qPCR employs polymerases and dyes that bind to DNA exclusively, so in order to quantify RNA using this method we must first make a **c**omplimentary **DNA** (**cDNA**) copy of the small RNA of interest. We generated a single cDNA copy for each copy of RNA using a viral reverse transcriptase, Superscript III, in a single long elongation. Using a single cycle prevents the primers from re-annealing to previously synthesized small RNAs, and makes certain each small RNA has an opportunity to be copied. This intermediate step has the added benefit of reducing a complex mixture of potential RNA templates to a single cDNA product, reducing the probability of off-site amplifications in the qPCR experiments. Additionally, DNA is more stable than RNA.

One limitation of the PCR reaction is its difficulty transcribing small RNAs. This is because the primers are nearly the same size as the small RNAs. To overcome this limitation, we used stem-loop primers (see Figure 2.3) to increase the length of small

RNAs as previously[84] described (detailed in Appendix D.1).

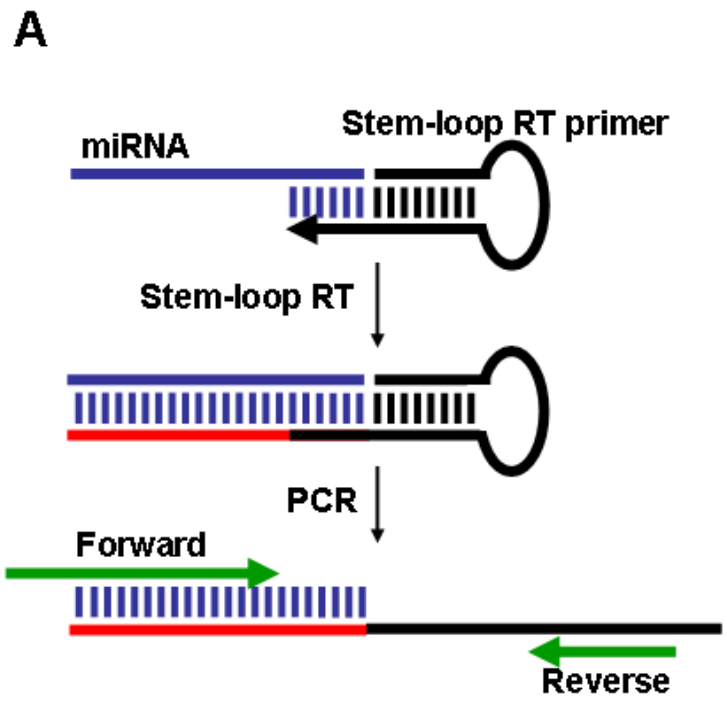

Figure 2.3: Schematic for Stem-loop Primer PCR Procedure - The stem-loop primer binds RNA, and cDNA (shown in red) is polymerized by Superscript III. The elongated DNA becomes is amplified and quantified using RT-qPCR. Picture taken from Varkonyi-Gasic *et al*[84].

Our reaction mixture was comprised of 1 μL 250 ng/μL appropriate primer (a full list of stem loop primers we used is in Table D.2), 1 μL 10 mM dNTPs, 50 ng total RNA, brought to a volume of 13 μL using nanopure water. We heated this mixture to 65°C for 5 minutes followed by a 1 minute incubation on ice, analogous to steps 1 and 2 in Figure 2.1. The contents were spun down at 13,000 rpm for 15 seconds. Then, 4 μL 5X 1st strand buffer, 1 μL 0.1M dithiothreitol (DTT), 1 μL RNAse Out, and 1 μL 200U SuperScriptIII (Invitrogen) were mixed into the tube. Ribonuclases (RNases) are pervasive and resilient proteins that we combat using RNAse Out, an RNase inhibitor, and DTT, which destabilizes RNAses[89]. The reverse transcription was run using the following parameters: 5 minutes at 25°C, an hour at 50°C, and

finally 15 minutes at 70°C. The 25°C stage is to ensure primer annealing before the 50°C elongation phase. The 70°C stage denatures reverse transcription proteins after they are not needed.

Finally, we quantified the cDNA concentrations of the reverse transcription product using RT-qPCR. We used Evagreen, an intercalating DNA dye suited for RT-qPCR[90,91] to detect cDNAs. Evagreen strongly fluoresces when bound to dsDNA, negligibly binds to ssDNA and does not bind to RNA. It uses a unique "release on demand" mechanism that does not inhibit PCR, and thus can be used at high concentrations to maximize fluorescence and detect scarce products. The emission intensity of Evagreen is directly proportional to the amount of cDNA in the reaction well. Plotting the total fluorescence as a function of cycle number results in a series of logarithmic curves corresponding to the concentration of DNA in each well throughout the experiment (Figure 2.4). At first, the DNA concentration in each sample is too low to be detected with Evagreen fluorescence. However, at a certain threshold fluorescence the DNA can be detectable. The cycle number at which the DNA passes this threshold is called the C_t value. The higher the starting cDNA concentration the earlier it can be detected by qPCR (and the lower the C_t value is).

The cDNA were diluted 5-fold with nanopure water and mixed with the qPCR reagents on ice (see Table 2.4 for final reaction conditions). The reaction mixture was loaded into a 96-well plate, 50 μL per well, and cycled in a Applied Biosystems 7500 Real Time PCR instrument. All reactions were run in quadruplicate.

To measure the relative abundance of the small RNAs, RT-qPCR was run using a relative quantitation assay. The samples were normalized to an endogenous control siRNA and analysed using the Applied Biosystems software.

RT-qPCR primers must be specific to the target DNA sequence and must not form primer dimers, both of which can amplify spurious sequences and thus increase Evagreen fluorescence. To determine specificity, we did DNA melting curve analysis

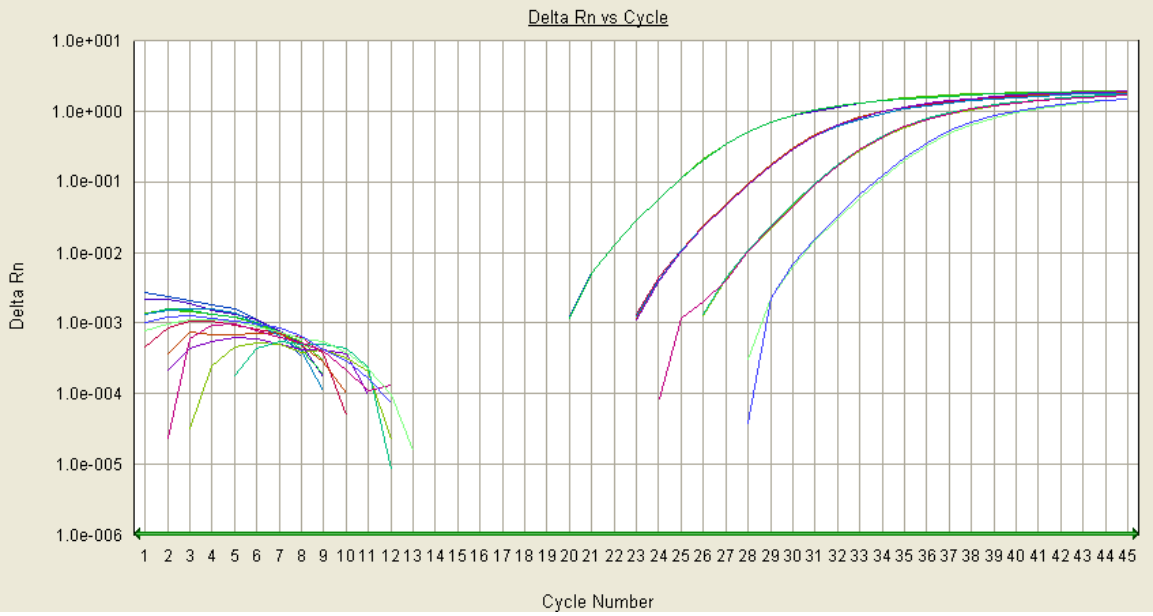

Figure 2.4: A Sample Amplification Plot for a Standard Curve Experiment - Plot of log (total Evagreen fluorescence) vs. cycle number for a 10-fold dilution series of cDNA. The reactions with higher starting concentrations amplify earlier (have lower C_t values) than the dilutions.

Stock	Final Concentration
10X Qiagen Buffer	1X
1 mM dNTP	200 μM
25 mM $MgCl_2$	1 mM
20X EvaGreen	1X
50X ROX	0.5X
5U/μL Qiagen Taq Polymerase	1.25 U/reaction
cDNA Template	2.5 ng/reaction
10 μM Primers	500 mM

Table 2.4: RT-PCR Reaction Conditions - List of reagents used in each well. For primer information, see Table D.3

immediately following RT-qPCR experiments, a method that is quicker and more informative than gel electrophoresis[92]. This method involves ramping the temperature of the qPCR plate gradually until all the DNA in the wells are melted. The instrument plots Evagreen fluorescence as a function of temperature*. Each DNA has a unique dissociation curve, whose shape and position is dependent on the AT:GC ratio, length, and primary structure of the DNA. A specific primer set will amplify a single DNA sequence, and so we would expect a single dissociation peak for a single amplification product. In contrast, non-specific primers will produce more than one product, and thus we expect various peaks for the different amplicons. To rule out the possibility that the fluorescence is an artifact of primer dimers or DNA contamination, we did control RT-qPCR experiments using RNA template instead of cDNA template.

2.5 Small RNAs Tested

We picked representative small RNAs from the 26G siRNA and 21U piRNA pathways to test if *rha-1* is involved in their respective pathways (see Figure 2.5). We also tested miRNAs and a snRNA genes as candidates for our internal reference genes, since they do not interact with *eri-1* or *rha-1*.

Additionally, we are testing expression of siRNAs in worms grown at both 16°C and 20°C to check if there is a difference between the two temperatures. The physiologically relevant temperature for *C. elegans* is 20°C. The sterility defects for our mutants occur between $23 - 25$°C, but the changes in fertility begin to occur at 20°C (K. Walstrom, personal communication).

*Recall, Evagreen fluoresces only when bound to dsDNA, and thus loss of fluorescence is an indicator of DNA strand separation.

RNA Class	RNA Name	RNA Sequence
miRNA	*mir-66*	CAU GAC ACU GAU UAG GGA UGU GA
	mir-77	UUC AUC AGG CCA UAG CUG UCC A
snRNA	*Y55F3BR.9 (sn2342)*	UCG GCU GUG AUG AUU UCC UAU UGC CGU UUA CCC GUC UGA GGA AAA CCG UGC UUG AUA CAA CUU GGA AAA GGC UGA GCC G
21U piRNA	*21UR-3442*	UAC UAG AGU GUU GAG AUU GUG
X-cluster	*X1051*	GUU ACU AGU ACG CUU UUA UGCC
Endo-siRNA	*K11D9.1*	GAU CUG GAA UAU GGC GUG AGA

Table 2.5: Small RNAs Tested - Name and sequence of the small RNAs used to test RNAi pathways *rha-1* might be involved in.

2.6 Determining Primer Efficiency

Assuming 100% primer efficiency, our cDNA is doubled in concentration every PCR cycle. In practice, RT-qPCR primers do not have the same performances due to different physical properties of the primers. For an accurate measurement of relative concentrations, it is essential to take primer efficiency into account [93].

To determine primer efficiency, we created a dilution series of cDNA (all other variables constant) and performed qPCR with absolute quantitation. These were our standard curve amplifications. The diluted cDNA reactions take more cycles to pass the detector threshold because they have less cDNA template to begin with. Since qPCR amplifies exponentially, plotting C_t vs. $\ln[cDNA]$ for each cDNA concentration results in a line. Fitting a line to the data using a linear regression and using Equation 2.1, we can solve for the primer efficiency.

$$E = 10^{\frac{-1}{\text{slope}}} \tag{2.1}$$

where E is primer efficiency and slope is $\frac{C_t}{\ln[cDNA]}$. Thus, slope of -3.32 corresponds to 100% primer efficiency; lower slopes indicate an efficiency of less than 100% and steeper slopes correspond to efficiencies higher than 100%. See Appendix D.2.1 for a sample calculation.

2.7 Relative Expression Data Analysis

We used the Pfaffl equation to calculate the relative expression of our genes.

$$R = \frac{E_{tar}^{\Delta C_t}\ (\text{target})}{E_{ref}^{\Delta C_t}\ (\text{reference})} \tag{2.2}$$

where R is the relative expression ratio, E_{ref} and E_{tar} are the efficiencies of the reference and target primers, and ΔC_t is the difference in C_t between the reference

and target strains.

Each measurement had some amount of error, which we reported with the data. Every quantification was repeated four times, giving us a standard deviation for C_t values. The root mean square error for the slope of our standard curve linear regressions were approximated with the equation

$$E_{\text{slope}} = \sqrt{1 - r^2} \times SD_y \tag{2.3}$$

where E_{slope} is the error of the slope, r^2 is the error of the linear regression equation, and SD_y is the standard deviation of all the y values in the dilution series (in this case, the C_t values were plotted on the y axis). The uncertainty for the relative quantitation function was determined by propagating the uncertainty of each variable through every mathematical operation.

Chapter 3

Results

"Results! Why, man, I have gotten a lot of results.
I know several thousand things that won't work."
-Thomas Edison

"There are three kinds of lies: lies, damned lies, and statistics."
-Sir Charles Wentworth Dilke

"A philosopher once said 'It is necessary for the very existence of science that the same conditions always produce the same results.' Well they don't!"
-Richard Feynman in *The Character of Physical Law*

3.1 Worm Genotype Integrity

Before beginning the small RNA quantification experiments, we made some quality control checks with our worm stocks. We verified our worm stocks were expressing the correct (mutant) alleles. We performed single worm PCR on the alleles and visualized the PCR products with DNA size standards on an agarose gel electrophoresis (see Appendix 2.2). All the worm genotypes were successfully verified (data not shown).

3.2 Determining Optimal Small RNA Extraction

We had the option of purifying small RNAs using a standard ethanol precipitation or the mirVana RNA Isolation Kit (Ambion). Both methods exclusively purify RNAs

from complex mixtures, but the ethanol precipitation is inexpensive.

We tested both methods to determine whether the ethanol precipitation would be sufficient for our experiments. We used synchronized wild-type worms grown at 16°C as an RNA source. Both methods gave satisfactory yields of total RNA (see Figures C.2 and C.3). We generated cDNA of our target genes using this RNA and confirmed using qPCR that both extraction methods obtained similar amplifications. Additionally, a melting curve and no template control analysis showed both methods were capable of specific RT-qPCR amplification. Thus, we used ethanol precipitation for RNA purification in all experiments.

3.3 Primer Specificity

We conducted a DNA melting curve experiment immediately following every RT-qPCR run (representative spectra taken from the 16°C N2 experiments are shown in Figures 3.1 – 3.6). Each DNA melting curve experiment was done in 16 individual reactions (in all four strains with four technical replicates each). The analysis of these experiments confirmed our primers specifically amplified a single product. The exception was the primer for *K11D9.1*, which consistently had substantial non-specific amplification in the melting curves (see Figure D.4). This could be due to primer-dimer artifacts. Note that the y-axis in Figures 3.1 – 3.6 should be the negative first derivative of DNA fluorescence.

3.4 Primer Efficiency

Based on our standard curve calculations (results in Table 3.1), most of our primers were of satisfactory quality. All the primers were at least 96% efficient. However, some primers replicated their targets with over 100% efficiency. These artificially high efficiencies are an artifact of Evagreen fluorescence of non-specific product amplification.

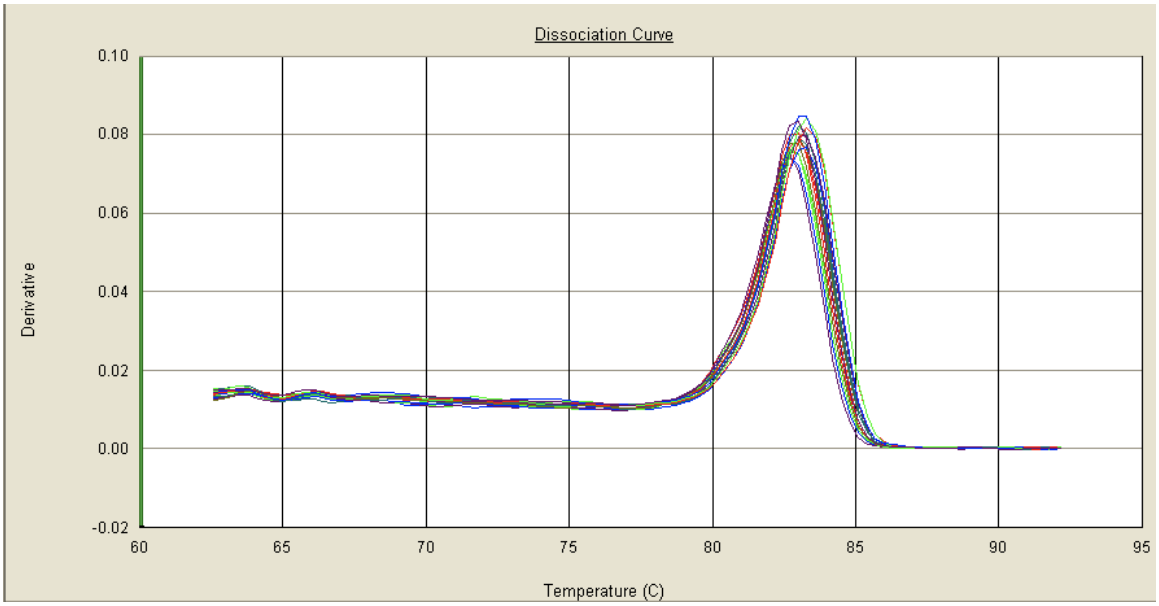

Figure 3.1: Dissociation Curve for *mir-66* 16°C N2 Relative Quantifications - Derivative of fluorescence versus temperature. The derivative elevates when the DNA strands are melted apart. The overlapping curves at a single peak indicates a single product is being amplified.

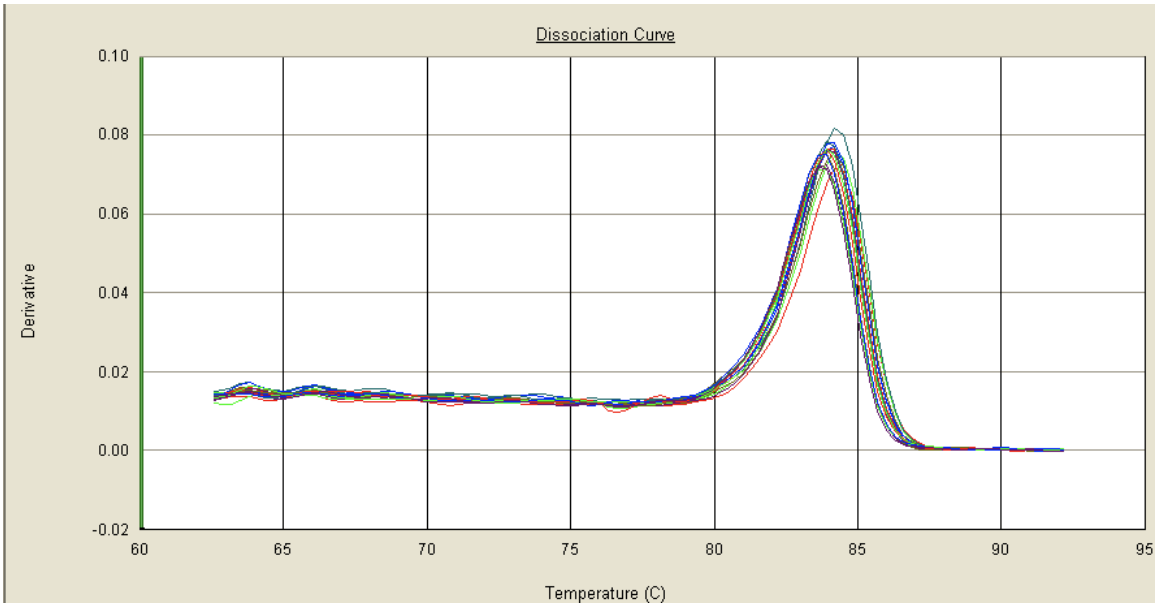

Figure 3.2: Dissociation Curve for *mir-77* 16°C N2 Relative Quantifications - Derivative of fluorescence versus temperature. The derivative elevates when the DNA strands are melted apart. The overlapping curves at a single peak indicates a single product is being amplified.

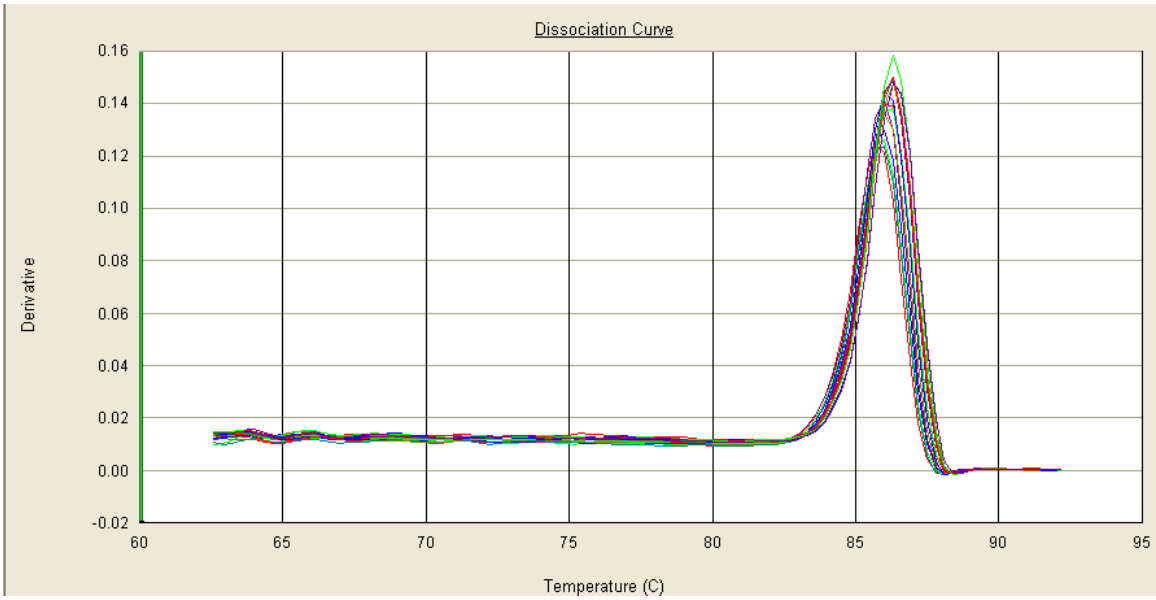

Figure 3.3: Dissociation Curve for *Y55F3BR (sn2342)* 16°C N2 Relative Quantifications - Derivative of fluorescence versus temperature. The derivative elevates when the DNA strands are melted apart. The overlapping curves at a single peak indicates a single product is being amplified.

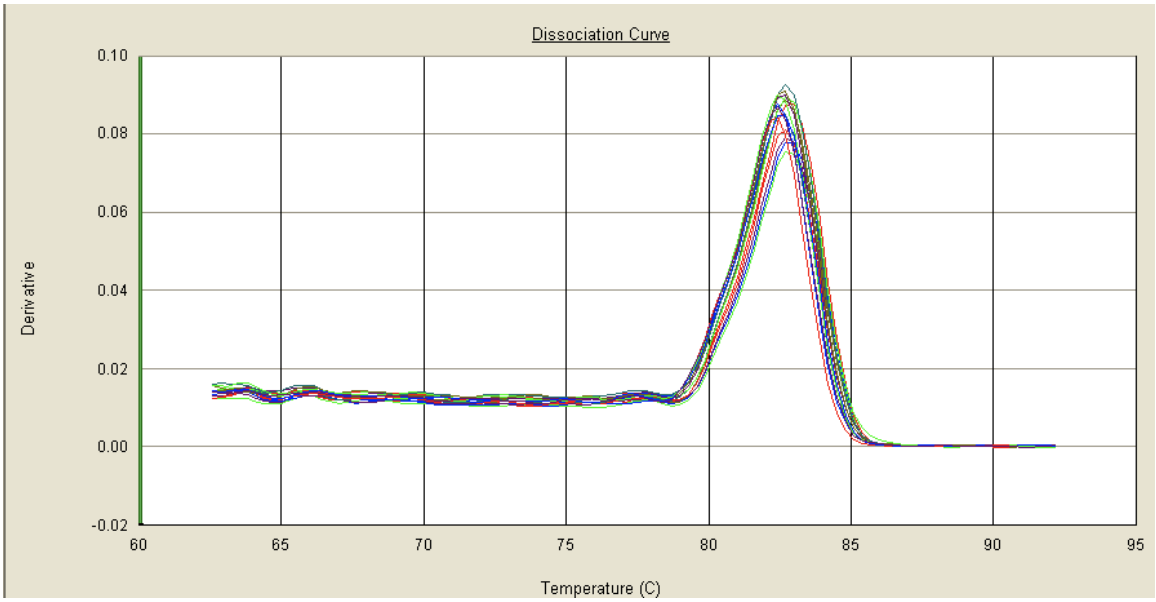

Figure 3.4: Dissociation Curve for *21UR-3442* 16°C N2 Relative Quantifications - Derivative of fluorescence versus temperature. The derivative elevates when the DNA strands are melted apart. The overlapping curves at a single peak indicates a single product is being amplified.

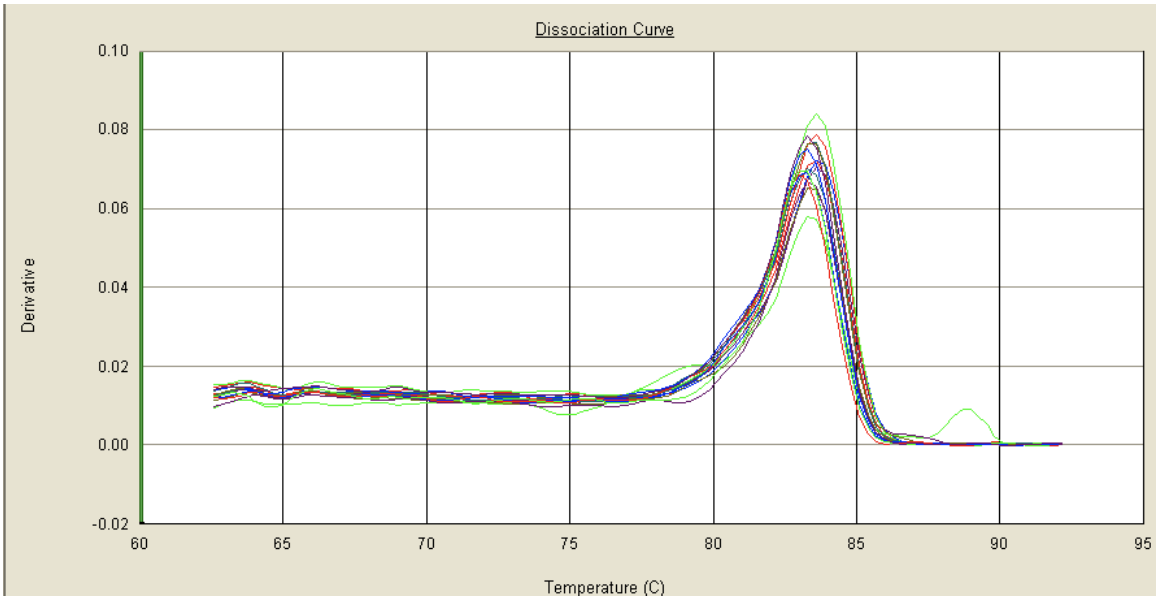

Figure 3.5: Dissociation Curve for *X1051* 16°C N2 Relative Quantifications - Derivative of fluorescence versus temperature. The derivative elevates when the DNA strands are melted apart. The overlapping curves at a single peak indicates a single product is being amplified.

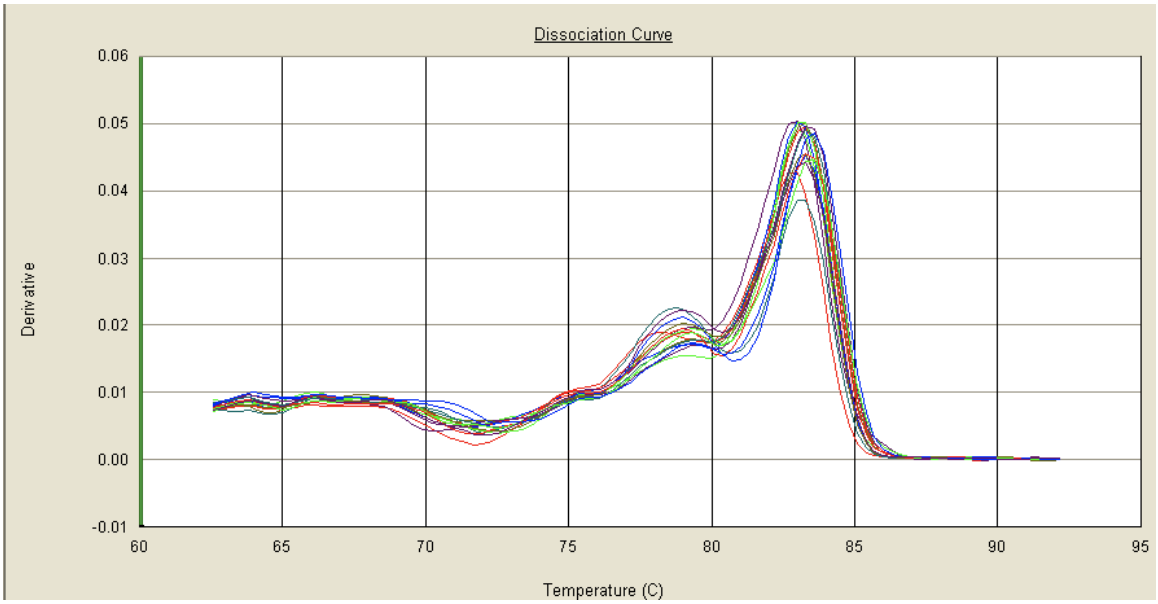

Figure 3.6: Dissociation Curve for *K11D9.1* 16°C N2 Relative Quantifications - Derivative of fluorescence versus temperature. The derivative elevates when the DNA strands are melted apart. The overlapping curves with two peaks indicate the primer is amplifying two products or that primer-dimers are forming and amplifying.

High efficiencies also occur if the reaction is contaminated with RNases or qPCR inhibitors.

RNA Name	RT-qPCR Primer Name	Primer Efficiency
mir-66	mir66for08	114.9%
mir-77	mir77for	96.1%
Y55F3BR.9 (sn2342)	Y55F3BR.9for08	96.1%
21UR-3442	21UR-3442for08	128.0%
X1051	X1051for08	147%
K11D9.1	K11D9_1efor08	1744%

Table 3.1: RT-qPCR Primer Efficiencies - Primer efficiencies of RT-qPCR primers. With the exception of K11D9_1efor08, the primers have reasonable efficiencies.

3.5 Relative RT-qPCR Results

The relative expression of all genes were tested in N2, *eri-1*, *rha-1*, and *rha-1;eri-1* worms grown at 16°C and 20°C. At first, we collected expression data using an absolute quantification assay. However, before completing the data set, we switched from using absolute to relative quantitation assays. Thus, we have two distinct data sets taken several months apart using the same cDNA. Unfortunately, the first data set had gaps which rendered most of it un-analysable. We were able to salvage some of this data by using a partial analysis. The two data sets were qualitatively analysed for trends.

In all experiments, the worms with the higher relative expression also had larger error bars. This is because increasing the ΔC_t parameter in Equation 2.2 increases the error of the entire function, even if the ΔC_t calculation itself does not have a large error.

To compensate for any differences in the amount of starting material, the must first be normalized. We did this by dividing a common variable to eliminate its effect on those data. This brings the sets into a common scale which can be meaningfully

compared. Our strategy to normalize our data was to use the same amount of template in each reaction and to find a reference gene which had constant expression in all our strains. To find a small RNA that could be used for normalization, we tested small RNAs that work in pathways unaffiliated with *eri-1* and *rha-1*. However, different RNAi pathways interact with each other, which complicates the search for a reference gene for endogenous RNAi.

We measured the expression of *mir-66*, *mir-77*, *Y55BR.9*, and *21UR-3442* in all genotypes at both temperatures. Of these, *21UR-3442* exhibited the most consistent C_t values across all mutants and temperatures (data shown in Table 3.2). Thus, we used *21UR-3442* as our reference gene to normalize our data. We compared the expression in each mutant strain to the expression levels in the wild-type N2 strain.

Unfortunately, the *21UR-3442* data had high deviation, which propagated through the rest of my calculations. Taking the partial derivative of the Pfaffl equation with respect to each term revealed that the *21UR-3442* ΔC_t term contributed the most error to the relative expression calculation. The 16°C experiments in the first data set and 20°C experiments from the second data set had especially large error, which is why those graphs have large error bars.

Data Set	N2	*eri-1*	*rha-1*	*rha-1;eri-1*
First 16°C	27.7 ± 0.2	27.2 ± 0.05	28.4 ± 0.12	27.32 ± 0.22
First 20°C	N.D.	N.D.	N.D.	N.D.
Second 16°C	28.52 ± 0.06	27.41 ± 0.03	26.98 ± 0.01	27.449 ± 0.00
Second 20°C	27.70 ± 0.18	27.16 ± 0.16	28.40 ± 0.05	27.32 ± 0.12

Table 3.2: Expression of *21UR-3442* in Both Datasets - The *21UR-3442* gene had the most similar expression across the different mutants and conditions, so we chose it as our reference gene to normalize our data. N.D., not determined.

In the *mir-66* and *mir-77* experiments, all strains had similar C_t values at both temperatures (see Tables 3.3 and 3.4). There were fluctuations in expression in the second *mir-77* data set, which is inconsistent with the first data set. The 20°C data set is also incomplete. We need more data to determine if there is a significant change

of expression in these RNAs.

Data Set	N2	*eri-1*	*rha-1*	*rha-1;eri-1*
First 16°C	1.0 ± 0.23	0.97 ± 0.18	1.98 ± 0.49	1.64 ± 0.41
First 20°C	N.D.	N.D.	N.D.	N.D.
Second 16°C	1.0 ± 0.07	0.78 ± 0.12	1.28 ± 0.30	0.88 ± 0.13
Second 20°C	1.0 ± 0.21	0.97 ± 0.20	N.D.	0.91 ± 0.17

Table 3.3: Relative Expression Data for *mir-66* - Relative expression of *mir-66* normalized using *21UR-3442* as a reference. In the first dataset, the overall expression of *mir-66* is almost flat in all conditions. In the second dataset, the two temperatures have similar expression and follow the same general trends as the first data set. In both datasets, the main contributing factor to the large error bars was the primer efficiency value, which had a large error. N.D., not determined.

Data Set	N2	*eri-1*	*rha-1*	*rha-1;eri-1*
First 16°C	1.0 ± 0.24	N.D.	0.87 ± 0.22	0.97 ± 0.24
First 20°C	N.D.	N.D.	N.D.	N.D.
Second 16°C	1.0 ± 0.07	0.52 ± 0.08	0.78 ± 0.27	0.33 ± 0.05
Second 20°C	1.0 ± 0.21	0.64 ± 0.13	N.D.	N.D.

Table 3.4: Relative Expression Data for *mir-77* - Relative expression of *mir-77* expression normalized using *21UR-3442* as a reference. In the first dataset, the expression was flat in both mutants. In the second dataset, there appears to be a larger change in the expression here than in the other miRNA results, but this experiment would have to be repeated to determine if the changes in expression are reproducible and significant. In both datasets, the main contributing factor to the large error bars was the primer efficiency calculation, which had one of the highest deviations. N.D., not determined.

In the *Y55F3BR.9* experiments, the *rha-1;eri-1*, *rha-1*, and *eri-1* mutants had progressively higher abundance at 16°C (see Table 3.5). These results were very consistent between both data sets. These results were unexpected, since snRNAs are not directly involved in endogenous RNAi. However, the 20°C experiments had flat expression in all mutants. We speculate the cause for snRNAs over-expression in these mutants is these mutants have so much extra RNA that needs to be spliced and processed.

In the *X1051* experiments, *eri-1* knockouts clearly lose siRNA expression (see

Data Set	N2	*eri-1*	*rha-1*	*rha-1;eri-1*
First 16°C	1.0 ± 0.23	6.21 ± 1.08	4.99 ± 1.73	1.40 ± 0.86
First 20°C	N.D.	N.D.	N.D.	N.D.
Second 16°C	1.0 ± 0.07	4.08 ± 1.18	2.97 ± 0.93	1.77 ± 0.36
Second 20°C	1.0 ± 0.22	1.29 ± 0.29	N.D.	0.52 ± 0.10

Table 3.5: Relative Expression Data for *Y55F3BR.9* - Relative expression of *Y55F3BR.9* in the both datasets normalized using *21UR-3442* as a reference. In the second dataset, The 16°C data follow the trends in relative expression with first data set. However, the 20°C worms seem to have flat expression. The 16°C *eri-1* worms had enormous variability in the technical replicates, giving it a very high error bar. In both datasets, the largest contributing factor to error was the C_t values due to poor technical replicates. N.D., not determined.

Table 3.6). There seems to be a slight enrichment in *rha-1* worms, but this result might not be significant due to large error in the *rha-1* data.

Data Set	N2	*eri-1*	*rha-1*	*rha-1;eri-1*
First 16°C	1.0 ± 0.27	N.D.	N.D.	0.00 ± 0.00
First 20°C	N.D.	N.D.	N.D.	N.D.
Second 16°C	1.0 ± 0.07	0.00 ± 0.00	1.44 ± 0.88	0.01 ± 0.16
Second 20°C	1.0 ± 0.21	0.00 ± 0.00	N.D.	0.00 ± 0.00

Table 3.6: Relative Expression Data for *X1051* - Relative expression of *X1051* in both datasets normalized using *21UR-3442* as a reference. In the first dataset, there was a loss of expression in the double-mutant. The main contributor to error in this data set was the primer efficiency value and the C_t value (due to bad technical replicates). In the second dataset, strains with defective *eri-1* had nearly no expression, in agreement with the trends in the first data set. The *rha-1* worms had low error values, but the combination of its large ΔC_t and high error in the efficiency value amplified the error component exponentially. The main contributing factor to the large error bars was the primer efficiency calculation, which had the highest deviation of the primers. N.D., not determined.

Chapter 4

Discussion

"The researches of many commentators have already thrown much darkness on this subject, and it is probable that, if they continue, we shall soon know nothing at all about it."

-Mark Twain

"Your theory is crazy...but it's not crazy enough to be true."

-Niels Bohr

4.1 Preflight Checks

The results of the single worm PCR affirmed that our worms were the expected genotype. The wild-type PCR product in the *rha-1* is 377 base-pairs long while the mutant PCR product (using different primers) is 527 base-pairs long due to the deletion mutation. Similarly, wildtype *eri-1* is 156 base-pairs long while the mutant is 179 base-pairs long due to the 23 base-pair insertion mutation. The gel analysis showed the bands were all the corrected sizes (data not shown).

The qPCR of RNAs extracted via ethanol precipitation and mirVana RNA purification kit showed that the ethanol precipitation had slightly lower C_t values, indicating it not only worked for small RNAs but also had some advantage over the mirVana kit (data not shown). This experiment also confirmed that our primers worked. The DNA melting curves for all primers (with the exception of the primer for *K11D9.1*) had a single peak indicating the primers were specific (see Section D.2).

The no template control and RNA template control reaction amplified late and had no PCR product. Thus, we concluded the ethanol precipitation was sufficient for our experiments and that treatment with DNases was not required.

4.2 Choosing a Reference Gene

We tested two miRNAs, *mir-66* and *mir-77*; a snRNA, *Y55F3BR.9*; and a member of the 21U RNA family, *21UR-3442* as potential reference genes.

Y55F3BR.9 was enriched in all mutants, with *rha-1;eri-1*, *rha-1*, and *eri-1* mutants having progressively higher expression. These result were unexpected, since snRNAs are not regulated by *eri-1* or *rha-1*. These results ruled out *Y55F3BR.9* as a potential reference gene, and suggest that the overexpression of genes in the mutants may require more snRNAs to process the excess mRNAs.

Both *mir-66* and *mir-77* had too much variability between the two strains. Interestingly, the relative expression profiles are the same for both genes: *rha-1* mutants have higher expression of miRNAs than *eri-1* mutants, and the double mutant rescues this phenotype. We don't know if the change in miRNA expression is significant or if it is a result of a general disruption in RNA metabolism.

The piRNA *21UR-3442* had similar expression in all strains. This ruled out any involvement of *rha-1* in the 21U piRNA pathway. It also provided us a reference gene to compare all other genes, although this was not ideal because expression was not completely flat across all mutants. Additionally, the root mean square error for the linear regression of *21UR-3442* primer efficiency was very high. This error propagated through all my other data during the relative expression calculation (see Equation 2.2). To make matters worse, the Pfaffl equation has exponential operations, which means the error increases exponentially as well.

4.3 RHA-1 and ERI-1 Might Work in a Common Pathway

My results are very preliminary and thus I cannot make strong inferences from them. The data is not statistically significant, has large error values, the relative expression calculations depend on a gene that is not ideal, and there are important gaps missing in the dataset (reviewed in Section 4.4). With this in mind, the following is an interpretation of the preliminary data.

The first data set has lower absolute error than the second data set for reasons I detail in the upcoming sections. Thus, the first data set has higher confidence overall.

The 20°C *rha-1* mutants had very low expression in all genes, an indication the experiments did not work. The data had standard deviations that were almost the same value as the measurements themselves. We revisited the UV/Vis spectra for this RNA extraction (see Figure C.12) and found a strong absorbance at 230 nm, an indication that the sample was contaminated with chaotropic salts, which can inhibit PCR reactions. Additionally, the spectra had an improper baseline subtraction, which led us to believe the RNA was almost 3 times more concentrated than it actually was. The combination of PCR inhibitors and lowered RNA template in the 20°C *rha-1* reactions is more likely than not the reason all these experiments failed. In light of this, I omitted all 20°C *rha-1* data from my results and discussion.

All the 16°C *rha-1* experiments have very high error bars and thus have low confidence levels. The A_{260}/A_{230} calculation of the 16°C *rha-1* UV/Vis spectra shows a very high amount of contamination, which is likely the culprit for the low quality of these data (see Table C.1). In general, the spectra for this RNA preparation shows it was very low quality. We did eventually extract new RNA from biological replicates, but due to time constrains were unable to repeat these experiments with higher quality RNA.

All the data for *K11D9.1* was too poor to make inferences. The RNAs have a very low cellular abundance, which lowered the precision and accuracy of RT-qPCR below reliable levels. Furthermore, the DNA melting curves for the *K11D9.1* primer indicated it was amplifying a second product, possibly primer-dimers. This casts doubt on all the fluorescence and efficiency calculations using this primer. The primer is also not specific to the gene. It is possible this is because we are using old *K11D9.1* sequencing data and thus are attempting to amplify sequencing artifacts. We expect *K11D9.1* to be under-expressed in *eri-1* mutants due to lack of endogenous RNAi.

As expected, mutations to *eri-1* eliminated expression of the *X1051* endogenous RNAs[1]. The increase in *X1051* expression in the 16°C *rha-1* worms is likely an artifact of high standard deviation, but the experiment should be repeated to check if the result is significant.

These data show that *rha-1* mutants do not have lowered concentrations of small RNAs in 26G genes. This seems to indicate RHA-1 is not involved in creation of 26G RNAs. However, experiments conducted in the Walstrom lab show that all the mutants have increased levels of mRNA targets of the 26G pathway, indicating that both *rha-1* and *eri-1* are necessary for proper 26G RNAi (C. Ortiz, personal communication). It is possible RHA-1 is involved in the 26G pathway downstream of 26G siRNA biogenesis. This would explain why 26G siRNA concentrations were unaffected in my RHA-1 knockout mutants while at the same time the 26G RNAi pathway failed to negatively regulate mRNAs. Perhaps *C. elegans* RHA-1 helps load 26G siRNAs into argonaute (similar to the human RHA model, Figure 1.3).

[1]Recall, ERI-1 functions in the 26G pathway, and worms expressing a null *eri-1* gene lack endogenous RNAi.

4.4 Our Data Quality is Poor

We can not make strong inferences from my data because it was very low quality. My experimental design has problems (see Section 4.4.3), the data needs to be expanded to be statistically significant (reviewed in Section 4.4.4), and there are technical problems with my experiments. Furthermore, this preliminary data has very high percent error. However, the absolute error is not very high in most of my experiments.

4.4.1 Random Error

RT-qPCR has random variability due to operator error, degradation of reagents over time, and differences between reagent lots[94]. In one study[94], the same experiment repeated by the same operator had 2 to 5-fold differences in the calculated copy numbers. However, that study was conducted in the year 2002, and since then there have been great improvements in the quality and dependability of qPCR kits and reagents, which has helped make qPCR experiments consistent and reproducible.

4.4.2 Systematic Errors

Small volumes of dilute samples are more difficult to handle because the slightest evaporation will significantly affect the concentration. I minimized this problem by centrifuging all samples briefly before pipetting. At low concentrations, molecules sticking to the sides of the tube or diffusing into the tubes' polymer matrix of the plastic tube become a substantial amount of variability.

Almost all the RNA UV/Vis spectra contained some amount of contamination at A_{230} known PCR inhibitors absorb, which means my reactions possibly contain PCR inhibitors. This is partially benign because lower concentrations of RNA have higher relative A_{230}. However, all RNA used from *rha-1* worms had very high amounts of

contaminants.

My experiments are roughly split into two data sets collected before and after winter. The more recent data set has a clear deterioration in data quality. The first data set has very good precision, with low standard deviation in the technical replicates and rare outliers. In contrast, the second data set has poor precision, with C_t values spanning more than one unit. Additionally, the C_t values between the data sets are not in agreement. Random error alone could not account for this change since both data sets were obtained using the same cDNA and protocols.

There were several changes that occurred between the collection of the two data sets. Many key reagents were replaced, including the Evagreen, ROX, and dNTPs stocks. We switched from Qiagen Taq in Qiagen PCR buffer to Bulldog Taq using a generic qPCR buffer. Additionally, the second data set was collected months after the worms were collected. Despite storing all qPCR precursors at -80°C, degradation still occurs. There is a possibility of RNA degradation from RNases or spontaneous hydrolysis. This degradation profoundly affects qPCR results[95].

While these might change the overall reaction kinetics, it does not explain why the technical replicates had so much variability. The sterile pipette tips the lab purchased sometimes had dust on the tips. When loading the 96-well plate into the qPCR instrument, I spotted tiny red fibres in the wells. Even though they are sterile, the fibres have a likelihood of interfering with the amplification. The fibers can also absorb fluorescent dyes or autofluoresce. The wells that dust or fibres fell into probably became outliers.

This streak of bad data also affects the standard curve experiments used to determine primer efficiency. Usually these experiments have very low deviation because the dilution is straightforward. High deviations make the efficiency calculation have a very large standard error, which propagates through all the analysis. Part of the reason for the poor quality in these experiments was the extremely low abundance of

the primer targets. I made new reverse transcription reactions at much higher concentrations, in some cases 2 orders of magnitude more concentrated, yet the efficiency experiments remained poor.

4.4.3 Flaws with the Experimental Design

Our experiments are measuring the difference the *eri-1* mutation has on the RNA levels. However, ERI-1 is only present in the developing somatic gonads and in some neurons. This is problematic, because we measure RNA levels using entire worms.

Our experiments were conducted with worms that had a random age distrubution. Thus, one of our assumptions is that the small worm fraction of our mixed stage worm collections had a negligible contribution to the total RNA extracted. However the small worms do make at least a small contribution of RNA. Additionally, worms of different ages have different gene expression profiles over the course of their lifetime.

Our experiments normalize the data to references so that we can see the relative amounts. We also use the same amount of RNA template in all reverse transcription reactions. This assumes that all adults worms of different ages have the same total RNA concentration in their body. If this is not the case, we are measuring relative concentrations of the genes but we lose other information.

Finally, the Pfaffl equation assumes that the efficiency of the primers remain the same throughout all amplification cycles. However, primer efficiency is a function of several variables including the abundance of template, which changes during the reaction[96,97].

4.4.4 Lack of Statistical Significance

To get past all the points of variability above, qPCR experiments need to go through several quality control checks to assure the data is indeed reproducible. They accomplish this by using biological and technical replicates. Biological replicates are

when you perform the same experiments using worms from different collections. If there is a big difference between the results, it means the worms were either grown in different conditions that would make their metabolism change, or that there was some other problem with how the RNA was extracted from the worms. Technical replicates are when you take RNA from a single biological set, and run the experiment multiple times using identical reagents, parameters, and procedures at the same time. Variations within technical replicates signal some sort of technical error, such as improperly mixing or contaminating one of the wells with foreign RNA or a substance that interferes with the qPCR reaction kinetics or qPCR detector.

The **m**inimum **i**nformation for **p**ublication of RT-**q**PCR **e**xperiments (**MIQE**) provides guidelines for high quality RT-qPCR experiments[98]. These guidelines delineate the minimum amount of technical and biological replicates needed before results are considered trustworthy. I did not use enough biological and technical replicates to satisfy these criteria. Unfortunately, a month's worth of my synchronized worm collections were destroyed in a lab catastrophe, which limited the amount of replicates I could do. I did eventually collect several biological replicates but did not have time to repeat the experiments with them.

4.5 Future Directions

"Would you tell me, please, which way I ought to go from here?"
"That depends a good deal on where you want to get to," said the Cat.
"–so long as I get SOMEWHERE," Alice added as an explanation.
"Oh, you're sure to do that," said the Cat, "if you only walk long enough."
-Alices's Adventure in Wonderland by Lewis Carroll

My preliminary results show that RHA-1 is not involved in the 21U RNAi pathway, so we should not persue those experiments further. Accurate quantification of the

K11D9.1 siRNAs has eluded the lab, so I recommend we abandon this siRNA. We should select new targets present at high cellular abundance from recent 26G siRNA sequencing data. We need to verify my results in the *X1051* experiments to fortify my conclusions. If it is the case that *rha-1* is not involved in the 26G pathway, it might be involved in the 22G RNAi pathway.

If I were to repeat my experiments, there are several things I would change. Some of the experiments were not performed in ideal conditions or were not optimized. One of the easier things to improve would be the primer efficiency calculations. Standard deviation is easier to lower in this measurement, and these errors heavily contribute to the final relative error because of the exponential operation the efficiency data undergoes. This needs to be done using a very high concentration of RNA, because extremely diluted RNA solutions cannot be accurately quantified by the qPCR instrument.

The analysis needs to be improved. The incomplete data sets made forming conclusions very difficult. Further, the second data set had a large standard deviation, which is not ideal. My good results need to be checked with biological and technical replicates to increase confidence in the data by increasing the n number. In most cases, I already have biological replicates collected, I simply did not have enough time to test them.

We need better internal references for more ideal normalizations. This gene would ideally have an expression within 0.5 C_t value in all strains. My experiments show that miRNAs and snRNAs are not good candidates for reference genes, and 21U RNAs seem to be a good class to explore.

I would use synchronized worms instead of mixed stage worms for my RNA extractions. Using mixed stage worms means we are extracting RNA from cells of very different tissue types, at different stages of differentiation, from animals at different developmental cycles. This, we should use synchronized worms to eliminate unneces-

sary sources of error and to improve reproducibility.

I would improve the quality of my RNA by using it promptly after purification to avoid RNA degradation. Alternatively, I could store RNA samples using RNA Later®, a product which permits RNA to be stored for years without degradation. However, I would first have to verify it does not interfere with qPCR kinetics. I would wash my RNA samples more thoroughly and a perform a second ethanol precipitation to remove contaminations. If this did not work, it might be wise to revert to using the mirVana RNA purification kits.

Some of our reagents were old and could have possibly become contaminated during their use by many different lab members. Additionally, it would be ideal to keep using the same reagents through the entire project and maybe even the same lot numbers.

Finally, there are more modern technologies available for qPCR, including instruments with better sensitivity and instruments that use capillaries to precisely mix the reactants and avoid contamination[95]. In the future, clean tips are paramount for RT-qPCR since it is such a sensitive technique. Special silicone tubes are marketed to prevent nucleic acids from sticking or leaching into the tubes, which I recommend for storing dilute RNA samples. There are digital motorized pipettes with many nozzles that make pipetting very quick, and minimize pipetting errors. Robots are also being employed to prepare the reaction mixes because they have extremely reproducible technique and are suited for repetitive tasks[94].

Bibliography

"The secret of creativity is knowing how to hide your sources."

-Albert Einstein

[1] Elgar G, Vavouri T. *Tuning in to the signals: noncoding sequence conservation in vertebrate genomes.* Trends in genetics : TIG 2008;24(7):344–52. doi:10.1016/j.tig.2008.04.005. 3

[2] Mercer T, Dinger M, Mattick J. *Long non-coding RNAs: insights into functions.* Nat Rev Genet 2009;10(3):155–159. 3

[3] Jinek, M; D, JA. *A three-dimensional view of the molecular machinery of RNA interference.* Nature 2009;457(7228):405–412. 3

[4] Fire A, Xu S, Montgomery M, *et al. Potent and specific genetic interference by double-stranded RNA in Caenorhabditis elegans.* Nature 1998;391(6669):806–811. 3

[5] Elbashir SM, Lendeckel W, Tuschl T. *RNA interference is mediated by 21- and 22-nucleotide RNAs.* Genes Dev 2001;15(2):188–200. 3, 8

[6] Costa FF. *Non-coding RNAs, epigenetics and complexity.* Gene 2008;410(1):9–17. doi:10.1016/j.gene.2007.12.008.

[7] Fischer SEJ. *Small RNA-mediated gene silencing pathways in C. elegans.* The international journal of biochemistry & cell biology 2010;42(8):1306–15. doi:10.1016/j.biocel.2010.03.006. 11, 14

[8] Moazed D. *Small RNAs in transcriptional gene silencing and genome defence.* Nature 2009;457(7228):413–20. doi:10.1038/nature07756. 3

[9] Chu CY, Rana TM. *Small RNAs: regulators and guardians of the genome.* J Cell Physiol 2007;213(2):412–9. doi:10.1002/jcp.21230. 3

[10] Gibney ER, Nolan CM. *Epigenetics and gene expression.* Heredity 2010;105(1):4–13. doi:10.1038/hdy.2010.54. 3

[11] Friedman RC, Farh KKH, Burge CB, *et al. Most mammalian mRNAs are conserved targets of microRNAs.* Genome Research 2008;19(1):92–105. 3

[12] Vastenhouw NL, Plasterk RHA. *RNAi protects the Caenorhabditis elegans germline against transposition.* Trends in genetics : TIG 2004;20(7):314–319. 3

[13] Haasnoot PCJ, Cupac D, Berkhout B. *Inhibition of virus replication by RNA interference.* J Biomed Sci 2003;10(6 Pt 1):607–616. doi:10.1159/000073526. 3

[14] Yigit E, Batista PJ, Bei Y, *et al. Analysis of the C. elegans Argonaute family reveals that distinct Argonautes act sequentially during RNAi.* Cell 2006; 127(4):747–57. doi:10.1016/j.cell.2006.09.033. 4, 11, 13

[15] Robb GB, Rana TM. *RNA helicase A interacts with RISC in human cells and functions in RISC loading.* Mol Cell 2007;26(4):523–37. doi:10.1016/j.molcel.2007.04.016. 6, 21

[16] Soejitno A, Wihandani D. *The therapeutic potential of RNA interference in controlling HIV-1 replication.* Acta medica ... 2009;. 5

[17] Bennasser Y, Yeung ML, Jeang KT. *RNAi therapy for HIV infection: principles and practicalities.* BioDrugs : clinical immunotherapeutics, biopharmaceuticals and gene therapy 2007;21(1):17–22. Review. 5

[18] Gondi CS, Rao JS. *Concepts in in vivo siRNA delivery for cancer therapy.* J Cell Physiol 2009;220(2):285–291. 5

[19] Castanotto D, Rossi JJ. *The promises and pitfalls of RNA-interference-based therapeutics.* Nature 2009;457(7228):426–433. 5

[20] Barik S. *Silence of the transcripts: RNA interference in medicine.* Journal of molecular medicine (Berlin, Germany) 2005;83(10):764–773. 5

[21] Kim VN, Han J, Siomi MC. *Biogenesis of small RNAs in animals.* Nat Rev Mol Cell Biol 2009;10(2):126–139. doi:doi:10.1038/nrm2632. 5, 7, 11

[22] Bernstein E, Caudy AA, Hammond SM, *et al. Role for a bidentate ribonuclease in the initiation step of RNA interference.* Nature 2001;409(6818):363–6. doi:10.1038/35053110. 5, 8

[23] Timmons L. *Endogenous inhibitors of RNA interference in Caenorhabditis elegans.* BioEssays : news and reviews in molecular, cellular and developmental biology 2004;26(7):715–8. doi:10.1002/bies.20078. 5, 8, 18, 19

[24] Qiu S, Adema CM, Lane T. *A computational study of off-target effects of RNA interference.* Nucleic Acids Res 2005;33(6):1834–47. doi:10.1093/nar/gki324. 8

[25] Macrae IJ, Zhou K, Li F, *et al. Structural basis for double-stranded RNA processing by Dicer.* Science (New York, NY) 2006;311(5758):195–198. 8, 10

[26] Liu Q, Paroo Z. *Biochemical principles of small RNA pathways.* Annu Rev Biochem 2010;79:295–319. doi:10.1146/annurev.biochem.052208.151733. 9, 10, 12, 13, 21

[27] Zhang S, Grosse F. *Multiple Functions of Nuclear DNA Helicase II (RNA Helicase A) in Nucleic Acid Metabolism.* Acta Biochim Biophys Sin 2004;36(3):177–183. doi:10.1093/abbs/36.3.177. 8

[28] Ye X, Paroo Z, Liu Q. *Functional anatomy of the Drosophila microRNA-generating enzyme.* J Biol Chem 2007;282(39):28373–28378. 8

[29] Batista PJ, Ruby JG, Claycomb JM, *et al. PRG-1 and 21U-RNAs interact to form the piRNA complex required for fertility in C. elegans.* Mol Cell 2008; 31(1):67–78. doi:10.1016/j.molcel.2008.06.002. 10, 14, 18

[30] Hammond SM, Bernstein E, Beach D, *et al. An RNA-directed nuclease mediates post-transcriptional gene silencing in Drosophila cells.* Nature 2000; 404(6775):293–296. 10

[31] Tabara H, Sarkissian M, Kelly WG, *et al. The rde-1 gene, RNA interference, and transposon silencing in C. elegans.* Cell 1999;99(2):123–132. 10

[32] Boisvert M, Simard M. *RNAi pathway in C. elegans: the argonautes and collaborators.* RNA interference 2008;21–36. doi:10.1007/978-3-540-75157-1_2. 10, 11, 14, 19

[33] Schwarz DS, Hutvagner G, Haley B, *et al. Evidence that siRNAs function as guides, not primers, in the Drosophila and human RNAi pathways.* Mol Cell 2002;10(3):537–548. 10

[34] Paroo Z, Liu Q, Wang X. *Biochemical mechanisms of the RNA-induced silencing complex.* Cell Res 2007;17(3):187–194. 10

[35] Tomari Y. *A Protein Sensor for siRNA Asymmetry.* Science (New York, NY) 2004;306(5700):1377–1380. 10

[36] Rand TA, Petersen S, Du F, *et al. Argonaute2 cleaves the anti-guide strand of siRNA during RISC activation.* Cell 2005;123(4):621–629. 10

[37] Liu J, Cao Z, Lu Y. *Functional nucleic acid sensors.* Chem Rev 2009; 109(5):1948–98. doi:10.1021/cr030183i. 10

[38] Elbashir SM, Martinez J, Patkaniowska A, *et al. Functional anatomy of siRNAs for mediating efficient RNAi in Drosophila melanogaster embryo lysate.* EMBO J 2001;20(23):6877–6888. 11

[39] Timmons L. *Ingestion of bacterially expressed dsRNAs can produce specific and potent genetic interference in Caenorhabditis elegans.* Gene 2001;263(1-2):103–112. doi:10.1016/S0378-1119(00)00579-5. 11, 18

[40] Conte D, Mello CC. *RNA interference in Caenorhabditis elegans.* Curr Protoc Mol Biol 2003;Chapter 26:Unit 26.3. 11

[41] Kennedy S, Wang D, Ruvkun G. *A conserved siRNA-degrading RNase negatively regulates RNA interference in C. elegans.* Nature 2004;427(6975):645–649. doi:10.1038/nature02320.1. 11, 18, 19

[42] Tabara H, Yigit E, Siomi H, *et al. The dsRNA binding protein RDE-4 interacts with RDE-1, DCR-1, and a DExH-box helicase to direct RNAi in C. elegans.* Cell 2002;109(7):861–871. 11

[43] Duchaine TF, Wohlschlegel Ja, Kennedy S, *et al. Functional proteomics reveals the biochemical niche of C. elegans DCR-1 in multiple small-RNA-mediated pathways.* Cell 2006;124(2):343–54. doi:10.1016/j.cell.2005.11.036. 11

[44] Maine EM. *An RNA-mediated silencing pathway utilizes the coordinated synthesis of two distinct populations of siRNA.* Mol Cell 2010;37(5):593–595. 14

[45] Pak J, Fire A. *Distinct populations of primary and secondary effectors during RNAi in C. elegans.* Science (New York, NY) 2007;315(5809):241–4. doi:10.1126/science.1132839. 14

[46] Gent JI, Lamm AT, Pavelec DM, *et al. Distinct phases of siRNA synthesis in an endogenous RNAi pathway in C. elegans soma.* Mol Cell 2010;37(5):679–689. 14

[47] Sijen T, Steiner FA, Thijssen KL, *et al. Secondary siRNAs result from unprimed RNA synthesis and form a distinct class.* Science (New York, NY) 2007; 315(5809):244–247. 14

[48] Gent JI, Schvarzstein M, Villeneuve AM, *et al. A Caenorhabditis elegans RNA-directed RNA polymerase in sperm development and endogenous RNA interference.* Genetics 2009;183(4):1297–1314. doi:10.1534/genetics.109.109686. 14

[49] Hutvagner G, Simard MJ. *Argonaute proteins: key players in RNA silencing.* Nat Rev Mol Cell Biol 2008;9(1):22–32. doi:10.1038/nrm2321. 15

[50] Han T, Manoharan AP, Harkins TT, *et al. 26G endo-siRNAs regulate spermatogenic and zygotic gene expression in Caenorhabditis elegans.* Proc Natl Acad Sci U S A 2009;106(44):18674–18679. 14, 17, 19

[51] Vasale JJ, Gu W, Thivierge C, *et al. Sequential rounds of RNA-dependent RNA transcription drive endogenous small-RNA biogenesis in the ERGO-1/Argonaute pathway.* Proc Natl Acad Sci U S A 2010;107(8):3582–3587. 16

[52] Wang G, Reinke V. *A C. elegans Piwi, PRG-1, regulates 21U-RNAs during spermatogenesis.* Current biology : CB 2008;18(12):861–7. doi:10.1016/j.cub.2008.05.009. 14, 18

[53] Ruby JG, Jan C, Player C, *et al. Large-scale sequencing reveals 21U-RNAs and additional microRNAs and endogenous siRNAs in C. elegans.* Cell 2006; 127(6):1193–207. doi:10.1016/j.cell.2006.10.040. 14, 18

[54] Kaufman EJ, Miska Ea. *The microRNAs of Caenorhabditis elegans.* Seminars in Cell & Developmental Biology 2010;21(7):728–737. 18

[55] Corrêa RL, Steiner FA, Berezikov E, *et al. MicroRNA-directed siRNA biogenesis in Caenorhabditis elegans.* PLoS Genet 2010;6(4):e1000903. doi:10.1371/journal.pgen.1000903.

[56] Bartel DP. *MicroRNAs: genomics, biogenesis, mechanism, and function.* Cell 2004;116:281–297. 18

[57] Lee RC, Ambros V. *An extensive class of small RNAs in Caenorhabditis elegans.* Science (New York, NY) 2001;294(5543):862–4. doi:10.1126/science.1065329. 18

[58] Lee Y, Ahn C, Han J, *et al. The nuclear RNase III Drosha initiates microRNA processing.* Nature 2003;425(6956):415–9. doi:10.1038/nature01957.

[59] Ambros V, Lee RC, Lavanway A, *et al. MicroRNAs and Other Tiny Endogenous RNAs in C. elegans.* Curr Biol 2003;13(10):807–818. doi:10.1016/S0960-9822(03)00287-2. 18, 23

[60] Simmer F, Tijsterman M, Parrish S, *et al. Loss of the putative RNA-directed RNA polymerase RRF-3 makes C. elegans hypersensitive to RNAi.* Current biology : CB 2002;12(15):1317–9. 18

[61] Roth BM, Pruss GJ, Vance VB. *Plant viral suppressors of RNA silencing.* Virus Res 2004;102(1):97–108. 18

[62] Gabel HW, Ruvkun G. *The exonuclease ERI-1 has a conserved dual role in 5.8S rRNA processing and RNAi.* Nature structural and molecular biology 2008;15(5):531–3. doi:10.1038/nsmb.1411. 18

[63] Pavelec DM, Lachowiec J, Duchaine TF, *et al. Requirement for the ERI/DICER complex in endogenous RNA interference and sperm development in Caenorhab-*

ditis elegans. Genetics 2009;183(4):1283–95. doi:10.1534/genetics.109.108134. 19

[64] Lee RC, Hammell CM, Ambros V. *Interacting endogenous and exogenous RNAi pathways in Caenorhabditis elegans.* RNA (New York, NY) 2006;12(4):589–97. doi:10.1261/rna.2231506. 19, 20

[65] He Y, Andersen GR, Nielsen KH. *Structural basis for the function of DEAH helicases.* EMBO Rep 2010;11(3):180–186. 19

[66] Ambrus AM, Frolov MV. *The diverse roles of RNA helicases in RNAi.* Cell Cycle 2009;8(21):3500–3505. 19, 21

[67] Eki T, Ishihara T, Katsura I, *et al. A genome-wide survey and systematic RNAi-based characterization of helicase-like genes in Caenorhabditis elegans.* DNA research : an international journal for rapid publication of reports on genes and genomes 2007;14(4):183–99. doi:10.1093/dnares/dsm016. 21

[68] Walstrom KM, Schmidt D, Bean CJ, *et al. RNA helicase A is important for germline transcriptional control, proliferation, and meiosis in C. elegans.* Mech Dev 2005;122(5):707–720. doi:10.1016/j.mod.2004.12.002. 21, 23

[69] Lee CG, Hurwitz J. *Human RNA helicase A is homologous to the maleless protein of Drosophila.* The Journal of biological chemistry 1993;268(22):16822–30. 21

[70] Hartman TR, Qian S, Bolinger C, *et al. RNA helicase A is necessary for translation of selected messenger RNAs.* Nature Structural and Mol Bio 2006;13(6):509–516. 21

[71] Fuller-Pace FV. *DExD/H box RNA helicases: multifunctional proteins with important roles in transcriptional regulation.* Nucleic Acids Res 2006;34(15):4206–4215. 21

[72] Buttner K, Nehring S, Hopfner KP. *Structural basis for DNA duplex separation by a superfamily-2 helicase.* Nature structural and molecular biology 2007; 14(7):647–652. 21

[73] Bolinger C, Yilmaz A, Hartman T, *et al. RNA helicase A interacts with divergent lymphotropic retroviruses and promotes translation of human T-cell leukemia virus type 1.* Nucleic Acids Res 2007;35(8):2629. 21

[74] Lawrence P, Rieder E. *Identification of RNA helicase A as a new host factor in the replication cycle of foot-and-mouth disease virus.* J Virol 2009;83(21):11356–11366. doi:10.1128/JVI.02677-08. 21

[75] DeVincenzo J, Lambkin-Williams R, Wilkinson T, *et al. A randomized, double-blind, placebo-controlled study of an RNAi-based therapy directed against respiratory syncytial virus.* Proc Natl Acad Sci U S A 2010;107(19):8800–8805. 21

[76] He QS, Tang H, Zhang J, *et al. Comparisons of RNAi approaches for validation of human RNA helicase A as an essential factor in hepatitis C virus replication.* J Virol Methods 2008;154(1-2):216–219. 21

[77] Bolinger C, Sharma A, Singh D, *et al. RNA helicase A modulates translation of HIV-1 and infectivity of progeny virions.* Nucleic Acids Res 2010;38(5):1686–96. doi:10.1093/nar/gkp1075. 21

[78] Roy B, Hu J, Guo X, *et al. Association of RNA helicase a with human immunodeficiency virus type 1 particles.* J Biol Chem 2006;281(18):12625. 21

[79] Schütz P, Wahlberg E, Karlberg T, *et al. Crystal structure of human RNA helicase A (DHX9): structural basis for unselective nucleotide base binding in a DEAD-box variant protein.* J Mol Biol 2010;400(4):768–82. doi:10.1016/j.jmb.2010.05.046. 21, 22

[80] Cordin O, Banroques J, Tanner NK, *et al. The DEAD-box protein family of RNA helicases.* Gene 2006;367:17–37. Undefined. 21

[81] Hilbert M, Karow AR, Klostermeier D. *The mechanism of ATP-dependent RNA unwinding by DEAD box proteins.* Biol Chem 2009;390(12):1237–1250. 22, 23

[82] Brenner S. *The genetics of Caenorhabditis elegans.* Genetics 1974;77(1):71–94. 22, 27

[83] Castoldi M, Benes V, Hentze MW, *et al. miChip: a microarray platform for expression profiling of microRNAs based on locked nucleic acid (LNA) oligonucleotide capture probes.* Methods (San Diego, Calif) 2007;43(2):146–152. 32

[84] Varkonyi-Gasic E, Wu R, Wood M, *et al. Protocol: a highly sensitive RT-PCR method for detection and quantification of microRNAs.* Plant methods 2007;3:12. doi:10.1186/1746-4811-3-12. 33, 34, 85

[85] Rutledge RG. *A Java Program for LRE-Based Real-Time qPCR that Enables Large-Scale Absolute Quantification.* PLoS ONE 2011;6(3):e17636. 33

[86] Bustin SA, Benes V, Nolan T, *et al. Quantitative real-time RT-PCR - a perspective.* J Mol Endocrinol 2005;34(3):597. 33

[87] Derveaux S, Vandesompele J, Hellemans J. *How to do successful gene expression analysis using real-time PCR.* Methods 2010;50(4):227–230. 33

[88] Cikos S, Koppel J. *Transformation of real-time PCR fluorescence data to target gene quantity.* Anal Biochem 2009;384(1):1–10. doi:10.1016/j.ab.2008.08.031. 33

[89] Chen Z, Ling J, Gallie DR. *RNase activity requires formation of disulfide bonds and is regulated by the redox state.* Plant Mol Biol 2004;55(1):83–96. 34

[90] Sang F, Ren J. *Capillary electrophoresis of double-stranded DNA fragments using a new fluorescence intercalating dye EvaGreen.* J Sep Sci 2006;29(9):1275–1280. 35

[91] Mao F, Leung WY, Xin X. *Characterization of EvaGreen and the implication of its physicochemical properties for qPCR applications.* BMC biotechnology 2007; 7:76. 35

[92] Ririe KM, Rasmussen RP, Wittwer CT. *Product Differentiation by Analysis of DNA Melting Curves during the Polymerase Chain Reaction.* Anal Biochem 1997;245(2):154–160. 37

[93] Ruijter JM, Ramakers C, Hoogaars WMH, *et al. Amplification efficiency: linking baseline and bias in the analysis of quantitative PCR data.* Nucleic Acids Res 2009;37(6):e45. 39

[94] Bustin SA. *Quantification of mRNA using real-time reverse transcription PCR (RT-PCR): trends and problems.* J Mol Endocrinol 2002;29(1):23. 54, 59

[95] FLEIGE S, PFAFFL M. *RNA integrity and the effect on the real-time qRT-PCR performance.* Molecular Aspects of Medicine 2006;27(2-3):126–139. 55, 59

[96] Rutledge RG, Stewart D. *Critical evaluation of methods used to determine amplification efficiency refutes the exponential character of real-time PCR.* BMC Molecular Biology 2008;9:96. 56

[97] Stolovitzky G, Cecchi G. *Efficiency of DNA replication in the polymerase chain reaction.* ... of Sciences of the United States ... 1996;. 56

[98] Taylor S, Wakem M, Dijkman G, *et al. A practical approach to RT-qPCR—Publishing data that conform to the MIQE guidelines.* Methods 2010;50(4):S1–S5. 57

Appendix A

Buffer Preparations

All buffers were sterilized before use unless otherwise noted.

A.1 M9 Buffer Preparation

To make 500 mL of M9 buffer, 5.65 g of Na_2HPO_4 ·7H2O, 1.5 g KH_2PO_4, 2.5 g NaCl, and 0.5 mL 1M $MgSO_4$ were mixed. The volume was brought to 500 mL with deionized water. Only M9 that did not form a white precipitate was used.

A.2 Tris/Ethylenediaminetetraacetic Acid (TE) Buffer Preparation

TE buffer is used to dissolve and protect RNA from degradation. A 40 mL solution of 10 mM Tris/0.1 mM EDTA solution was prepared by adding 400 μL of 1 M Tris buffer (pH 8.0) and 8 μL of 0.5 M EDTA to 39.59 μL of nanopure water.

A.3 Potassium Phosphate Buffer Preparation

To make 1M potassium phosphate buffer, 30 mL 1M K_2HPO_4 was mixed with 70 mL 1M KH_2PO_4 and adjusted to a pH of 6.0.

A.4 Single Worm Lysis Buffer Recipe

The recipe for our lysis buffer is as follows:

50 mM KCl

10 mM Tris pH 8.2

2.5 mM $MgCl_2$

0.45% NP-40

0.45% Tween 20

0.01% gelatin

A.5 SB Buffer Preparation

To make a 20X SB buffer solution, NaOH was diluted with 400 mL of deionized water. The pH was brought to 8.0 by adding solid boric acid. Finally, this mixture was diluted to a final volume of 500 mL using deionized water.

Appendix B

Worm Maintenance

B.1 Worm Food

B.1.1 rNGM Plate Preparation

In a 500 mL bottle, 8.5 g agar, 1.5 g NaCl, 3.75 g bacteriological peptone, and approximately 485 mL of deionized water were combined and sterilized by autoclave. After cooling in an oven, 170 μL of 15 mg/mL cholesterol, 0.5 mL 1M $MgSO_4$, 0.5 mL 1M $CaCl_2$, and 12.5 mL 1M Potassium phosphate buffer (pH 6.0) were added with mixing after each addition. The rNGM was poured into petri dishes using sterile technique. The plates were left at room temperature overnight to solidify.

B.1.2 *Escherichia coli* Preparation

OP50 was streak plated and a colony was inoculated in Luria broth. The culture was grown with shaking at 37°C overnight.

B.1.3 Seeded Rich Nematode Growth Medium (rNGM) Plates

Solidified rNGM plates were seeded with *E. coli* OP50 by spreading two drops of OP50 culture on the surface of sterile rNGM plates. The spreader was bathed in ethanol and flamed before every application. The walls of the plate were avoided. The OP50 lawn was permitted to grow on the plates at room temperature (20-25°C) overnight before the plates were stored at 4°C.

B.2 Worm Stock Maintenance

Worm stocks fed a diet of *E. coli* OP50 strain by maintaining them on seeded rNGM plates. All stocks were maintained at 16°C. Before the plates were depleted of OP50, the worms were "chunked" onto a fresh seeded rNGM plates. Chunking is a method for transferring worms to a new plate which involves slicing a chunk of the agar using a sterilized scalpel and placing the agar chunk on a 16°C seeded rNGM plate. The worms crawl off the chunk and populate the plate.

Appendix C

RNA Purification

C.1 RNA Extraction Using TRIzol Reagent

For 10 μL of packed frozen worms, 100 μL of TRIzol was added and mixed vigorously as the worms thawed. Once the worms were thawed, 1 μL of β-mercaptoethanol was added, and the mixture was mixed vigorously for 5 minutes followed by a 10 minute incubation at room temperature and an additional 2 minutes of mixing. The β-mercaptoethanol breaks disulfide bonds proteins and ribonucleases, which disrupt their tertiary and quaternary structure. This breaks open the bodies and cells of the worms, releasing their contents into solution. TRIzol has many components that denature RNases that would otherwise quickly degrade the small RNAs we are interested in quantifying. The mixture was then centrifuged at 12,000 rpm in a cooled microcentrifuge for 10 minutes in order to pellet the large cellular debris. The supernatant was transferred to a sterile tube, vigorously mixed with 20 μL of chloroform, and incubated at room temperature for 3 minutes. This tube was spun at 12,000 rpm in a cooled microcentrifuge for 15 minutes. At this point, the mixture was partitioned into two immiscible solvents of different polarities. The top aqueous fraction contained the RNA from the worms, the bottom fraction contained organic molecules,

with DNA dissolved at the interface. The top fraction was carefully transferred to a sterile tube and its volume was measured.

At this point, we purified our RNA either by a series of ethanol precipitations (Section C.2) or by using a mirVana RNA purification kit. We used ethanol precipitations for our relative quantitation experiments after we determined the two methods were comparable (data in Section 3.2).

C.2 Purification of Total RNA Using Ethanol Precipitation

To the aqueous RNA mixture, 0.1 volumes of 3 M sodium acetate (pH 5.3) and 3 volumes of 100% ethanol were added successively and incubated on ice for 10 minutes. This mixture was spun in a cooled microcentrifuge at 12,000 rpm for 10 minutes and the supernatant discarded, leaving a white pellet. This pellet contains the RNA; however it has a high salt concentration that needs to be removed before the RNA can be used for experiments. The pellet was washed with 190 μL of 75% ethanol and re-spun for 1 minute. The supernatant was decanted and the pellet was allowed to air dry for 5 minutes. The pellet was re-suspended in 50 μL of nanopure water and stored at -80°C. The RNA concentration was quantified using UV/Vis (see Appendix C.3 for details and a sample calculation).

C.3 RNA Concentration Quantification

"Trying to determine the structure by UV spectroscopy was like trying to determine the structure of a piano by listening to the sound it made while being dropped down a flight of stairs."

-Francis Crick

RNA concentration was quantified using ultraviolet/visible light spectrometry. Absorbance was measured in the spectrum of light between 230 nm^{-1} to 360 nm^{-1} using an Olis Cary-14 Spectrophotometer. We zeroed the instrument using TE, and assigned the TE spectrum as the baseline for RNA measurements. Purified RNA was diluted 111-fold with TE buffer in a 1 cm quartz cuvette.

The concentration of RNA was then calculated using the Beer-Lambert Law,

$$A = \epsilon \times l \times c \tag{C.1}$$

where A is measured absorbance, ϵ is the extinction coefficient, l is the path length, and c is the concentration. RNA has a characteristic absorption at 260 nm where the aromatic bases absorb light. RNA's extinction coefficient is 40 $\mu L\ \mu g^{-1}\ cm^{-1}$. The measured concentration is then multiplied by the dilution factor to give the RNA concentration of extracted RNA.

For example, for an A_{260} of 0.08:

$$c = \frac{A}{\epsilon \times l}$$

$$c = \frac{0.08}{33\ \mu L \mu g^{-1}\ cm^{-1} \times 1\ cm} = 0.08 \times 40\ \mu g/mL$$

$$c = 3.2\ \mu g\ mL^{-1}$$

Finally, the measured concentration is multiplied by the dilution factor d to determine the sample concentration:

$$C_{sample} = c \times d$$

$$C_{sample} = 3.2\ \mu g\ mL^{-1} \times 111 = 355.2\ \mu g\ \mu L^{-1}$$

Most of the UV/Vis spectra indicate there are contaminations by phenol, chaotropic salts, or guanadinium isotheiocynate, which are leftover byproducts of the TRIzol RNA extraction. This might be an artifact because low RNA concentrations have an A_{260}/A_{230} ratio closer to 1.0. The only samples with major contamination are the *rha-1* samples. The 20°C *eri-1* worms seem to be impossibly pure.

Condition	**Strain**	A_{260}/A_{230}	A_{260}/A_{280}	**Concentration** $(ng/\mu L)$
16°C	N2	1.27	2.12	753.91
	eri-1	1.24	1.95	293.04
	rha-1	0.29	N/A	114.55
	rha-1;eri-1	1.24	1.76	276.61
20°C	N2	1.47	2.21	447.11
	eri-1	3.97	2.76	477.3
	rha-1	0.86	1.25	618.49
	rha-1;eri-1	1.67	1.95	668.22

Table C.1: UV/Vis Data for RNA Samples - Calculations for UV/Vis data. The A_{260}/A_{230} measures contamination with chaotropic salts; 2.0 is considered a good ratio. The A_{260}/A_{280} measures protein contamination, samples between 1.8 and 2.1 are considered pure RNA.

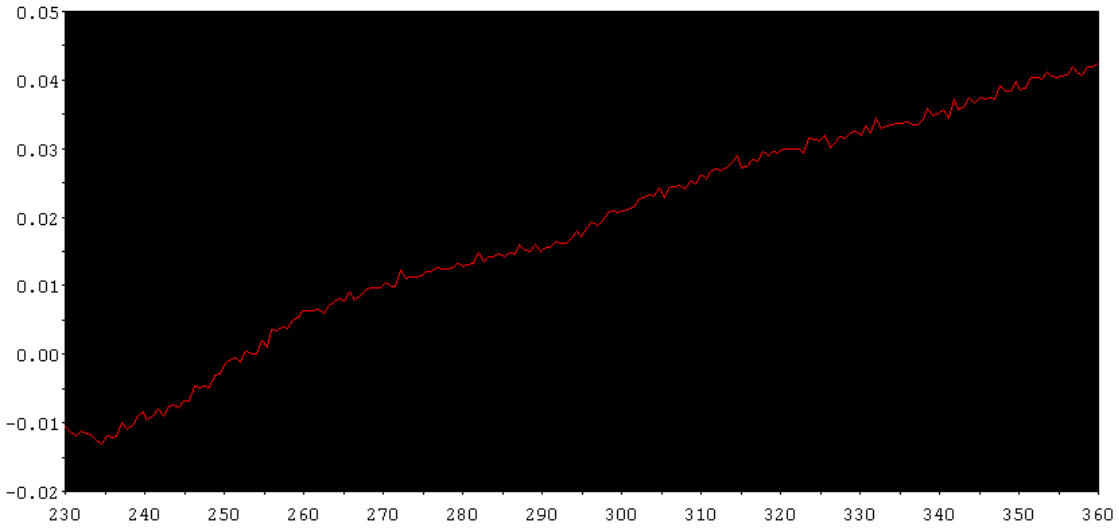

Figure C.1: TE Blank UV/Vis Spectra for 11/3/10 Quantifications - Plot of absorbance vs wavelength. We took a spectra of our TE buffer to zero our instrument. This spectra was assigned as the baseline and subtracted from subsequent spectra.

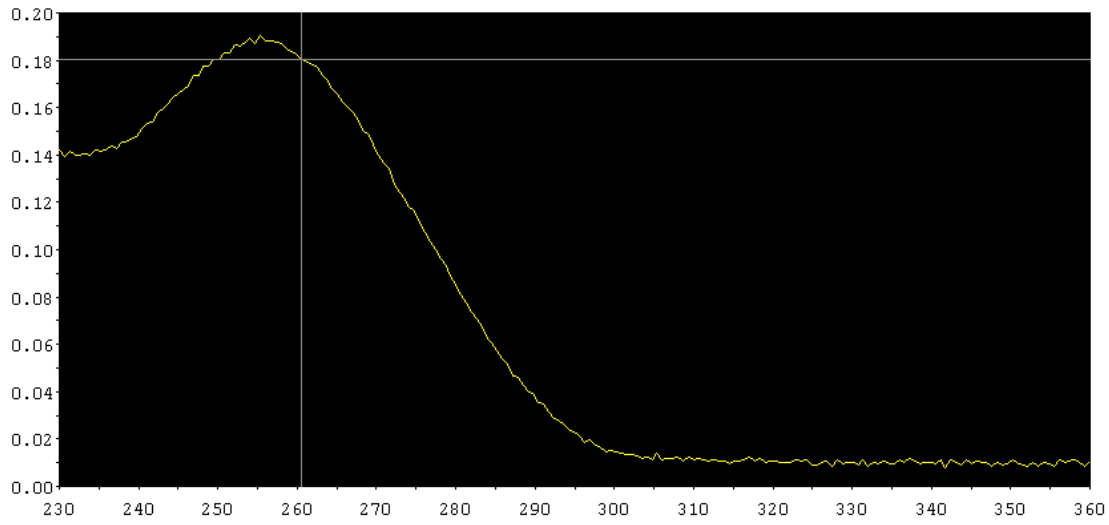

Figure C.2: UV/Vis Spectra of RNA Isolated From Synchronized N2 Worms Grown at 16C (Purified by Ethanol Precipitation) - Plot of absorbance vs wavelength. Calculations are shown in Table C.1. This RNA was used to determine if we needed to use mirVANA kits to purify RNA.

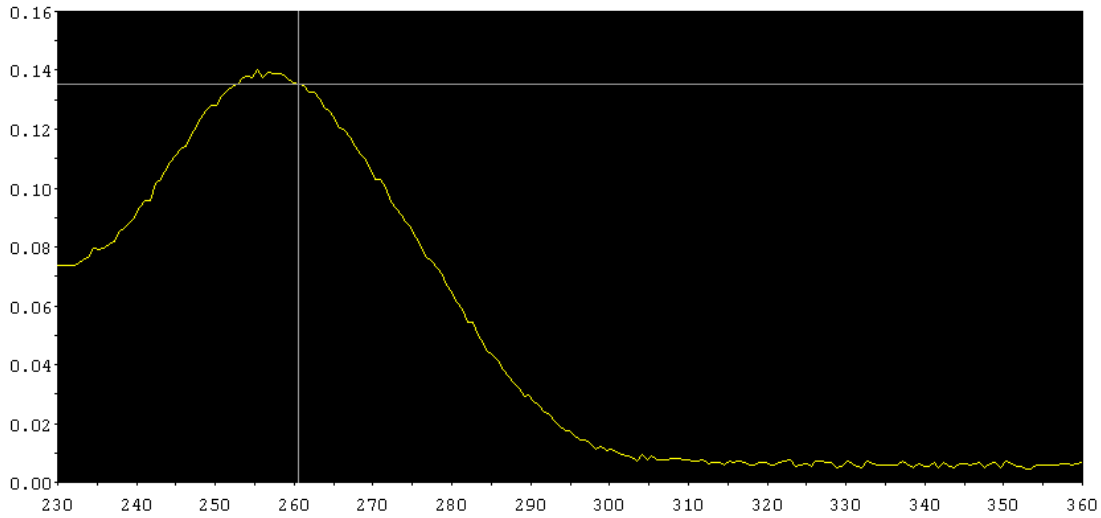

Figure C.3: UV/Vis Spectra of RNA Isolated From Synchronized N2 Worms Grown at 16C (Purified with Ambion mirVANA Kit) - Plot of absorbance vs wavelength. Calculations are shown in Table C.1. This RNA was used to determine if we needed to use mirVANA kits to purify RNA.

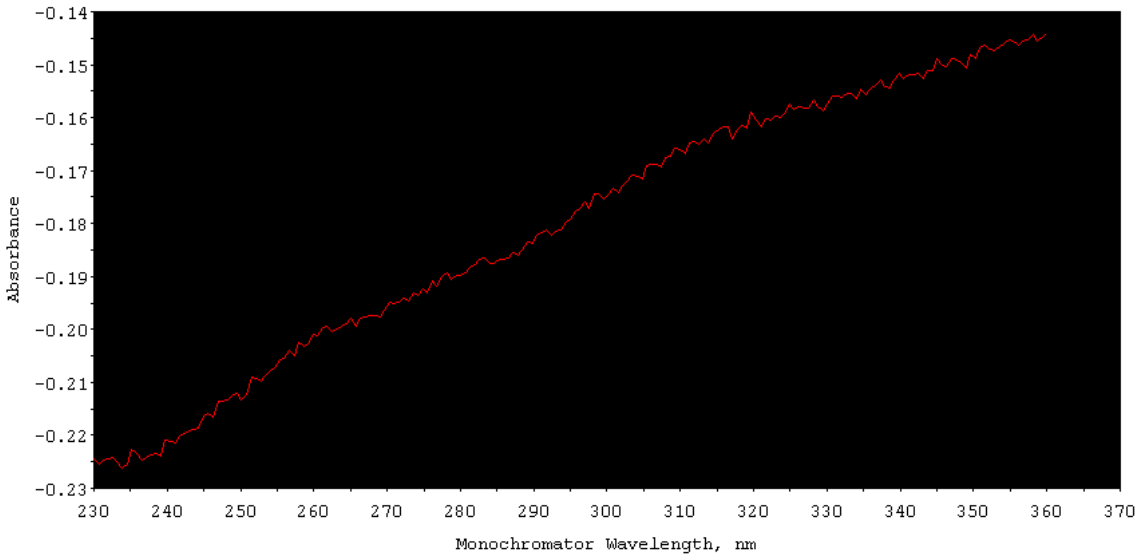

Figure C.4: TE Blank UV/Vis Spectra for 9/15/10 Quantifications - We took a spectra of our TE buffer to zero our instrument. This spectra was assigned as the baseline and subtracted from the following spectra.

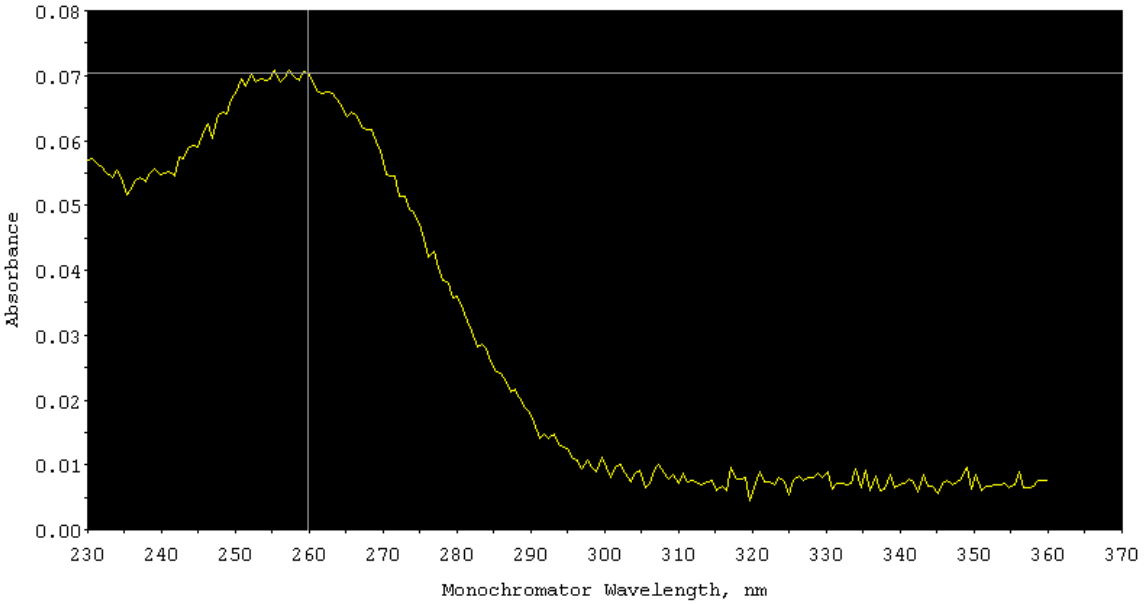

Figure C.5: UV/Vis Spectra of RNA Extracted From *eri-1* Strain Grown at 16°C - Plot of absorbance vs wavelength. Calculations are shown in Table C.1. This RNA was used in our relative quantitation experiments.

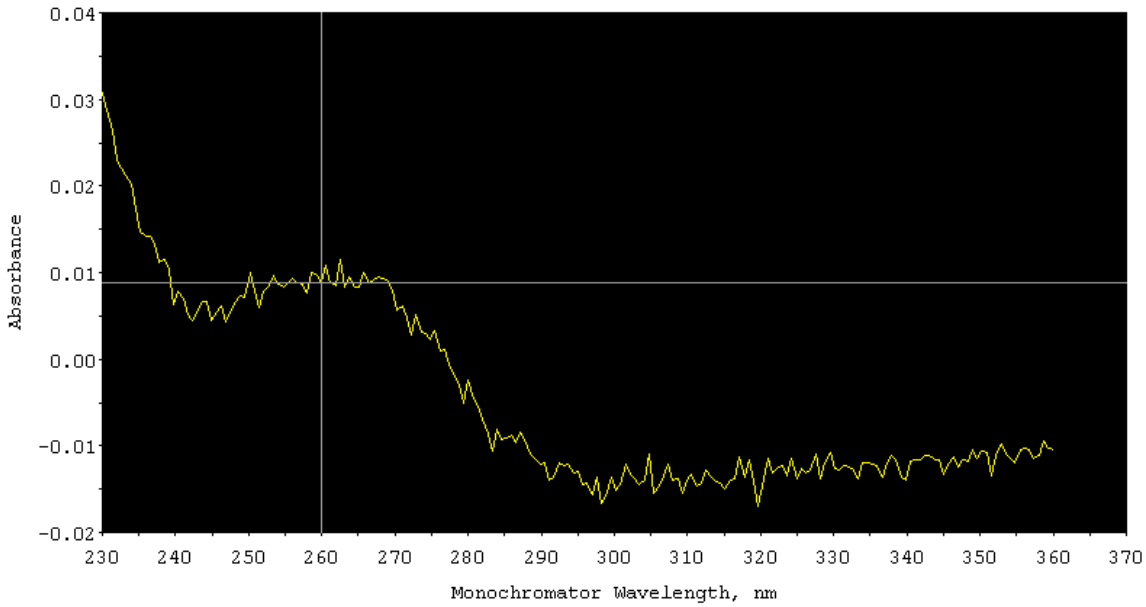

Figure C.6: UV/Vis Spectra of RNA Extracted From *rha-1* Strain Grown at 16°C - Plot of absorbance vs wavelength. Calculations are shown in Table C.1. This RNA was used in our relative quantitation experiments.

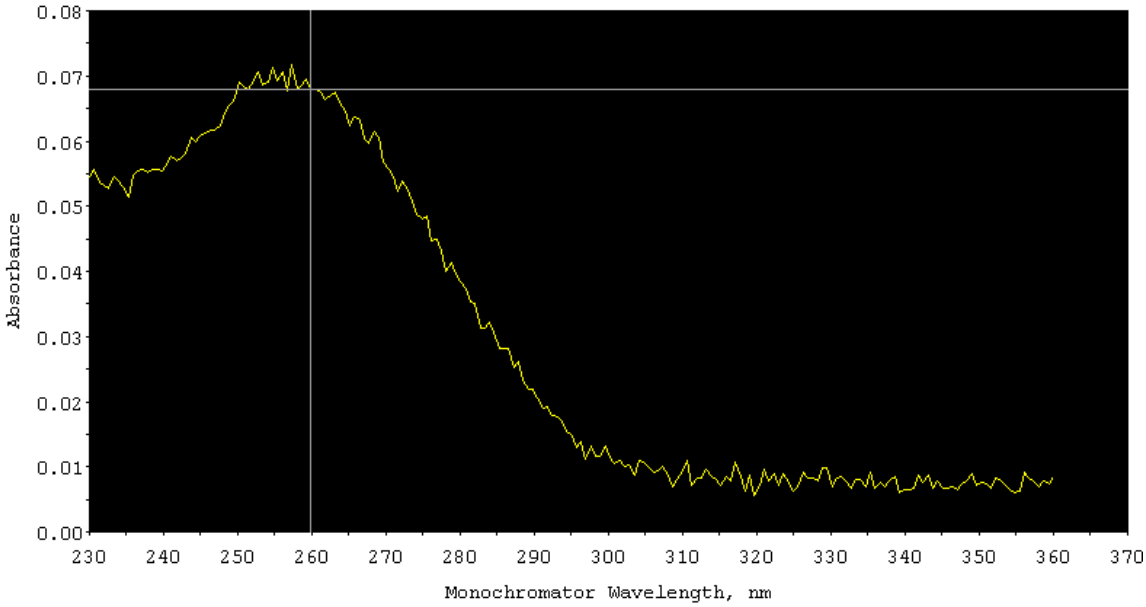

Figure C.7: UV/Vis Spectra of RNA Extracted From *rha-1;eri-1* Strain Grown at 16°C - Plot of absorbance vs wavelength. Calculations are shown in Table C.1. This RNA was used in our relative quantitation experiments.

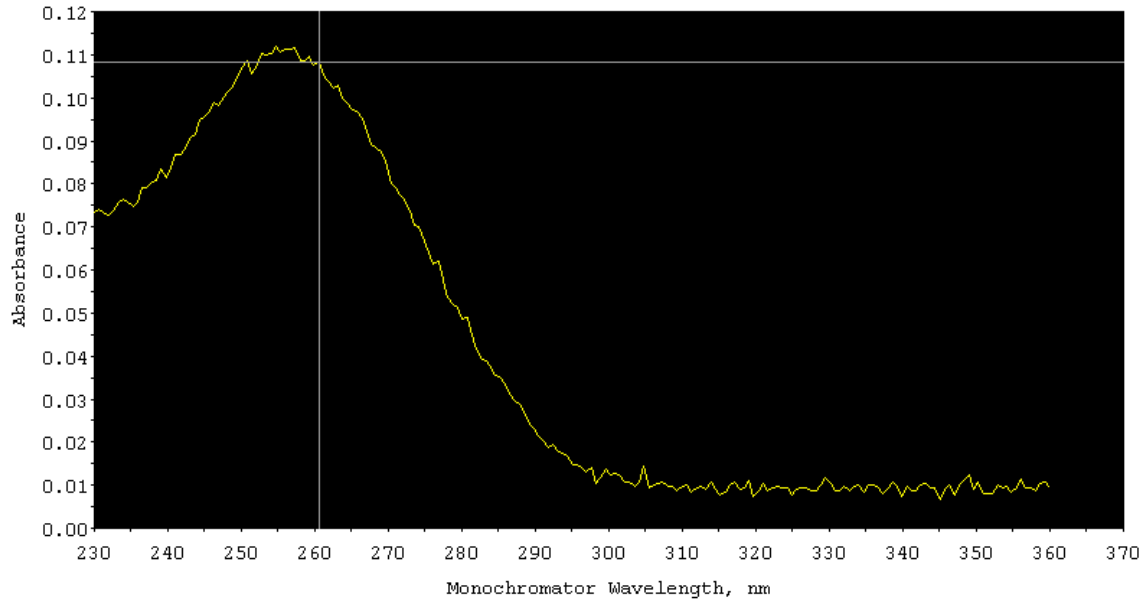

Figure C.8: UV/Vis Spectra of RNA Extracted From N2 Strain Grown at 20°C - Plot of absorbance vs wavelength. Calculations are shown in Table C.1. This RNA was used in our relative quantitation experiments.

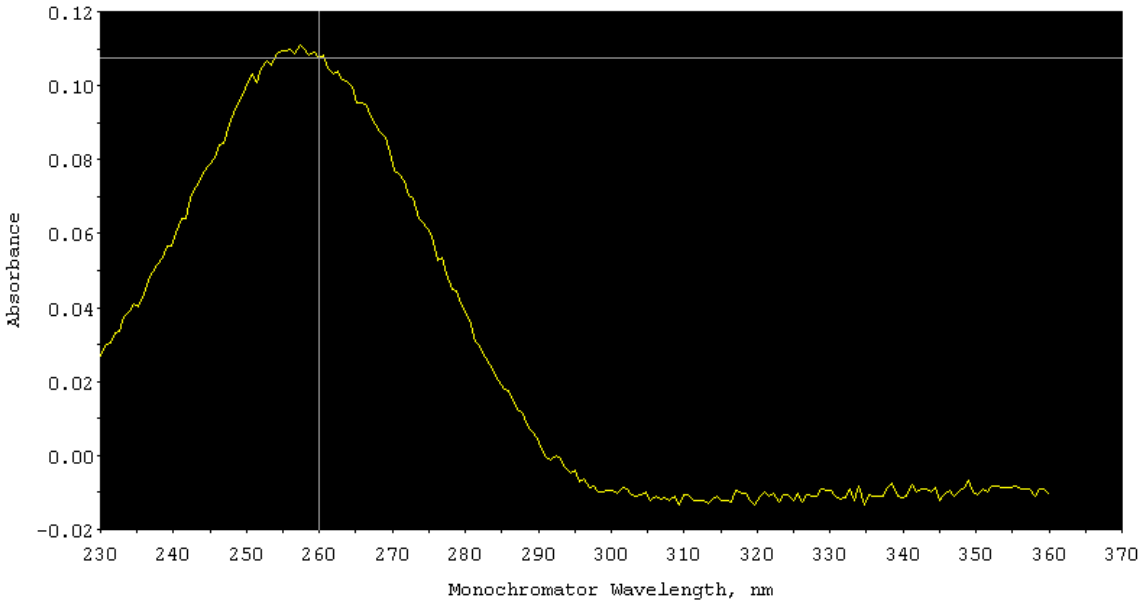

Figure C.9: UV/Vis Spectra of RNA Extracted From *eri-1* Strain Grown at 20°C - Plot of absorbance vs wavelength. Calculations are shown in Table C.1. This RNA was used in our relative quantitation experiments.

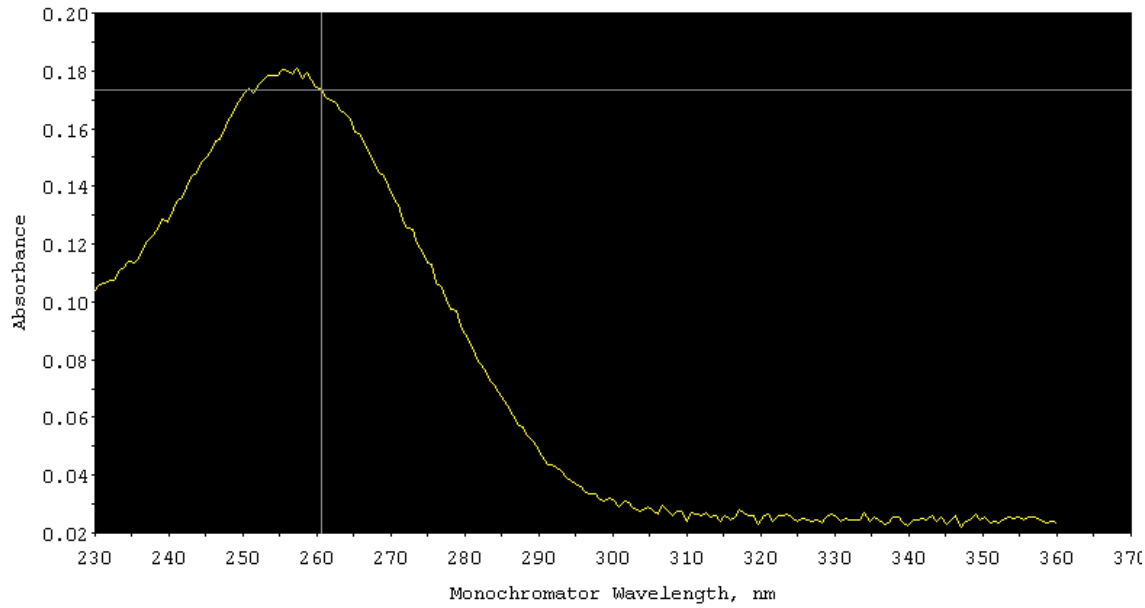

Figure C.10: UV/Vis Spectra of RNA Extracted From *rha-1;eri-1* Strain Grown at 20°C - Plot of absorbance vs wavelength. Calculations are shown in Table C.1. This RNA was used in our relative quantitation experiments.

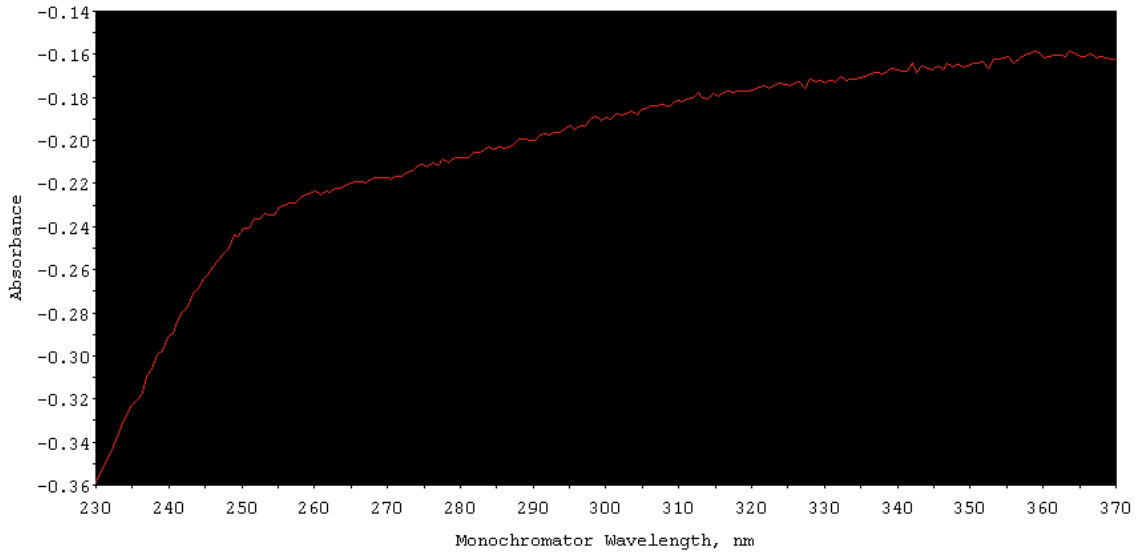

Figure C.11: TE Blank UV/Vis Spectra for 3/23/11 Quantifications - Plot of absorbance vs wavelength. We took a spectra of our TE buffer to zero our instrument. This spectra was assigned as the baseline and subtracted from the following spectra.

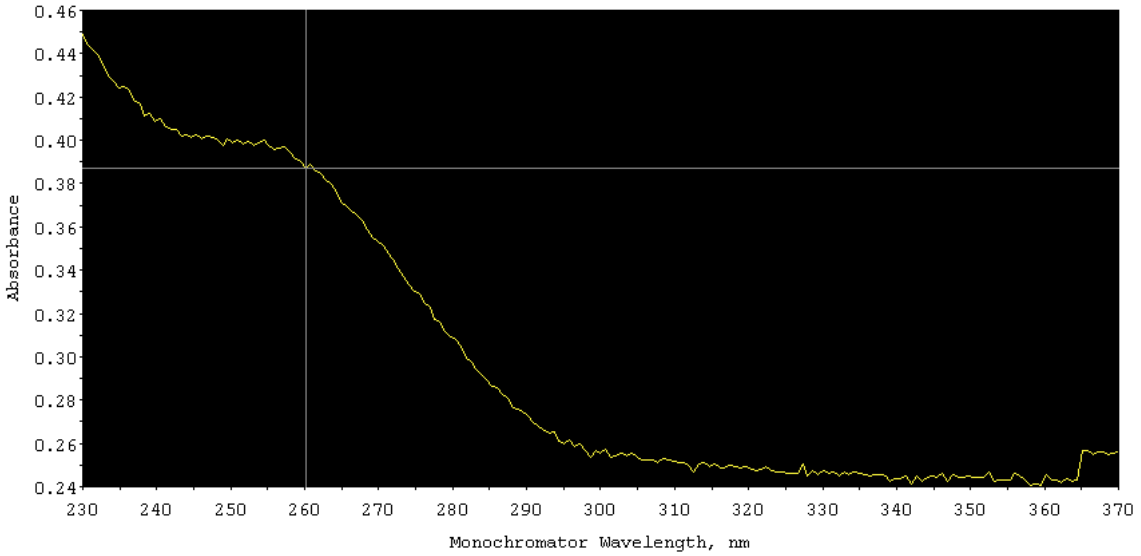

Figure C.12: UV/Vis Spectra of RNA Extracted From *rha-1* Strain Grown at 20°C - Plot of absorbance vs wavelength. Calculations are shown in Table C.1. This RNA was used in our relative quantitation experiments.

Appendix D

Primer Information

D.1 Primers Used

We used different primers for the single worm PCR (see Table D.1), reverse transcriptions (see Table D.2), and RT-qPCR experiments (see Table D.3). For the reverse transcription primers, we used a design similar to the one described by Varkonyi-Gasic *et al*[84] (see Figure 2.3). The general structure is:

GTTGGCTCTGGTGCAGGGTCCGAGGTATTCGCACCAGAGCCAAC-6 nt

where "6 nt" is the a 6 nucleotide-long segment that is complimentary to the target small RNA. The primer has self complimentary regions, so it forms a stem loop with itself and forms base-stacking interactions with the small RNA. The composition of the primer raises the melting temperature of the primer-RNA duplex to about 59°C.

Genotype tested	Primer Name	Primer Sequence
eri-1(mg366)	eri-1a	GAT AAA ACT TCG GAA CAT ATG GGG C
	eri-1b	ACT GAT GGG TAA GGA ATC GAA GAC G
rha-1(tm329)	3430	TCA AGC GAG GTG AAG CAC TTG AC
	2221	GGC TAC ACT GCT TTC GGA AAT TCC
	3784	ATT CGC AGC AAG ACT CCA ACA G

Table D.1: Primers Used for Single Worm PCR - Name and sequence of all primers used in single worm PCR experiments.

D.2 Primer Specificities

The following are the DNA melting curve spectra for the primer specificity experiments (discussed in Section 2.4.2).

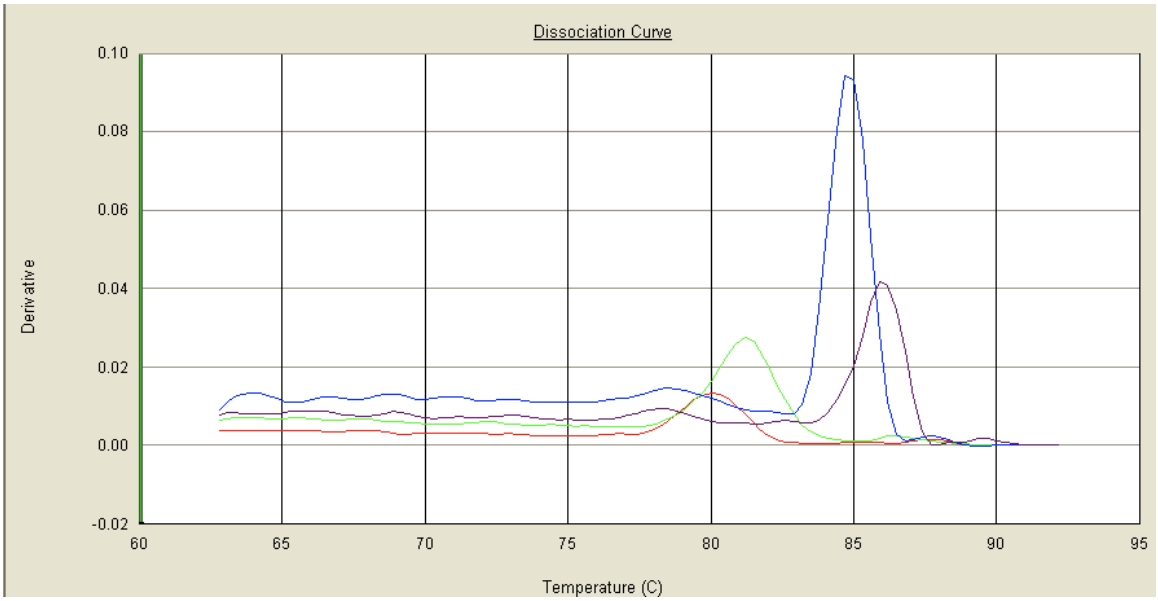

Figure D.1: DNA Melting Curve for Y55F3BR.9for08 No Template Control - Plot of derivative as a function of temperature. The amplification curves had C_t values of range 41-43, indicating little to no product amplification. The curves do not overlap, indicating the amplifications are due to spurious binding.

RNA Name	Reverse Transcription Primer Name	Reverse Primer Sequence
21UR-3442	21UR-3442RT	GTT GGC TCT GGT GCA GGG TCC GAG GTA TTC GCA CCA GAG CCA ACC ACAA
Y55F3BR.9 (sn2342)	Y55F3BR.9RT	GTT GGC TCT GGT GCA GGG TCC GAG GTA TTC GCA CCA GAG CCA ACC GGCT
X1051	X1051RT	GTT GGC TCT GGT GCA GGG TCC GAG GTA TTC GCA CCA GAG CCA ACG GCA TA
K11D9.1	K11D9_1eRT	GTT GGC TCT GGT GCA GGG TCC GAG GTA TTC GCA CCA GAG CCA ACT CTC AC
mir-66	mir66RT	GTT GGC TCT GGT GCA GGG TCC GAG GTA TTC GCA CCA GAG CCA ACT CAC AT
mir-77	mir77_RT	GTT GGC TCT GGT GCA GGG TCC GAG GTA TTC GCA CCA GAG CCA ACT GGA CA

Table D.2: Reverse Transcription Primers Used - Information regarding primers used in reverse transcriptions to generate cDNA copies of the small RNAs. See Figure 2.3 for description of stem loop primers.

RNA Name	RT-qPCR Primer Name	Primer Sequence
21UR-3442	21UR-3442for08	CGG CGG TAC TAG AGT GTT GAG ATT G
Y55F3BR.9 (sn2342)	Y55F3BR.9for08	GCG GCG GCT GTG ATG ATT T
X1051	X1051for08	CGG CGG GTT ACT AGT ACG CTT TTA TG
K11D9.1	K11D9_1efor08	TGC GGG ATC TGG AAT ATG GCG
mir-66	mir66for08	TGC CGC ATG ACA CTG ATT AGG G
mir-77	mir77for	AGC CCT TCA TCA GGC CAT AGC

Table D.3: RT-qPCR Primers Used - Information regarding primers used in qPCR to quantify cDNA product from reverse transcriptions. For all of these primers, the same universal primer was used (univ_RT primer with the sequence GTGCAGGGTCC-GAGGT).

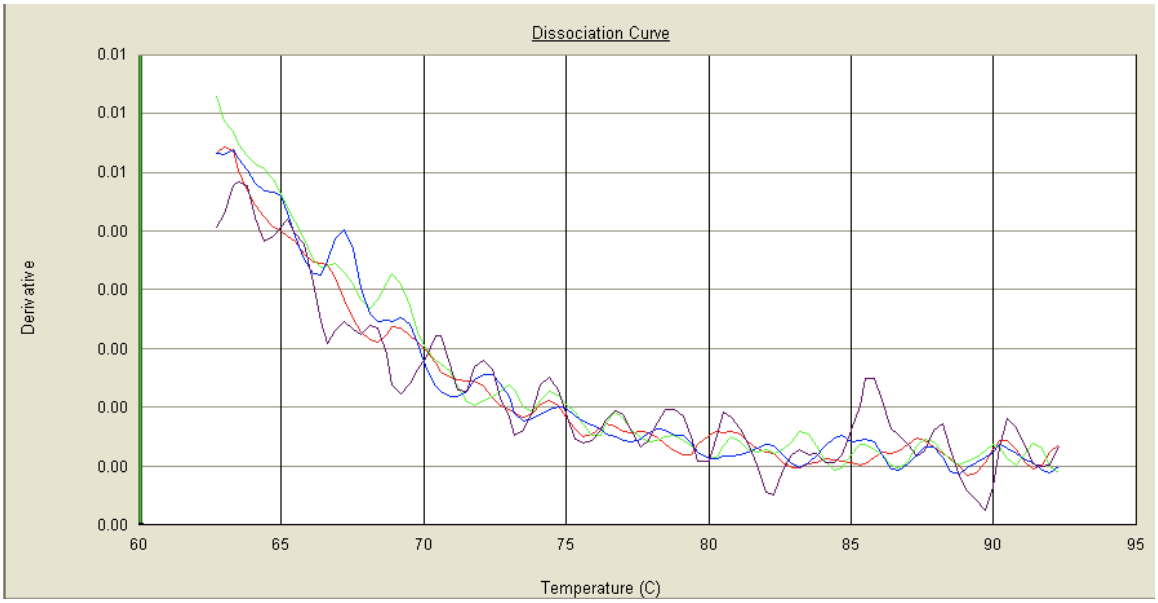

Figure D.2: DNA Melting Curve for X1051for08 No Template Control - Plot of derivative as a function of temperature. The amplification curves had C_t values above the detectable range, indicating little to no product amplification. The curves do not overlap, indicating the amplifications are due to spurious binding.

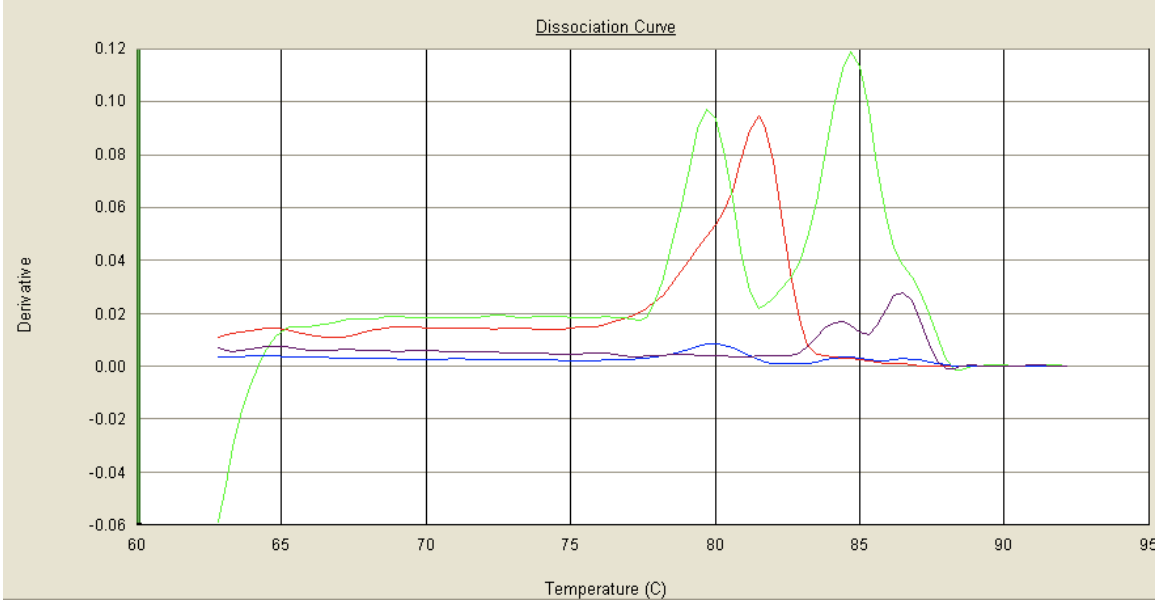

Figure D.3: DNA Melting Curve for 21UR-3442for08 No Template Control - Plot of derivative as a function of temperature. The amplification curves had C_t values ranging between 38-44, indicating little to no product amplification. Additionally, the y-axis has a very small range. The curves do not overlap, indicating the amplifications are due to spurious binding.

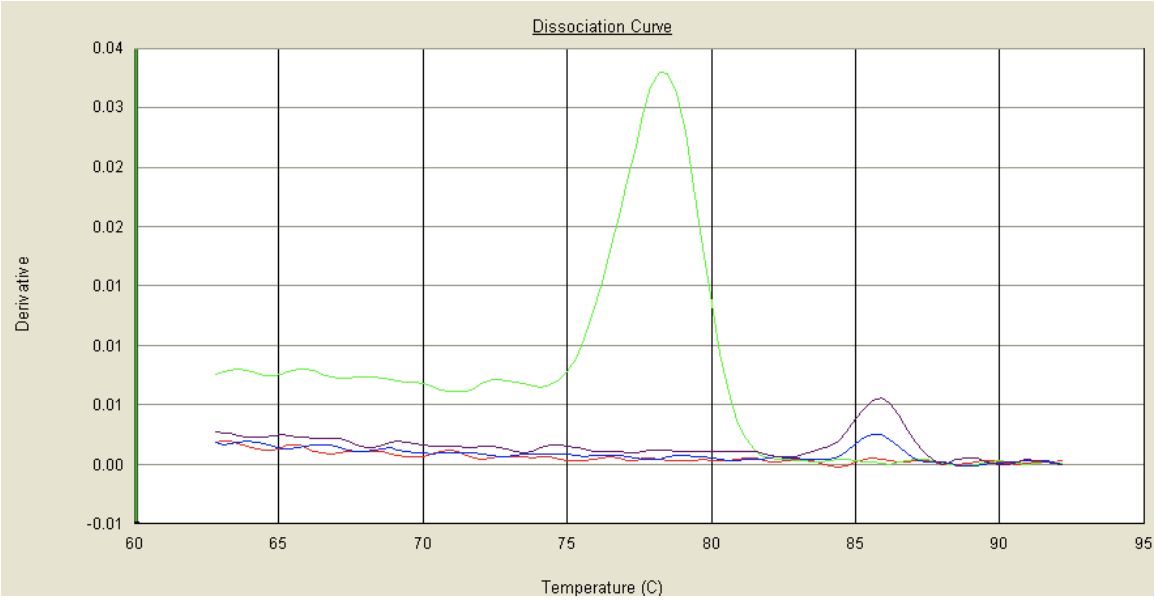

Figure D.4: DNA Melting Curve for K11D9_1efor08 No Template Control - Plot of derivative as a function of temperature. The amplification curves C_ts greater than or equal to 43, indicating little to no product amplification. The curves do not overlap, indicating the amplifications are due to spurious binding.

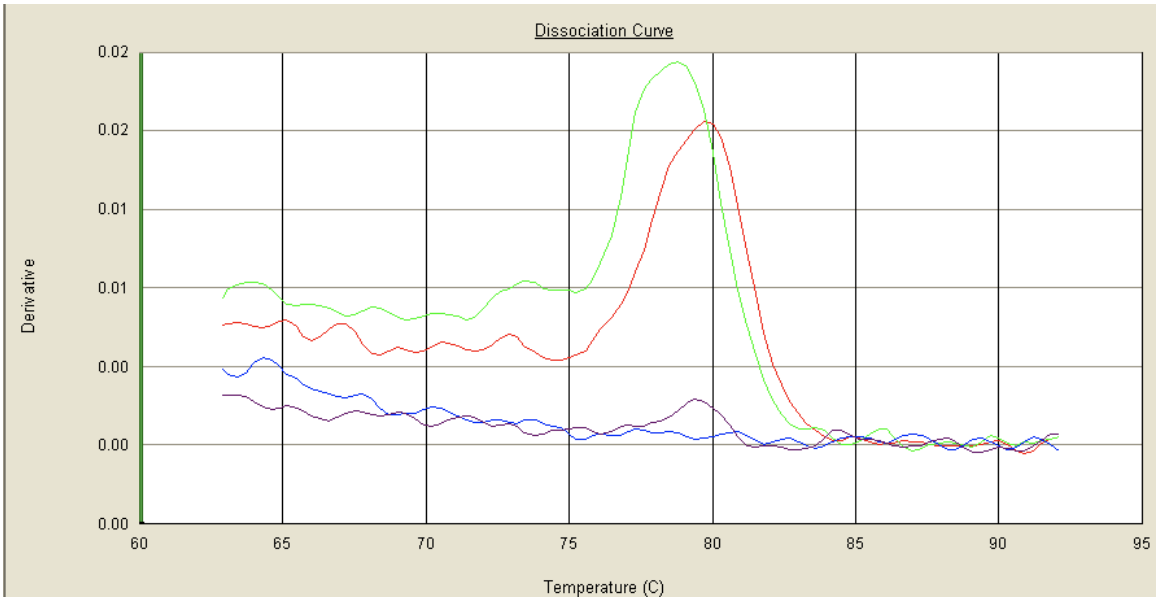

Figure D.5: DNA Melting Curve for mir66for08 No Template Control - Plot of derivative as a function of temperature. The amplification curves had C_t values greater than or equal to 43, indicating little to no product amplification. The curves do not overlap, indicating the amplifications are due to spurious binding.

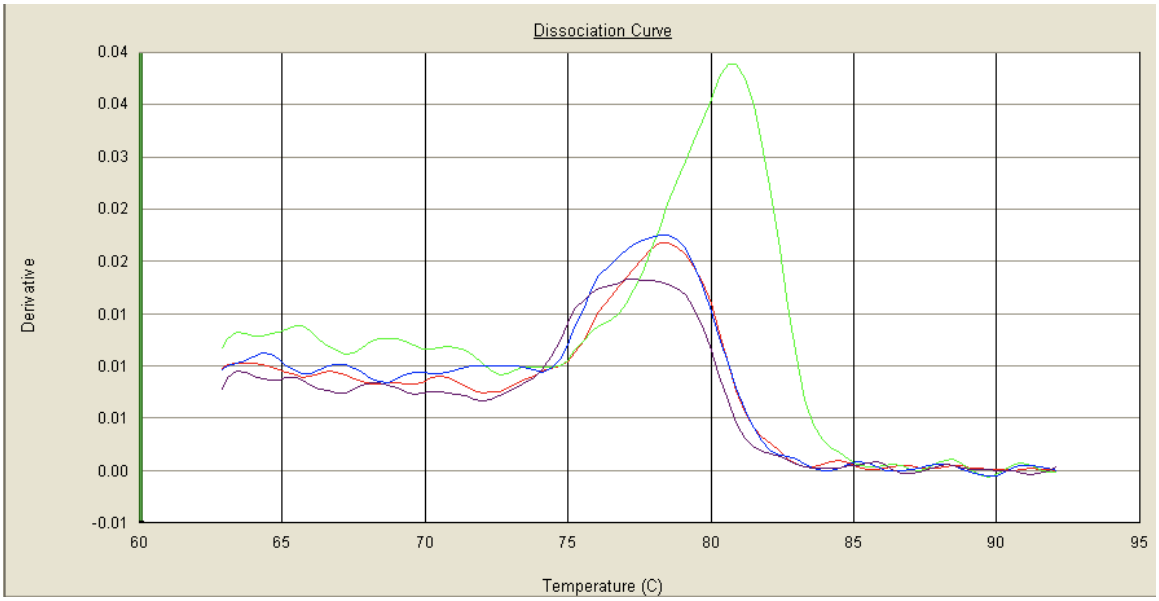

Figure D.6: DNA Melting Curve for mir77for No Template Control - Plot of derivative as a function of temperature. The amplification curves had a C_t range of 38-41, indicating little to no product amplification. The curves do not overlap, indicating the amplifications are due to spurious binding.

D.2.1 Primer Efficiency Quantification

The following are the linear regressions for the primer efficiency dilution series experiments. To calculate primer efficiency, we used Equation 2.1. For example, for a standard curve with a slope of -3.6,

$$E = -1 + 10^{\frac{-1}{\text{slope}}}$$

$$E = -1 + 10^{\frac{-1}{-3.6}}$$

$$E = -1 + 10^{1.896} = -1 + 1.897 = 0.897$$

or, efficiency is equal to 89.7%. This means each round of qPCR amplifies 1.897 the amount of DNA. Note, the Pfaffl definition for efficiency designated 1.0 as no efficiency and 2.0 as 100% efficiency.

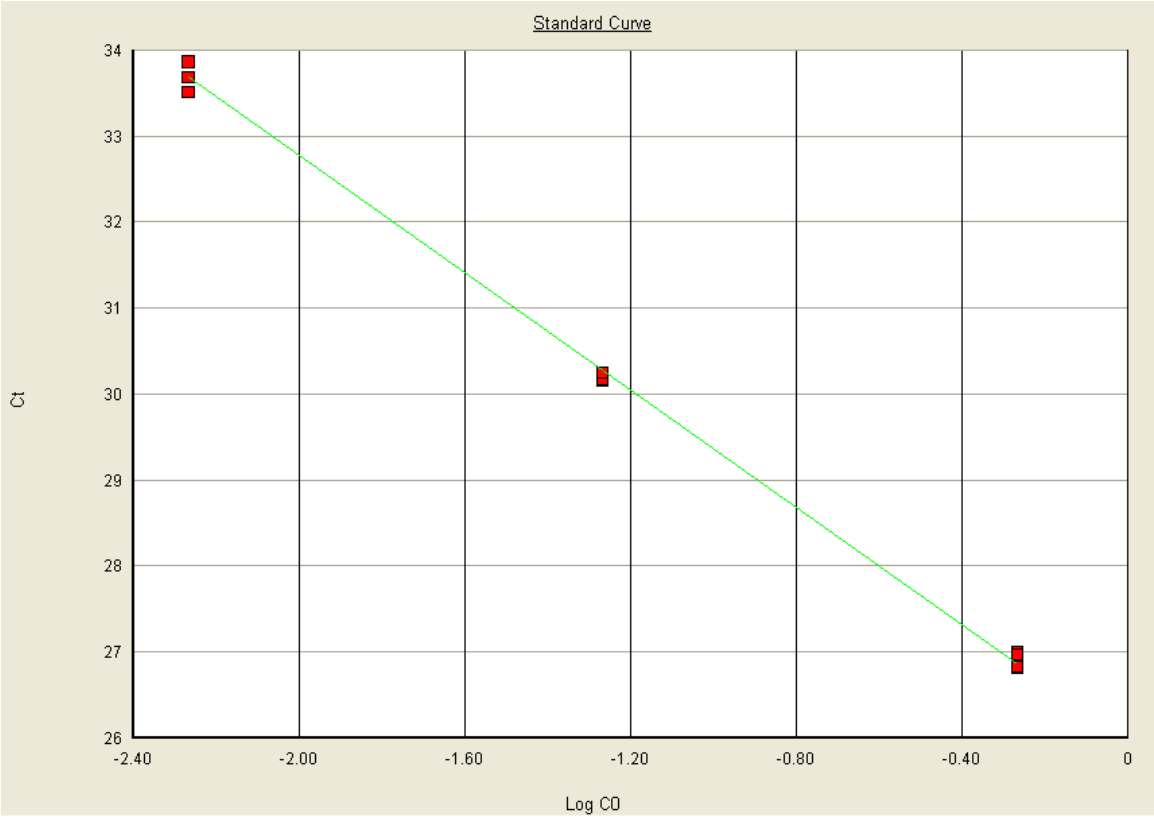

Figure D.7: Standard Curve for Y55F3BR.9for08 - Plot of C_t vs. $\ln[cDNA]$ for a 10-fold dilution series of cDNA. cDNA amounts in the dilution series are as follows: 1.25 ng, 0.125 ng, 0.00125 ng, and 0.000125 ng. The slope was -3.42 ($r^2 = 0.998$), corresponding to an efficiency of 96.1%.

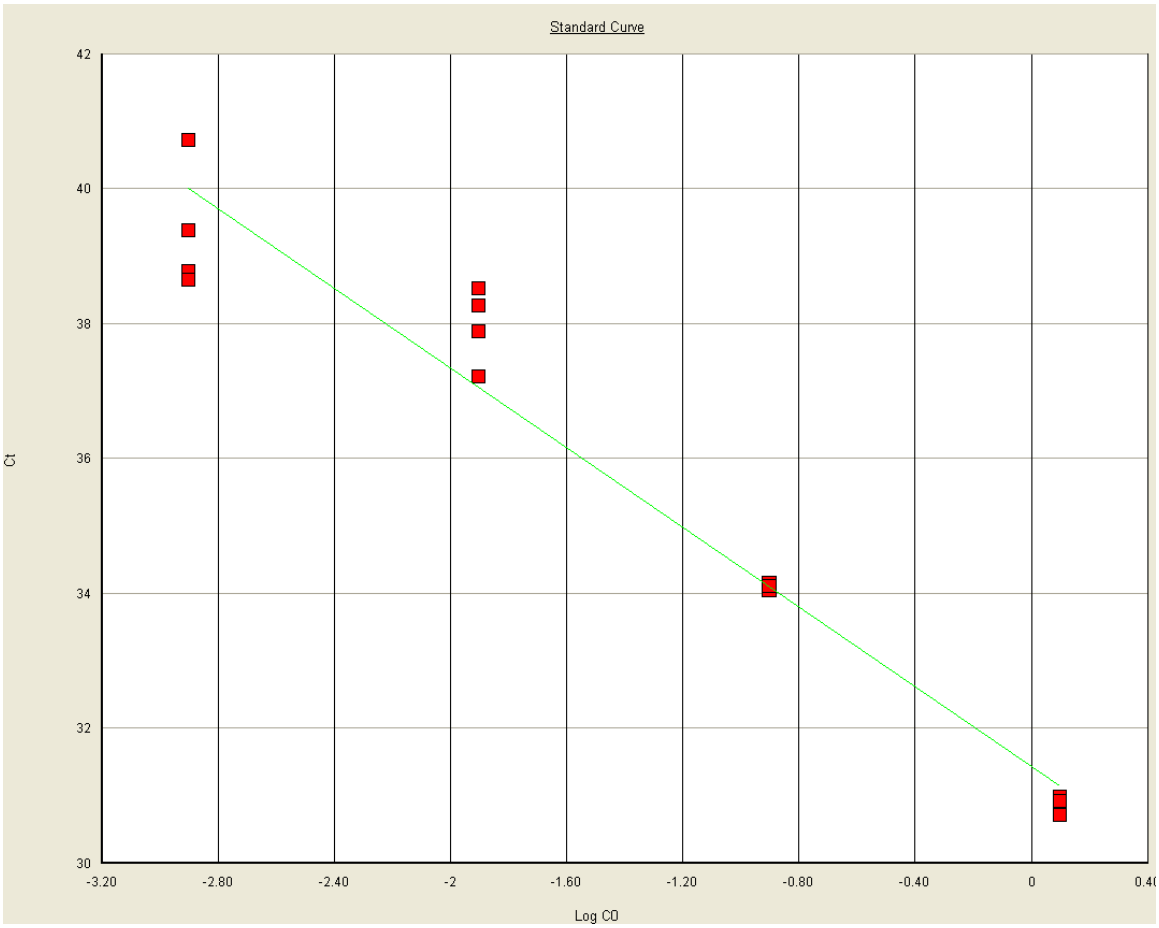

Figure D.8: Standard Curve for X1051for08 - Plot of C_t vs. $\ln[cDNA]$ for a 10-fold dilution series of cDNA. cDNA amounts in the dilution series are as follows: 1.25 ng, 0.125 ng, 0.00125 ng, and 0.000125 ng. The slope was -2.55 ($r^2 = 0.950$), corresponding to an efficiency of 147%.

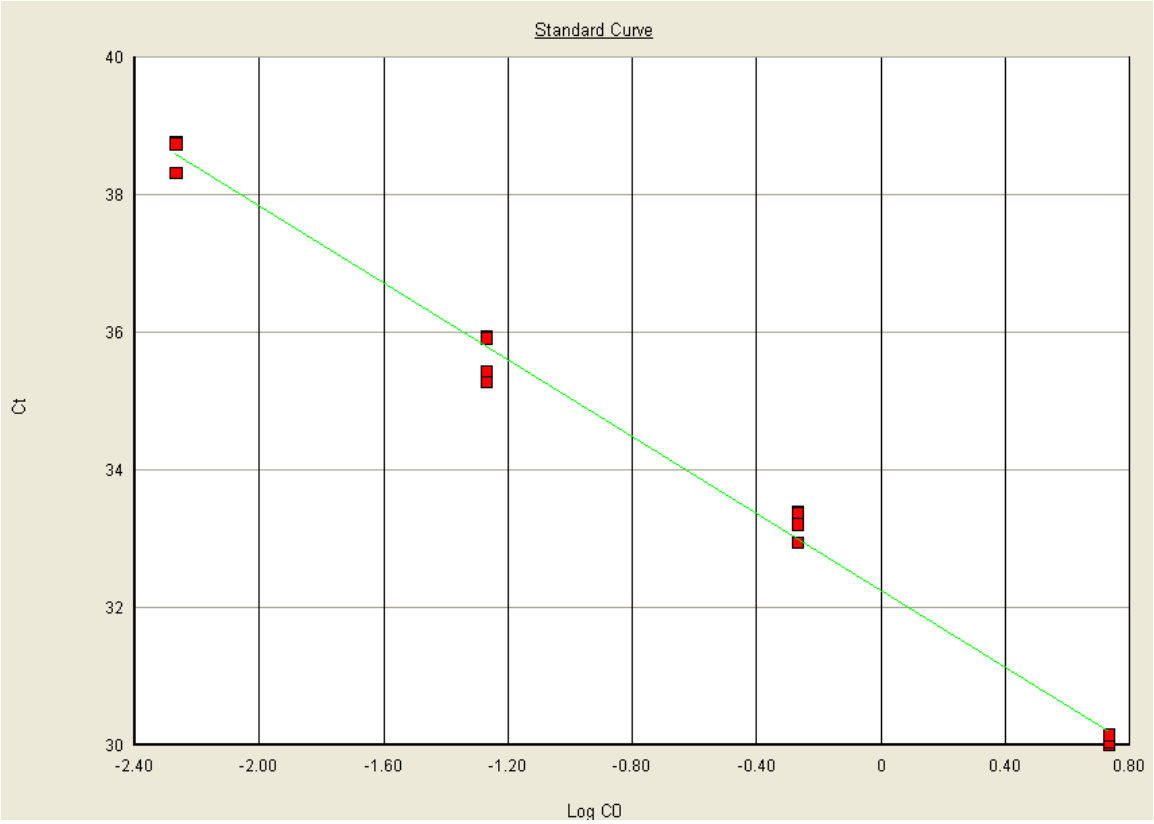

Figure D.9: Standard Curve for 21UR-3442for08 - Plot of C_t vs. $\ln[cDNA]$ for a 10-fold dilution series of cDNA. cDNA amounts in the dilution series are as follows: 1.25 ng, 0.125 ng, 0.00125 ng, and 0.000125 ng. The slope was -2.79 ($r^2 = 0.993$), corresponding to an efficiency of 131.013%.

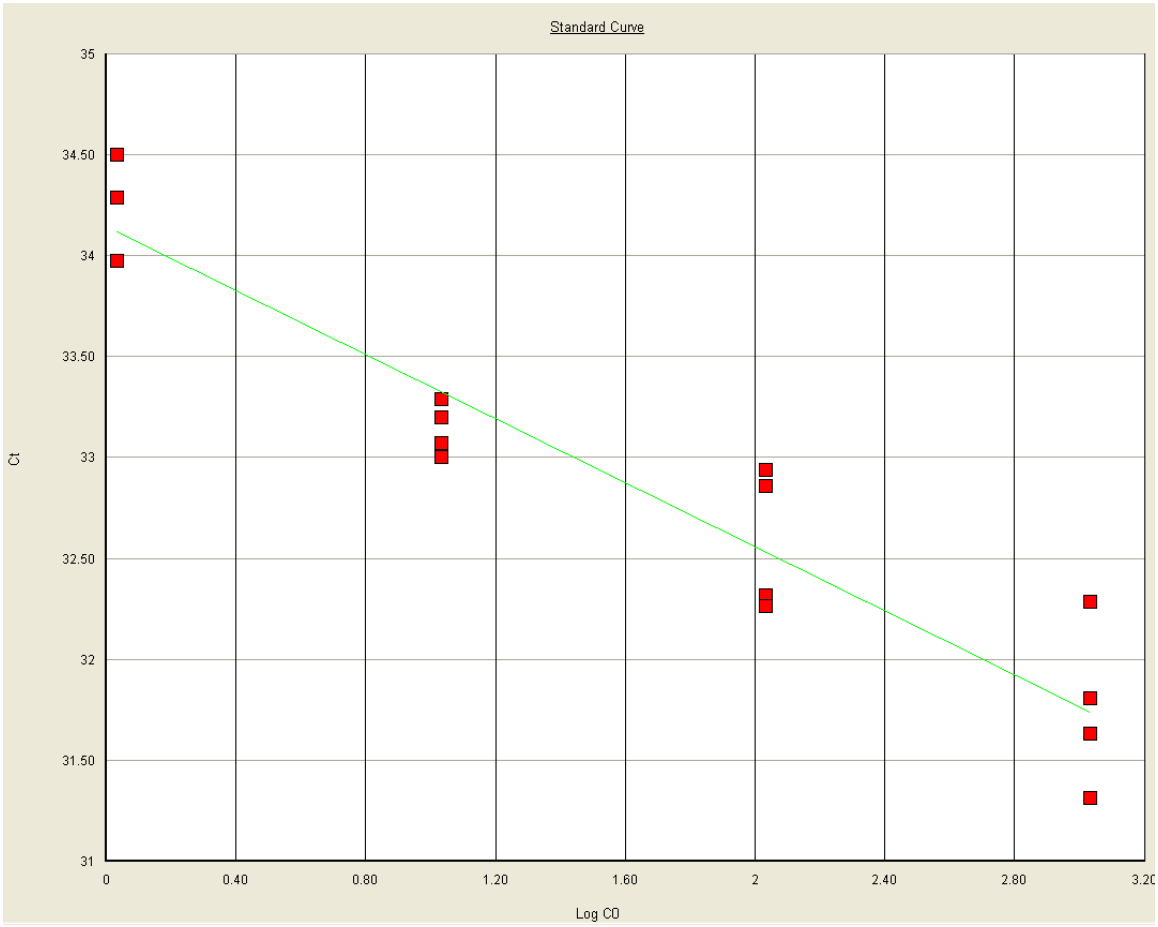

Figure D.10: Standard Curve for K11D9_1efor08 - Plot of C_t vs. $\ln[cDNA]$ for a 10-fold dilution series of cDNA. cDNA amounts in the dilution series are as follows: 1079.4 ng, 107.9 ng, 10.79 ng, and 1.07 ng. The slope was -0.79 ($r^2 = 0.897$), corresponding to an efficiency of 1744%. Note: This primer is of exceedingly low quality!

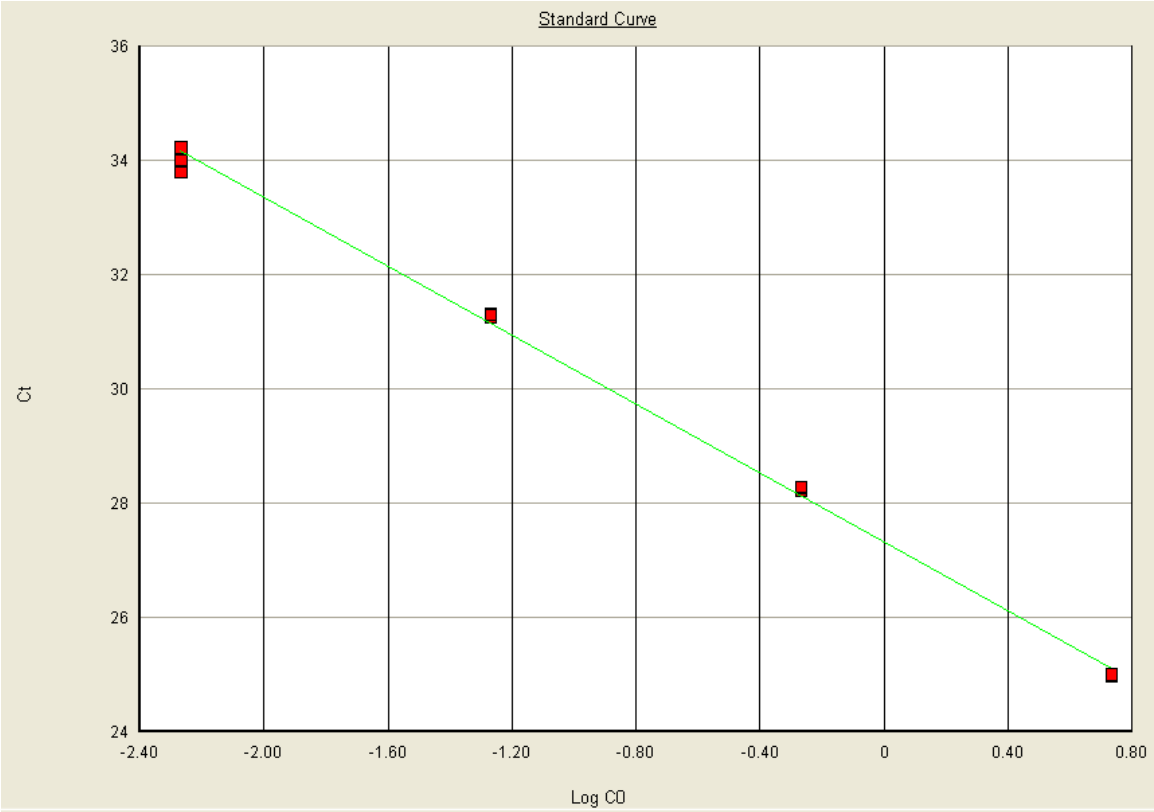

Figure D.11: Standard Curve for mir66for08 - Plot of C_t vs. $\ln[cDNA]$ for a 10-fold dilution series of cDNA. cDNA amounts in the dilution series are as follows: 1.25 ng, 0.125 ng, 0.00125 ng, and 0.000125 ng. The slope was -3.01 ($r^2 = 0.998$), corresponding to an efficiency of 114.89%.

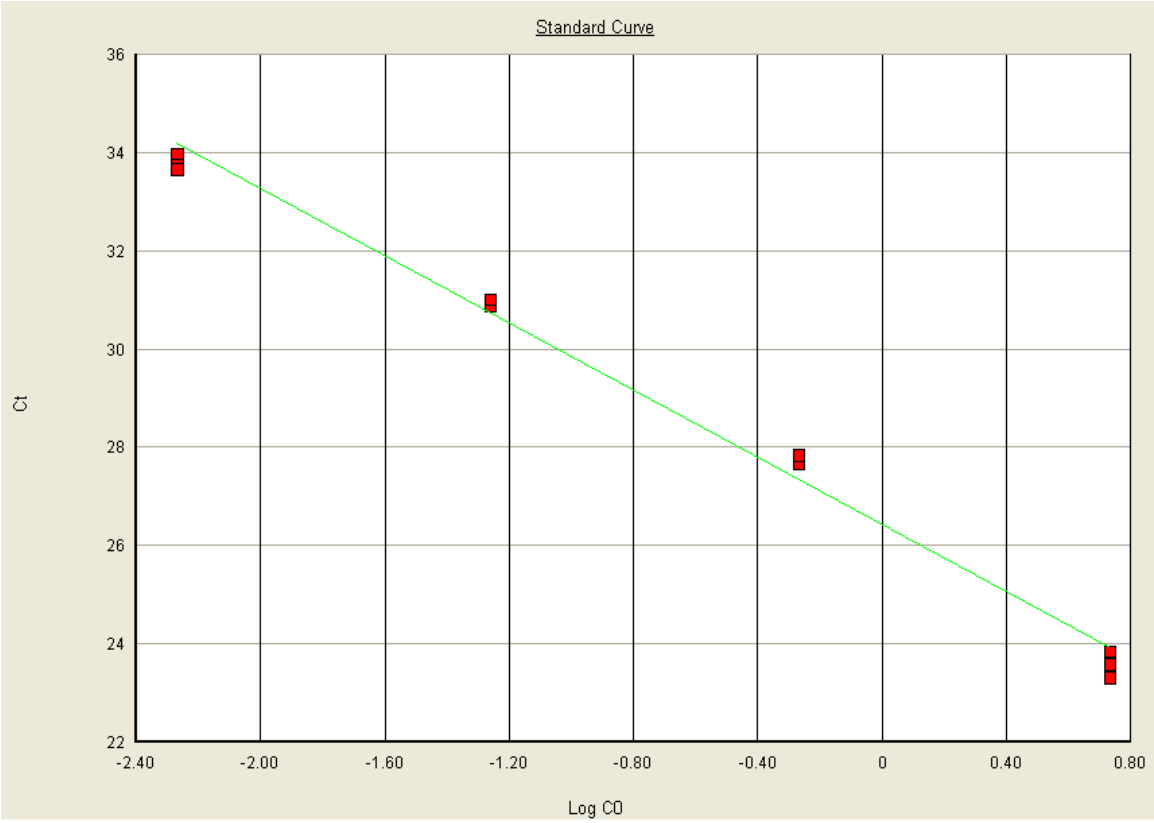

Figure D.12: Standard Curve for mir77for - Plot of C_t vs. $\ln[cDNA]$ for a 10-fold dilution series of cDNA. cDNA amounts in the dilution series are as follows: 1.25 ng, 0.125 ng, 0.00125 ng, and 0.000125 ng. The slope was -3.42 ($r^2 = 0.991$), corresponding to an efficiency of 96.06%.